NASA Contractor Report 3301

An Interaction Algorithm for Prediction of Mean and Fluctuating Velocities in Two-Dimensional Aerodynamic Wake Flows

A. J. Baker and J. A. Orzechowski

CONTRACT NAS1-14855
JULY 1980

NASA

NASA Contractor Report 3301

An Interaction Algorithm for Prediction of Mean and Fluctuating Velocities in Two-Dimensional Aerodynamic Wake Flows

A. J. Baker and J. A. Orzechowski
Computational Mechanics Consultants, Inc.
Knoxville, Tennessee

Prepared for
Langley Research Center
under Contract NAS1-14855

NASA
National Aeronautics
and Space Administration

Scientific and Technical
Information Office

1980

TABLE OF CONTENTS

SUMMARY

A theoretical analysis is presented yielding sets of partial differential equations for determination of turbulent aerodynamic flowfields in the vicinity of an airfoil trailing edge. A four-phase interaction algorithm is derived to facilitate the analysis. Following input, the first computational phase is an elementary viscous-corrected two-dimensional potential flow solution yielding an estimate of the inviscid-flow induced pressure distribution. Phase C involves solution of the turbulent two-dimensional boundary layer equations up to the trailing edge, with transition to a two-dimensional parabolic Navier-Stokes equation system describing the near-wake merging of the upper and lower surface boundary layers. An iteration provides refinement of the potential flow induced pressure coupling to the viscous flow solutions. The final phase, if desired, is a complete two-dimensional Navier-Stokes analysis of the wake flow in the immediate vicinity of trailing edge. A finite element numerical algorithm is presented which is applicable to solution of all partial differential equation sets of the inviscid-viscous aerodynamic interaction algorithm. Numerical results of prediction in the wake of a NACA 63-012 airfoil are compared to experimental data.

INTRODUCTION

Turbulent boundary layer flows departing the trailing edge of an aerodynamic surface are experimentally verified to be strong sources of noise. Alteration of the aerodynamic surface can alter far-field intensity by local absorbtion as well as modifications to the turbulent flow structure prior to departing the trailing edge. A considerable volume of experimental data has been obtained for the case of a jet flow directed over a surface. Attention is now turning to aeroacoustic analysis of the near-field wake associated with airfoil flowfields induced solely by forward flight.

This report presents a theoretical analysis yielding sets of partial differential equations governing turbulent aerodynamic flowfields in the vicinity of a trailing edge. It is a generalization of the parabolic procedure developed by Baker and Manhardt (ref. 1) for analysis of slot jet flows and downstream of the sharp trailing edge terminus of a planar flap. The solution procedure developed herein is a viscous-inviscid interaction algorithm and is applicable to analysis of subsonic two-dimensional airfoils at angle of attack. The primary requirement of this algorithm is accurate numerical prediction of the detailed distributions of mean and fluctuating velocity fields in the immediate trailing edge vicinity.

To accomplish this goal, the four phase interaction algorithm presented in Table 1 has been developed. The input phase serves its standard purpose. Phase B is an inexpensive iterative sequence wherein the Laplacian ($2D\phi$) is repeatedly solved for the potential flow over an airfoil which is sequentially augmented in thickness distribution by computed estimates of the viscous boundary layer displacement thickness distribution δ^*. This solution provides the initial estimate of the inviscid flow pressure distribution imposed upon the subsequent solutions.

In Phase C, the consequentially more complete (and expensive) two-dimensional boundary layer (2DBL) and parabolic Navier-Stokes (2DPNS) equation systems are solved in the trailing edge vicinity. The 2DPNS solution yields detailed distributions of the mean and fluctuating velocity correlations, as well as the computed distribution of efflux velocity $\tilde{u}_2(x_1)$ from the 2DPNS domain. The $2D\phi$ solution from Phase B is repeated, using this "onset" velocity boundary condition specification, producing a refined inviscid flow pressure field. This sequence of 2DBL, 2DPNS and $2D\phi$ solutions is repeated as necessary to yield a common solution for the coupling pressure distribution.

The terminal Phase D solution is probably not required for sharp trailing edge airfoils at small angles of attack. It is required to determine the immediate vicinity trailing edge solution for a blunt-based airfoil. The requirement of Phase D is to refine the prediction of the 2DPNS solution within the immediate trailing edge vicinity, and is accomplished by the more expensive solution of the complete time-averaged, two-dimensional Navier-Stokes (2DNS) equations. An appropriate 2DNS solution domain is determined and boundary conditions applied thereon from the 2DPNS solution. The 2DPNS solution also provides the initial conditions for the iterative solution to 2DNS.

Table 1

VISCOUS-INVISCID AERODYNAMIC INTERACTION ALGORITHM

PHASE	OPERATION	
A.	Input	1. Problem specified by M_∞, C, t/C, α, Re $\equiv$ (Mach No., chord, thickness distribution, angle of attack, Reynolds No.)
B.	Viscous-Corrected Potential Computation ($2D\phi$)	1. Solve $\nabla^2\phi = 0$ on basic airfoil and wake centerline 2. Solve integral boundary layer equation for δ^* 3. Extrapolate δ^* onto wake 4. Repeat B. 1-3 until $\delta^*(x)$ is stationary
C.	Turbulent Boundary Layer, Parabolic Solutions (2DBL/2DPNS)	1. Initialize $\tilde{u}_1(x_2)$ from data or Cole's Law across $\delta(x_1)$ at $x_1/C \approx 0.9$ 2. Establish polar coordinate system on $0.9 < x_1/C \leq 1.0$ if required. 3. Execute 2DBL on $0.9 < x_1/C < 1.0$ using inviscid C_p. 4. Initialize 2DPNS at $x_1/C \approx 1.0$ 5. Execute 2DPNS on $1.0 < x_1/C < 1.2$ using inviscid C_p. 6. Modify $2D\phi$ boundary conditions using 2DBL/2DPNS solution for $\tilde{u}_2$ "onset" velocity 7. Compute $2D\phi$ to refine inviscid C_p distribution. 8. Repeat C.2-7 until C_p stationary.
D.	Complete Navier-Stokes Solution (2DNS)	1. Identify appropriate 2DNS solution domain spanning $x_1/C \approx 1.0 \pm \epsilon$ 2. Obtain initial-boundary conditions from 2DBL/2DPNS solutions 3. Solve complete Navier-Stokes Equations

This report presents derivation of the appropriate differential equation systems including closure for turbulence. A finite element numerical algorithm is developed that is applicable to solution of each system of the identified differential equation systems. Numerical predictions with the algorithm, for Phases A through C, are presented and compared with experimental data for a NACA 63-012 airfoil at zero angle of attack.

SYMBOLS

a_i	boundary condition coefficient
c	coefficient
C	chord length
C_f	skin friction coefficient
C_p	pressure coefficient
d	ordinary differential
D	diffusion coefficient
e	finite element index
f	function of known argument; coordinate curve
g	function; source term
h	metric coefficient; mesh parameter; integration step size
H	boundary layer shape factor
k	turbulence kinetic energy; polynomial degree
K	generalized diffusion coefficient
ℓ	differential operator; length scale
L	differential operator
M	Mach number; number of finite elements spanning R^n
n	unit normal vector; nodes per element; dimensionality

N	finite element interpolation function
p	pressure; generalized parameter; iteration index
q	generalized dependent variable
Q	generalized discretized dependent variable
R	domain of elliptic operator
Re	Reynolds number
S	finite element assembly operator
t	time
T	temperature
u_i	velocity vector
u, U	reference velocity
x_i	Cartesian coordinate system
$y+$	friction velocity Reynolds number
α	parameter
γ	ratio of specific heats
∂R	boundary of solution domain R^n
δ	Kronecker delta; boundary layer thickness; increment
δ^*	boundary layer displacement thickness
Δ	increment
ε	turbulence dissipation function; convergence criteria
θ	boundary layer momentum thickness
η_i	transformed coordinate system
ξ_i	transformed coordinate system
κ	Karman coefficient
λ	multiplier

ν	kinematic viscosity; general diffusion coefficient
ρ	density
σ_{ij}	mean flow Stokes stress tensor
τ	Reynolds stress tensor; wall shear; differential element
ϕ	velocity potential function
χ	generalized initial-value operator
ψ	conservation potential function
ζ_i	finite element natural coordinate system
ω	turbulence damping factor
Ω	global solution domain

Superscripts:

e	effective value
n	dimension of R
t	turbulent
T	matrix transpose
+	turbulence correlation function
~	mass-weighted time-average
$\overline{\quad}$	time average
^	unit vector
´	mass-weighted fluctuating component; ordinary derivative

Subscripts:

∞	global reference condition
e	finite element domain
i,j,k,ℓ	tensor indices

I	freestream reference condition
n	normal
o	initial condition
t	time derivative
w	wall reference condition

Notation:

{ }	column matrix
[ ]	square matrix
$\cup$	union
$\cap$	intersection
ϵ	belongs to
| |	absolute value

PROBLEM DESCRIPTIONS

Overview

The several differential equation systems required for the viscous-inviscid aerodynamic interaction algorithm are each derived from the complete Navier-Stokes equations. The distinguishing feature of aerodynamic flows is their fundamental unidirectionality as induced by the forward flight of the aircraft. Of course, local regions of separated, i.e. omnidirectional, flows can be induced by adverse pressure gradients and/or abrupt changes in geometry. An example of the former occurs on the trailing edge upper surface of an airfoil at sufficiently large angle of attack. A blunt trailing edge illustrates the latter. All but the complete Navier-Stokes equation descriptions have imbedded in their derivation the assumption of unidirectionality. This assumption greatly simplifies the attendant numerical solutions as well as producing considerable cost savings in computer time. The interaction algorithm concept is basically an overt attempt to enjoy these benefits to the fullest extent. The appropriate differential equation systems are developed in this section.

Time-Averaged Navier-Stokes Equations

A state point in single species fluid mechanics is expressed within solution of a coupled nonlinear partial differential equation system describing conservation of mass, momentum and energy. Unique solutions can be obtained upon closure of this system by specification of constitutive behavior and boundary conditions. In Cartesian tensor notation the non-dimensional conservation form of the Navier-Stokes equation system for isoenergetic flow is

$$L(\rho) \equiv \frac{\partial \rho}{\partial t} + \frac{\partial}{\partial x_j}(\rho u_j) = 0 \tag{1}$$

$$L(\rho u_i) \equiv \frac{\partial}{\partial t}(\rho u_i) + \frac{\partial}{\partial x_j}\left[\rho u_j u_i + p\delta_{ij} - Re^{-1}\sigma_{ij}\right] = 0 \tag{2}$$

The dependent variables in equations (1)-(2) have their usual interpretation in fluid mechanics, i.e. ρ is mass density, u_j is the velocity vector, p is the static pressure, and σ_{ij} is the Stokes stress tensor

$$\sigma_{ij} \equiv \mu\left[\frac{\partial u_i}{\partial x_j} + \frac{\partial u_j}{\partial x_i}\right] - \frac{2\mu}{3}\frac{\partial u_k}{\partial x_k}\delta_{ij} \tag{3}$$

where μ is the dynamic viscosity. The equation of state for a perfect gas closes the definition, and the Reynolds number $Re = \rho_\infty U_\infty \ell / \mu_\infty$ where ℓ is a characteristic scale length.

Equations (1)-(3) are valid descriptions for both laminar and turbulent flows. For the latter, however, the solution becomes tractible in a practical sense only after time-averaging. While more definitive resolutions are the subject of current research, (c.f. (ref. 2), the conventional mass-weighted time-averaging is assumed adequate for the present requirements. Therefore, c.f. Cebeci and Smith (ref. 3), the Reynolds decomposition is defined as

$$u_j(x_i,t) \equiv \tilde{u}_j(x_i) + u_j''(x_i,t) \tag{4}$$

The mass-weighted time-average velocity is defined as

$$\tilde{u}_j \equiv \overline{\rho u_j}/\bar{\rho} \tag{5}$$

and

$$\overline{\rho u_i''} \equiv \lim_{T\to\infty} \int_t^{t+T} (\rho u_i - \bar{\rho}\tilde{u}_i)dt \equiv 0 \tag{6}$$

This operation yields the important relation

$$\overline{\rho u_i u_j} = \bar{\rho}\tilde{u}_i\tilde{u}_j + \overline{\rho u_i'' u_j''} \tag{7}$$

Substituting equations (4)-(5) into (1)-(3), time averaging and collecting terms yields the time-averaged Navier-Stokes equations for isoenergetic flow.

$$L(\bar{\rho}) = \frac{\partial \bar{\rho}}{\partial t} + \frac{\partial}{\partial x_j}[\tilde{u}_j\bar{\rho}] = 0 \tag{8}$$

$$L(\bar{\rho}\tilde{u}_i) = \frac{\partial(\bar{\rho}\tilde{u}_i)}{\partial t} + \frac{\partial}{\partial x_j}\left[\tilde{u}_j(\bar{\rho}\tilde{u}_i) + \bar{p}\delta_{ij} - \bar{\sigma}_{ij} + \overline{\rho u_i'' u_j''}\right] = 0 \tag{9}$$

The solution of various simplified forms of equations (8)-(9) is required for the aerodynamic wake flow analysis. The following sections establish the appropriate sub-systems.

Viscous-Corrected Potential Flow

The first requirement of the interaction solution algorithm is to compute a viscous-corrected two-dimensional potential flow distribution, Phase B in Table 1. The solution domain is a "sufficiently" large region surrounding the airfoil and the wake trajectory. The airfoil will become augmented in thickness distribution during the sequence of viscous corrections, see Figure 1.

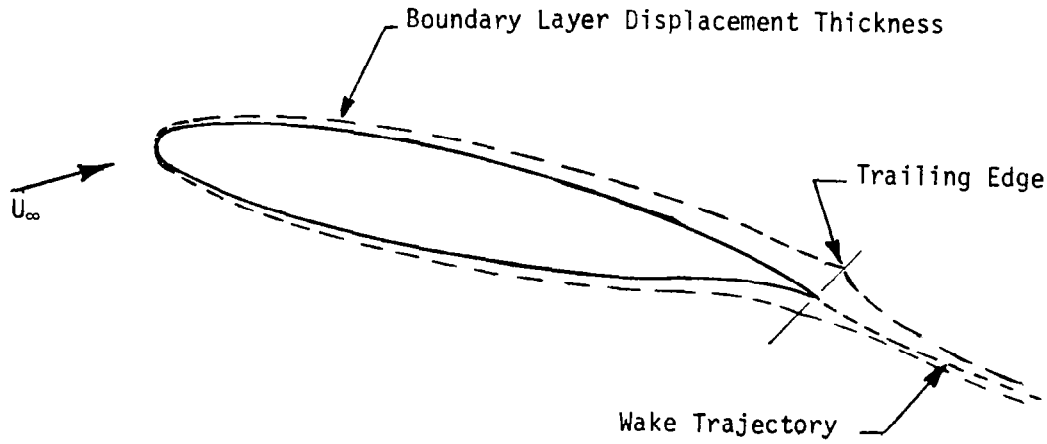

Figure 1. Illustration of Viscous-Corrected Potential Flow Solution Requirements

The differential equations governing the two-dimensional potential and integral viscous boundary layer flows are trivial subclasses of equations (8)-(9). Define the gradient of the perturbation potential function $\phi(x_i)$ as the difference between the reference and local velocity vectors, i.e.

$$u_i(x_j) \equiv U_\infty \left[\hat{\varepsilon}_i - \frac{\partial \phi}{\partial x_i}\right] \tag{10}$$

For all Mach numbers below transonic, and for all irrotational, isentropic, inviscid, steady and turbulence-free flows, equations (8)-(9) collapse to the elementary Laplacian

$$L(\phi) = \frac{\partial^2 \phi}{\partial x_i^2} = \nabla^2 \phi = 0 \tag{11}$$

The boundary condition for solution of equation (11) is established from the defining equation (10) by the inner product with the unit normal $\hat{n}_i$ as

$$\mathcal{L}(\phi) = \frac{\partial \phi}{\partial x_i} \hat{n}_i - \hat{\varepsilon}_i \hat{n}_i + U_\infty^{-1} u_i \hat{n}_i = 0 \tag{12}$$

If the contour with normal $\hat{n}_i$ corresponds to an inviscid streamline, for example, the boundary layer displacement thickness δ^*, the last term in equation (12) vanishes identically. If not, the last term corresponds to the inviscid entrainment velocity component $u^{\perp}$. In either instance, equations (11)-(12) represent a well-posed Neumann problem, and $\phi \equiv 0$ is set at one location (only) on the $2D\phi$ boundary.

Segments of the potential flow solution domain coincide with the viscous displacement surface δ^* and its extrapolation into the wake. The distribution of δ^* is estimated during Phase B by solution of the integral form of the steady flow continuity and $\tilde{u}_1$ momentum equations (8)-(9). The resultant differential equation is written on θ, the boundary layer momentum thickness, as (c.f., ref. 3)

$$L(\theta) = \frac{d\theta}{dx} + \frac{\theta}{u} (H+2) \frac{du}{dx} - \frac{1}{2} C_f = 0 \tag{13}$$

In equation (13), $u(x_1)$ is the potential velocity at the boundary layer edge, $H \equiv \delta^*/\theta$ is the boundary layer shape factor, and C_f is the skin friction coefficient. Using the Ludweig-Tillman formula,

$$C_f \equiv 0.246(10)^{-0.678H} \, Re^{-0.268} \tag{14}$$

and the length scale θ is used in evaluating the Reynolds number.

The primary output of this computational sequence is the potential flow pressure distribution induced on the airfoil and wake flow solution domains.

$$C_p \equiv 1 - \frac{\rho u_i u_i}{\rho_\infty U_\infty^2} \tag{15}$$

Upon substitution of equation (10) and resolution into scalar components on the local normal-tangent coordinate system (n, s), with unit vectors $(\hat{n}, \hat{t})$, equation (15) becomes

$$C_p = (\hat{\varepsilon}.\hat{n})^2 + 2 \frac{\partial \phi}{\partial s} (\hat{\varepsilon}.\hat{t}) - \left(\frac{\partial \phi}{\partial s}\right)^2 \tag{16}$$

This completes definition of the equation systems required to be solved within Phase B of the interaction algorithm.

Turbulence Closure Model

The Phase C and D differential eq-ation systems require identification of a turbulence closure model, since time-averaging has introduced the dynamic Reynolds stress $-\overline{\rho u_i' u_j'}$ into the mean flow differential equation system (8)-(9). For the aerodynamic wake flows of interest, it is reasonable to assume

$$\overline{\rho u_i' u_j'} \approx \bar{\rho}\,\overline{u_i' u_j'} \tag{17}$$

The exact differential equation for the kinematic Reynolds stress tensor $-\overline{u_i' u_j'}$ is (c.f. ref. 3, 4)

$$L(\overline{u_i' u_j'}) = \frac{\partial}{\partial t}(\overline{u_i' u_j'}) + \frac{\partial}{\partial x_k}(\tilde{u}_k \overline{u_i' u_j'}) + \left[\overline{u_j' u_k'}\frac{\partial \tilde{u}_i}{\partial x_k} + \overline{u_i' u_k'}\frac{\partial \tilde{u}_j}{\partial x_k}\right]$$

$$+ 2\bar{\nu}\,\overline{\frac{\partial u_i'}{\partial x_k}\frac{\partial u_j'}{\partial x_k}} + \overline{\frac{p}{\rho}\left[\frac{\partial u_i'}{\partial x_j} + \frac{\partial u_j'}{\partial x_i}\right]}$$

$$+ \frac{\partial}{\partial x_k}\left[\overline{u_i' u_j' u_k'} - \bar{\nu}\,\overline{\frac{\partial u_i' u_j'}{\partial x_k}} + \overline{\frac{p}{\rho}(\delta_{jk} u_i' + \delta_{ik} u_j')}\right] = 0 \tag{18}$$

where $\bar{\nu}$ is the kinematic viscosity $\bar{\mu}/\bar{\rho}$. An additional differential equation is required established, usually written on a turbulence dissipation rate funtion. Assuming dissipation occurs in the sub-scale and is isotropic, the corresponding turbulence dissipation rate ε is defined by the contraction of the fourthterm in equation (18) as

$$\frac{2}{3}\delta_{ij}\varepsilon \equiv 2\bar{\nu}\,\overline{\frac{\partial u_i'}{\partial x_k}\frac{\partial u_j'}{\partial x_k}} \tag{19}$$

The transport equation for dissipation function ε is

$$L(\varepsilon) = \frac{\partial \varepsilon}{\partial t} + \frac{\partial}{\partial x_k}(\tilde{u}_k \varepsilon) + 2\bar{\nu}\,\overline{\frac{\partial u_i'}{\partial x_k}\frac{\partial u_i'}{\partial x_\ell}\frac{\partial u_k'}{\partial x_\ell}}$$

$$+ 2\overline{\left[\nu \frac{\partial^2 u_i'}{\partial x_k \partial x_\ell}\right]^2} + \frac{\partial}{\partial x_k}\left[\bar{\nu}\,\overline{u_k' \frac{\partial u_i'}{\partial x_\ell}\frac{\partial u_i'}{\partial x_\ell}} + \overline{\frac{\nu}{\rho}\frac{\partial p}{\partial x_i}\frac{\partial u_k'}{\partial x_i}}\right] = 0 \qquad (20)$$

Equations (18) and (20) constitute seven partial differential equations, and are not closed since the third order correlations are undefined. Additional differential equations could be established, but they in turn would involve undefined higher order terms. Hence, modeling of third order correlations is usually invoked at a level of completeness dependent upon the dimensionality and geometrical complexity of the physical system.

Launder, Reece and Rodi (ref. 5) present a comprehensive analysis of a Reynold's stress closure hypothesis and numerical results for several allied classes of flows, see also Hanjalic and Launder (ref. 6). Gessner and Emery (ref. 7) report an order of magnitude analysis of the Launder closure model, for the parabolic flow approximation in Cartesian coordinates that yields an algebraic equation system for the Reynolds stress field in terms of dominant mean flow gradients and the turbulence kinetic energy field k.

$$k \equiv \frac{1}{2}\overline{u_i' u_i'} \qquad (21)$$

From tensor field theory, see also reference 8, the existence of a Reynold's stress constitutive equation is assured and of the form

$$-\overline{u_i' u_j'} = -\alpha_1 \overline{u_k' u_k'}\,\delta_{ij} + \alpha_2 E_{ij} + \alpha_3 E_{ik}E_{kj} + \ldots \qquad (22)$$

Equation (22) displays the symmetry required of a stress tensor since

$$E_{ik} \equiv \left[\frac{\partial \tilde{u}_i}{\partial x_k} + \frac{\partial \tilde{u}_k}{\partial x_i}\right] \qquad (23)$$

The α may be determined from some sub-dimensional flows. For example, in two-dimensional boundary layer flow wherein only $-\overline{u_1' u_2'}$ remains significant, the form of equation (22) must agree with the familiar two-equation closure model

$$- \overline{u_1' u_2'} = C_\nu \frac{k^2}{\varepsilon} \frac{\partial \tilde{u}_1}{\partial x_2} \tag{24}$$

where C_ν is an empirical constant (0.09). Comparing equations (22) and (24) yields $\alpha_2 = C_\nu k^2/\varepsilon$.

The tensor generalization of Gessner and Emery's analysis for three-dimensional parabolic flows can be established. The first three terms in the expansion of equation (22) are

$$- \overline{u_i' u_j'} = -k\alpha_{ij} + C_4 \frac{k^2}{\varepsilon} \left[\frac{\partial \tilde{u}_i}{\partial x_j} + \frac{\partial \tilde{u}_j}{\partial x_i}\right] + C_2 C_4 \frac{k^3}{\varepsilon^2} \left[\frac{\partial \tilde{u}_i}{\partial x_k} + \frac{\partial \tilde{u}_k}{\partial x_i}\right]\left[\frac{\partial \tilde{u}_k}{\partial x_j} + \frac{\partial \tilde{u}_j}{\partial x_k}\right] + \ldots \tag{25}$$

This form is achieved using the model of Launder, et al (ref. 5) for the triple correlations in equations (18)-(20). The diagonal tensor α_{ij} is defined as

$$\alpha_{ij} = \frac{1}{3k} \left(\overline{u_\ell' u_\ell'}\right) a_i \delta_{ij} \tag{26}$$

The coefficients a_i permit anisotropy in the turbulence normal stress field. For $a_1 \equiv C_1$, $a_2 \equiv a_3 \equiv C_3$, the C_i are defined by Launder, Reese and Rodi (ref. 5) as

$$C_1 \equiv \frac{22(C_{\phi 1} - 1) - 6(4C_{\phi 2} - 5)}{33(C_{\phi 1} - 2C_{\phi 2})}$$

$$C_2 \equiv \frac{4(3C_{\phi 2} - 1)}{11(C_{\phi 1} - 2C_{\phi 2})}$$

$$C_3 \equiv \frac{22(C_{\phi 1} - 1) - 12(3C_{\phi 2} - 1)}{33(C_{\phi 1} - 2C_{\phi 2})}$$

$$C_4 \equiv \frac{44C_{\phi 1} - 22C_{\phi 1}C_{\phi 2} - 128C_{\phi 2} - 36C_{\phi 2}^2 + 10}{165(C_{\phi 1} - 2C_{\phi 2})^2} \tag{27}$$

Here $C_{\phi 1}$ and $C_{\phi 2}$ are the "universal" empirical constants derived by Hanjalic and Launder (ref. 6). The suggested values are $C_{\phi 1} = 2.8$ and $C_{\phi 2} = 0.45$.

The algebraic Reynold's stress model developed by Gessner and Emery (ref. 7) retained most first-order terms in the expansion. Equation (25), simplified in accordance with the parabolic assumption, but retaining all first and second-order terms yields

$$\overline{u_1'u_1'} = C_1 k - 2C_4 \frac{k^2}{\varepsilon} \frac{\partial \tilde{u}_1}{\partial x_1} - C_2 \frac{k}{\varepsilon} C_4 \frac{k^2}{\varepsilon} \left[\left(\frac{\partial \tilde{u}_1}{\partial x_2} \right)^2 + \left(\frac{\partial \tilde{u}_1}{\partial x_3} \right)^2 \right]$$

$$\overline{u_2'u_2'} = C_3 k - 2C_4 \frac{k^2}{\varepsilon} \frac{\partial \tilde{u}_2}{\partial x_2} - C_2 \frac{k}{\varepsilon} C_4 \frac{k^2}{\varepsilon} \left(\frac{\partial \tilde{u}_1}{\partial x_2} \right)^2$$

$$\overline{u_3'u_3'} = C_3 k - 2C_4 \frac{k^2}{\varepsilon} \frac{\partial \tilde{u}_3}{\partial x_3} - C_2 \frac{k}{\varepsilon} C_4 \frac{k^2}{\varepsilon} \left(\frac{\partial \tilde{u}_1}{\partial x_3} \right)^2$$

$$\overline{u_1'u_2'} = - C_4 \frac{k^2}{\varepsilon} \frac{\partial \tilde{u}_1}{\partial x_2}$$

$$\overline{u_1'u_3'} = - C_4 \frac{k^2}{\varepsilon} \frac{\partial \tilde{u}_1}{\partial x_3}$$

$$\overline{u_2'u_3'} = - C_4 \frac{k^2}{\varepsilon} \left[\frac{\partial \tilde{u}_2}{\partial x_3} + \frac{\partial \tilde{u}_3}{\partial x_2} \right] - C_2 \frac{k}{\varepsilon} C_4 \frac{k^2}{\varepsilon} \frac{\partial \tilde{u}_1}{\partial x_2} \frac{\partial \tilde{u}_1}{\partial x_3} \qquad (28)$$

The retained second-order terms are the C_4-premultiplied expressions in $\overline{u_i'u_i'}$ and $\overline{u_2'u_3'}$. These terms provide the elliptic boundary value character required for solution of the transverse momentum equations as initial-boundary value problems. Under the parabolic order of magnitude analysis, Gessner et al. (ref. 7) obtained the parabolic form of the dissipation function as

$$\varepsilon = - \left(\overline{u_1'u_2'} \frac{\partial \tilde{u}_1}{\partial x_2} + \overline{u_1'u_3'} \frac{\partial \tilde{u}_1}{\partial x_3} \right) \qquad (29)$$

With equations (25)-(26) established, the aerodynamic interaction algorithm solution requirement for turbulence closure is considerably moderated, since only equation (18) contracted over i and j need be solved in concert with equation (20). Again employing the model of Launder, Reece and Rodi (ref. 5), the final form is

$$L(k) = \frac{\partial k}{\partial t} + \frac{\partial}{\partial x_j}\left[\tilde{u}_j k - \left(C_k \frac{k}{\varepsilon}\overline{u_i' u_j'} + \tilde{\nu}\delta_{ij}\right)\frac{\partial k}{\partial x_i}\right]$$

$$+ \overline{u_i' u_j'}\frac{\partial \tilde{u}_i}{\partial x_j} + \varepsilon = 0 \qquad (30)$$

$$L(\varepsilon) = \frac{\partial \varepsilon}{\partial t} + \frac{\partial}{\partial x_j}\left[\tilde{u}_j \varepsilon - C_\varepsilon \frac{k}{\varepsilon}\overline{u_i' u_j'}\frac{\partial \varepsilon}{\partial x_i}\right]$$

$$+ C_\varepsilon^1 \overline{u_i' u_j'}\frac{\varepsilon}{k}\frac{\partial \tilde{u}_i}{\partial x_j} + C_\varepsilon^2 \frac{\varepsilon^2}{k} = 0 \qquad (31)$$

The various C_k and C_ε^α are empirical model constants.

Parabolic Solution Algorithm

Following completion of the Phase B viscous-corrected potential flow solution, the next requirement is solution of the two-dimensional parabolic Navier-Stokes (2DPNS) equations for the pre- and post- trailing edge flowfields. The familiar boundary layer equations are a subset of the 2DPNS system. There are four assumptions required satisfied for 2DPNS to be a valid flowfield description, specifically:

1. The flow is steady.

2. A dominant mean flow direction is omnipresent.

3. In this direction only, diffusion is negligible compared to all other processes including convection, and

4. Overall elliptic boundary value character can be enforced by pressure coupling with a complete-dimensional inviscid (potential) flow solution.

The steady viscous and turbulent aerodynamic flows under study meet all four requirements except in a region of separation as induced either by a sufficient adverse pressure gradient or abrupt change in geometry. Excluding these, the 3DPNS partial differential equation system is readily established from the complete Navier-Stokes equations (8)-(9), and turbulence kinetic energy and dissipation equations (30)-(31) as

$$L(\bar{\rho}) = \frac{\partial}{\partial x_i}(\bar{\rho}\tilde{u}_i) = 0 \tag{32}$$

$$L(\bar{\rho}\tilde{u}_1) = \frac{\partial}{\partial x_i}(\bar{\rho}\tilde{u}_i\tilde{u}_1) + \frac{\partial \bar{p}}{\partial x_1} - \frac{\partial}{\partial x_\ell}\left[\frac{\bar{\mu}}{Re}\frac{\partial \tilde{u}_1}{\partial x_\ell} - \overline{\rho u_1' u_\ell'}\right] = 0 \tag{33}$$

$$L(\bar{\rho}\tilde{u}_2) = \frac{\partial}{\partial x_i}(\bar{\rho}\tilde{u}_i\tilde{u}_2) + \frac{\partial \bar{p}}{\partial x_2} - \frac{\partial}{\partial x_\ell}\left[\frac{\bar{\mu}}{Re}\left(\frac{\partial \tilde{u}_2}{\partial x_\ell} + \frac{\partial u_\ell}{\partial x_2}\right) - \overline{\rho u_2' u_\ell'}\right] = 0 \tag{34}$$

$$L(\bar{\rho}\tilde{u}_3) = \frac{\partial}{\partial x_i}(\bar{\rho}u_i u_3) + \frac{\partial \bar{p}}{\partial x_3} - \frac{\partial}{\partial x_\ell}\left[\frac{\bar{\mu}}{Re}\left(\frac{\partial \tilde{u}_3}{\partial x_\ell} + \frac{\partial \tilde{u}_\ell}{\partial x_3}\right) - \overline{\rho u_3' u_\ell'}\right] = 0 \tag{35}$$

$$L(k) = \frac{\partial}{\partial x_i}(\bar{\rho}\tilde{u}_i k) - \frac{\partial}{\partial x_i}\left[\bar{\rho}\left(\frac{\bar{\nu}}{Re} + C_k\frac{k}{\varepsilon}\overline{u_i' u_k'}\right)\frac{\partial k}{\partial x_k}\right] + \overline{\rho u_i' u_k'}\frac{\partial \tilde{u}_k}{\partial x_i} + \bar{\rho}\varepsilon = 0 \tag{36}$$

$$L(\varepsilon) = \frac{\partial}{\partial x_i}(\bar{\rho}\tilde{u}_i\varepsilon) - \frac{\partial}{\partial x_i}\left[\bar{\rho}\left(C_3\,\overline{u_i' u_k'}\,\frac{k}{\varepsilon}\right)\frac{\partial \varepsilon}{\partial x_k}\right] + C_\varepsilon^1\,\overline{\rho u_i' u_\ell'}\,\frac{\varepsilon}{k}\frac{\partial \tilde{u}_k}{\partial x_\ell} + C_\varepsilon^2\bar{\rho}\varepsilon^2/k = 0 \tag{37}$$

Equations (32)-(37) are generally valid on two- and three-dimensional space dependent solely upon summation index limits. The 2DPNS limited summation index convention is $1 \le i \le 2$ and $\ell = k = 2$, while 3DPNS $1 \le i \le 3$ and $2 \le \ell, k \le 3$. The x_1 axis is assumed aprallel to the predominant flow direction, and the various C_α remain the model correlation coefficients. Furthermore, the dilitation term from the Stoke's laminar stress tensor, equation (3) has been deleted from equations (33)-(35) as negligibly small.

For the $\tilde{u}_1$ equation, upon inserting and expanding terms in the Reynolds stress, the divergence term becomes

$$\frac{\partial}{\partial x_\ell}\left[\frac{\bar{\mu}}{Re}\frac{\partial \tilde{u}_1}{\partial x_\ell} - \overline{\rho u_1' u_\ell'}\right] = \frac{\partial}{\partial x_\ell}\left[\left(\frac{\bar{\mu}}{Re} + C_4\frac{\bar{\rho}k^2}{\varepsilon}\right)\frac{\partial \tilde{u}_1}{\partial x_\ell}\right] \tag{38}$$

Defining an effective diffusion coefficient

$$\nu^{eff} \equiv \frac{\bar{\nu}}{Re} + C_4\left(\frac{k}{\varepsilon}\right)k \tag{39}$$

the diffusion expression for $\tilde{u}_1$ in 2DPNS is the familiar form

$$\frac{\partial}{\partial x_\ell}\left[\frac{\bar{\mu}}{Re}\frac{\partial \tilde{u}_1}{\partial x_\ell} - \overline{\rho u_1' u_\ell'}\right] = \frac{\partial}{\partial x_\ell}\left[\bar{\rho}\nu_{eff}\frac{\partial \tilde{u}_1}{\partial x_\ell}\right] \tag{40}$$

The divergence terms in the remaining momentum equations are

$$\frac{\partial}{\partial x_\ell}\left[\frac{\bar{\mu}}{Re}\left(\frac{\partial \tilde{u}_k}{\partial x_\ell} + \frac{\partial \tilde{u}_\ell}{\partial x_k}\right) - \overline{\rho u_k' u_\ell'}\right] = \frac{\partial}{\partial x_\ell}\left[\bar{\rho}\nu_{eff}\left(\frac{\partial \tilde{u}_k}{\partial x_\ell} + \frac{\partial \tilde{u}_\ell}{\partial x_k}\right)\right]$$

$$- \frac{\partial}{\partial x_\ell}\left[\bar{\rho} k \alpha_{k\ell} - \bar{\rho} C_2 \frac{k}{\varepsilon} C_4 \frac{k}{\varepsilon} k \frac{\partial \tilde{u}_1}{\partial x_k}\frac{\partial \tilde{u}_1}{\partial x_\ell}\right] \tag{41}$$

where addition of terms involving shear of the alternative transverse plane mean velocity component $\tilde{u}_\ell$ and the dominant component $\tilde{u}_1$ are now present.

The divergence term common to both the k and ε equations contains three terms. After inserting equation (25), the first term in the expansion is

$$\frac{\partial}{\partial x_i}\left[C_q \bar{\rho}\frac{k}{\varepsilon}\overline{u_i' u_\ell'}\frac{\partial q}{\partial x_\ell}\right] = \frac{\partial}{\partial x_\ell}\left[\frac{2}{3} C_q \bar{\rho}\frac{k^2}{\varepsilon}\frac{\partial q}{\partial x_\ell}\right] \tag{42}$$

where q represents either k or ε. Note that equation (42) is fundamentally identical to the Reynold's stress contribution to equation (39) with C_4 replaced by C_q. For $2C_q/3 \approx C_4$, equation (39) yields the effective viscosity as the representative major diffusion contribution throughout 2DPNS. When inserted into equation (36), the second term in the expansion of $\overline{u_i' u_j'}$ vanishes identically in the parabolic approximation. However, the third term yields a non-vanishing diffusion-type contribution for both the k and ε equations as

$$\frac{\partial}{\partial x_k}\left[C_q \bar{\rho}\frac{k}{\varepsilon} C_2 \frac{k}{\varepsilon} C_4 \frac{k}{\varepsilon} k \left(\frac{\partial \tilde{u}_1}{\partial x_k}\right)\left(\frac{\partial \tilde{u}_1}{\partial x_\ell}\right)\frac{\partial q}{\partial x_\ell}\right]$$

Hence, an anisotropic divergence-based transport of both k and ε is permitted for a non-symmetric three-dimensional $\tilde{u}_1$ velocity field.

The production terms for both k and ε are basically identical, with the latter multiplied by $C_{\varepsilon}^{1}\left(\frac{k}{\varepsilon}\right)^{-1}$. The Reynold's stress-velocity shear contraction simplifies to the following form under the parabolic approximation.

$$-\overline{\rho u_i'' u_k''}\,\frac{\partial \tilde{u}_i}{\partial x_k} = \bar{\rho} C_4 \frac{k^2}{\varepsilon}\left[\frac{\partial \tilde{u}_1}{\partial x_\ell}\frac{\partial \tilde{u}_1}{\partial x_\ell}\right] + 2\bar{\rho} C_2 \frac{k}{\varepsilon} C_4 \frac{k}{\varepsilon} k \left(\frac{\partial \tilde{u}_1}{\partial x_1}\right)\left[\frac{\partial \tilde{u}_1}{\partial x_\ell}\frac{\partial \tilde{u}_1}{\partial x_\ell}\right] \tag{43}$$

The first term is identical to the familiar boundary layer form. The second term may be negligible due to the appearance of $\partial\tilde{u}_1/\partial x_1 \ll \partial\tilde{u}_1/\partial x_\ell$.

Pressure Resolution and Mass Conservation

The procedure to enforce pressure coupling and computational conservation of mass is required. As described in Table 1, the first step following initiation of a $\tilde{u}_1$ velocity profile in Phase C is integration of the 2DBL form of the 2DPNS equations. This procedure establishes an initial distribution of $\tilde{u}_2$ that satisfies the continuity equation, as well as to initialize distributions of k, ε and ν_{eff} in the absence of data. In 2DBL, equations (33), (36) and (37) are solved for $\tilde{u}_1$, k and ε, while the continuity equation (32) is solved directly for $\tilde{u}_2$ as

$$L(\bar{\rho}) = \frac{\partial(\bar{\rho}\tilde{u}_2)}{\partial x_2} + \frac{\partial(\bar{\rho}\tilde{u}_1)}{\partial x_1} = 0 \tag{44}$$

Equation (44) is an initial-value problem, the direct solution of which specifically enforces continuity. The integration is initiated at the airfoil surface using the specified value of (suction) velocity V_w, i.e., $\tilde{u}_2(x_1, 0) \equiv V_w(x_1)$. The second term in equation (44) is the axial (x_1) derivative of $\tilde{u}_1$, an accurate evaluation of which results following a few integration steps of equations (33), (36) and (37).

The pressure distribution through the boundary layer in 2DBL is established from the familiar order of magnitude analysis of equation (34) as

$$L(\bar{\rho}\tilde{u}_2) = \frac{\partial}{\partial x_2}\left[\bar{p} + \bar{\rho}\,\overline{u_2'' u_2''}\right] = 0 \tag{45}$$

Equation (45) is a linear ordinary differential equation solved exactly in terms of the appropriate Reynolds stress component.

Within the 2DPNS equation system, pressure coupling to the freestream inviscid flow, and the distribution throughout the viscous flow domain, is contained within solution of a transverse plane Poisson equation. Forming the divergence of equations (34) plus (35) for steady flow, and recalling the limited summation convention, this equation is

$$L(\bar{p}) = \frac{\partial}{\partial x_\ell}\left[\frac{\partial \bar{p}}{\partial x_\ell} + \frac{\partial}{\partial x_j}\left(\bar{\rho}\tilde{u}_j\tilde{u}_\ell\right) - \frac{\partial}{\partial x_k}\left(\bar{\sigma}_{\ell k} - \overline{\rho u_\ell'' u_k''}\right)\right] = 0 \tag{46}$$

The aerodynamic interaction algorithm is based upon the observation that the solution of the linear, elliptic Poisson equation (46) consists of complementary and particular solutions as

$$\bar{p}(x_i) = p_c(x_i) + p_p(x_i) \tag{47}$$

By definition, the complementary solution satisfies the homogeneous form of equation (46)

$$L(p_c) = \frac{\partial^2 p_c}{\partial x_\ell^2} = 0 \tag{48}$$

subject to the known boundary conditions for $\bar{p}(x_i)$, which corresponds to the bounding inviscid flow pressure distribution. Therefore, on 2DPNS domain segments coincident with the inviscid flow,

$$\bar{p}(\bar{x}_\ell) = p^I(\bar{x}_\ell) = p_c(\bar{x}_\ell) \tag{49}$$

where $\bar{x}_\ell$ indicates x_ℓ constrained to the boundary of the 2DPNS solution domain. Elsewhere, the appropriate boundary condition is vanishing normal gradient.

$$\ell(p_c) = \frac{\partial p_c}{\partial x_\ell}\hat{n}_\ell = 0 \tag{50}$$

The particular solution p_p is any function satisfying equation (46) with homogeneous boundary conditions on 2DPNS boundary segments coincident with the freestream. Elsewhere, a gradient boundary condition can be established from the inner product of equations (34)-(35) with the surface normal. Since the convection term vanishes identically at a wall or symmetry plane, the constraint is

$$\ell(p_p) = \frac{\partial p_p}{\partial x_\ell}\hat{n}_\ell - \frac{\partial}{\partial x_k}\left[\bar{\sigma}_{\ell k} - \overline{\rho u_k' u_\ell'}\right]\hat{n}_\ell = 0 \tag{51}$$

Since the laminar viscosity term is negligible everywhere away from a wall, equation for p_p can be simplified to the inviscid form,

$$L(p_p) = \frac{\partial}{\partial x_\ell}\left[\frac{\partial p_p}{\partial x_\ell} + \frac{\partial}{\partial x_j}\left(\bar{\rho}\tilde{u}_j\tilde{u}_\ell + \overline{\rho u_\ell' u_j'}\right)\right] = 0 \tag{52}$$

Equations (47)-(52) define the pressure-coupled interaction algorithm, as well as a solution procedure for pressure distributions in the equation solutions. Since the current requirement is solely two-dimensional, the 2DPNS algorithm becomes identical with 2DBL for flows upstream of the trailing edge terminus. Since $\ell = 2$ only, equation (48) becomes

$$\frac{d^2 p_c}{dx_2^2} = 0 \tag{53}$$

Applying $p_c = p^I$ at the freestream and equation (50) at the wall, the solution is p_c = constant = p^I, i.e. the complementary pressure is the inviscid flow pressure imposed across the boundary layer. Similarly, since p_p vanishes at the freestream, the solution of equation should agree essentially with the boundary layer form, equation (45).

This redundancy does not hold for two-dimensional flows downstream of the trailing edge terminus for non-zero angles of attack. On $x_1/C > 1$, the upper and lower surface inviscid pressures are equal only for the planar wake associated with zero angle of attack. Designating the levels as p_u^I and p_ℓ^I, equation (48) becomes a two-point boundary value problem, the solution to which is a linear interpolation between the end point values. Hence, the distribution of p_c in 2DPNS is known a priori. Equation (52) is solved directly with $p_p \equiv 0$ at each end point. The x_1-derivatives in the non-homogeniety cannot be deleted since local strong accelerations occur parallel to x_1 immediately downstream of the trailing edge.

The final requirement within 2DPNS is explicit computational enforcement of conservation of mass. An implicit enforcement occurs in the non-homogeniety in the particular pressure Poisson equation by direct insertion of the continuity equation. The explicit enforcement is accomplished within the finite element solution algorithm by considering the continuity equation as a differential constraint in the PNS solution statements for transverse velocity. Looking to the variational calculus for guidance, a suitable measure

of mass conservation is a potential function ψ, wherein the Laplacian of ψ is equated to the error in exact satisfaction of the continuity equation (32), by the computed mean velocity mass flux, i.e.

$$L(\phi) \equiv \frac{\partial}{\partial x_\ell}(\bar{\rho}\frac{\partial \psi}{\partial x_\ell}) - \frac{\partial}{\partial x_i}(\tilde{\rho}\tilde{u}_i) = 0 \qquad (54)$$

The boundary conditions for ψ are arbitrary and may include the derivative constraint

$$\ell(\phi) = \frac{\partial \psi}{\partial x_\ell}\hat{n}_\ell = 0 \qquad (55)$$

as well as setting $\psi \equiv 0$ at select locations. In this regard, ψ exhibits much of the character of velocity potential function associated with the 2Dϕ solution. However, in the context of a differential constraint, the gradient of ψ acts in the manner of a pressure gradient in the PNS solution statement. Importantly, the PNS solution is acceptable only upon equation (54) becoming computationally homogeneous, whereupon $\psi \approx 0$ throughout. Hence, interpretation of the gradient of ψ as a velocity or pressure contribution is correspondingly a computational zero.

Finally, for algorithm stability in the computation of subsonic flows, the particular pressure distribution computed during the current iterate of the overall interaction algorithm is applied solely within the transverse momentum equation. The previous iterate distribution is added to the current distribution of complementary pressure to form the x_1-pressure gradient for $\tilde{u}_1$. In the limit of convergence, the computed particular pressure distribution takes on a computationally stationary value.

Coordinate Systems

Only for an airfoil with cusped trailing edge can the locally Cartesian boundary layer coordinate system be carried directly into the wake. For a non-zero trailing edge included angle, it is necessary to transform to a polar coordinate system well upstream of the trailing edge terminus, to "rotate" the upper and lower boundary layers to a planar coincidence at the trailing edge. Figure 2 illustrates the geometry for a sharp edged airfoil, and $x_1/C = 0.9$ is selected as the point to initiate transformation to polar coordinates. The intersection of the two rays, perpendicular to the local tangent to the airfoil at $x_1/C = 0.9$ and 1.0, defines the origin of the polar coordinate system. (Only the lower surface system is shown; the operations on the upper surface are identical.) The exterior potential flow solution, Phase B, or experimental data on $\tilde{u}_1$ determines the boundary layer thickness δ at $x_1/C = 0.9$. The 2DBL/2DPNS domain intersection with the lower free-stream is extrapolated on $x_1/C > 0.9$ and into the downstream wake as

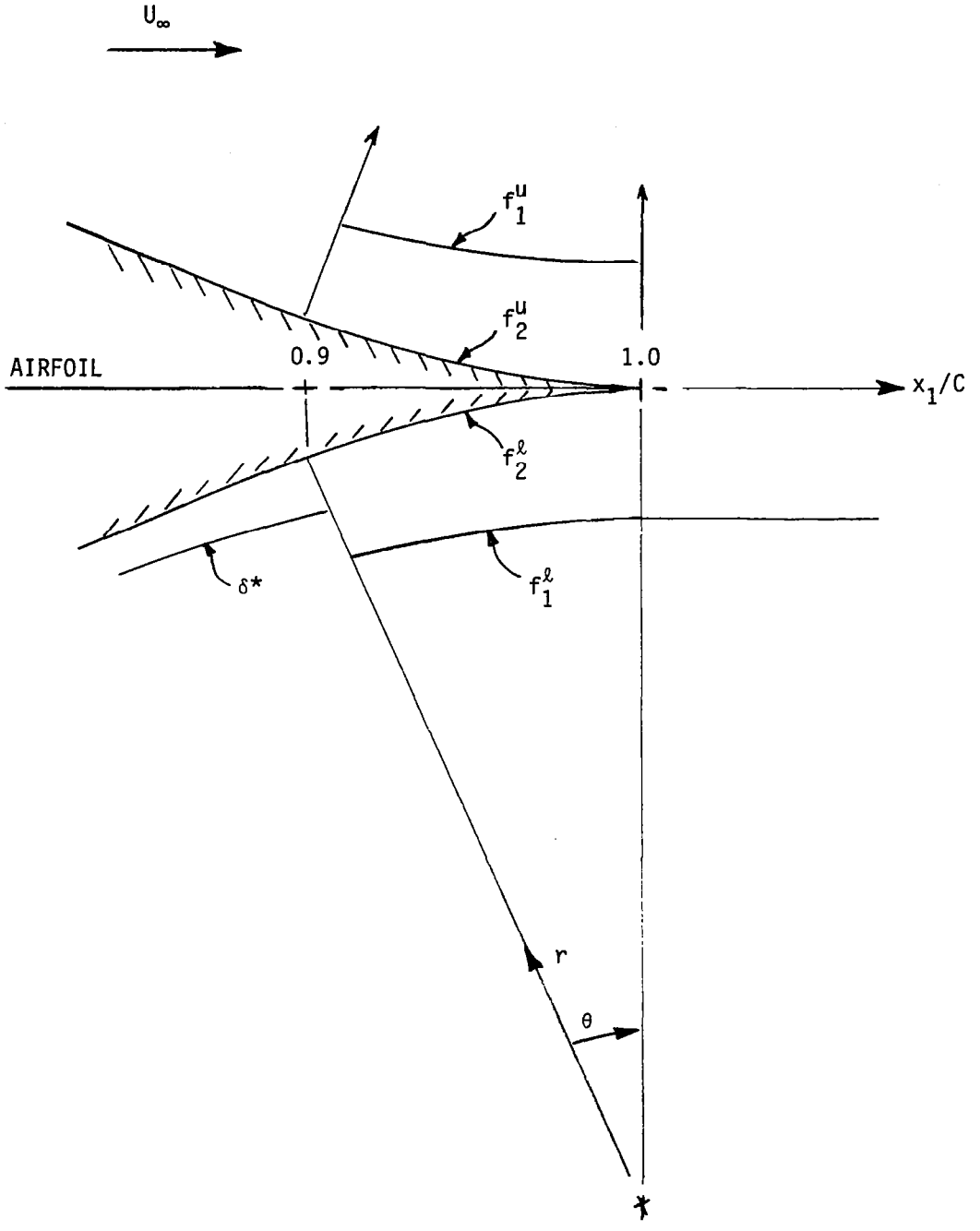

Figure 2. Coordinate Systems for 2DBL/2DPNS Solutions

the curve noted, f_1^{ℓ}. The computational requirement is that the region defined by this curve, and the airfoil surface or wake trajectory, contain $\delta(x_1)$. The extrapolation can be refined, if required, during the iteration sequence within Phase C, but it is not required to be a coordinate surface of the polar coordinate system $x_i = \{\theta,r\}$. Specifically, this boundary is assumed expressed in the form

$$f_1(x_1) = \bar{r}_1 (1 + a_1\theta) \tag{56}$$

where $\bar{r}_1$ is the radial coordinate of $f_1(x_1/C = 0.9)$, and a_1 is an input parameter to produce the desired scaling. The other surface of the 2DBL domain is the airfoil contour, assumed expressed as

$$f_2(x_1) = \bar{r}_2(1 + a_2\theta) \tag{57}$$

On the interval $0.9 \leq x_1/C \leq 1.0$, the 2DBL/2DPNS equations are cast onto the $x_i \equiv \{\theta,r\}$ coordinate system. The predominant velocity component is $\tilde{u}_\theta$. For example, equation (33) takes the form,

$$L(\tilde{u}_\theta) = \frac{1}{r}\bar{\rho}\tilde{u}_\theta \frac{\partial \tilde{u}_\theta}{\partial \theta} + \bar{\rho}\tilde{u}_r \frac{\partial \tilde{u}_\theta}{\partial r} + \frac{1}{r}\bar{\rho}\tilde{u}_r\tilde{u}_\theta + \frac{1}{r}\frac{\partial p_c}{\partial \theta} - \frac{\partial}{\partial r}\left[\rho\nu_{eff}\left(\frac{\partial u_\theta}{\partial r} - \frac{\tilde{u}_\theta}{r}\right)\right] = 0 \tag{58}$$

Derivatives in the remaining members of each equation set are correspondingly expressed. A grid stretching coordinate transformation, that uniformly scales the viscous flow domain on the interval bounded by f_1 and f_2, is

$$\theta' = \theta$$
$$r' = \frac{r - f_1(\theta)}{[f_2(\theta) - f_1(\theta)]f^{-1}} \tag{59}$$

where f is a normalizing factor. Using the chain rule, the θ-derivative in equation (58) becomes

$$\frac{\partial}{\partial \theta} = \frac{\partial}{\partial \theta'} - \left[\frac{f_1'}{(f_2-f_1)f^{-1}} + r' \frac{f_2' - f_1'}{f_2 - f_1}\right]\frac{\partial}{\partial r'} \tag{60}$$

where superscript prime denotes the θ-ordinary derivative. Dividing by r, and repeating the operation for the radial derivative, yields the final forms

$$\frac{1}{r}\frac{\partial}{\partial\theta} = \frac{1}{r}\frac{\partial}{\partial\theta'} - \left[h_2 + r'h_3\right] \qquad \frac{\partial}{\partial r'}\frac{\partial}{\partial r} = h_1\frac{\partial}{\partial r'} \tag{61}$$

The h_i, $1 \leq i \leq 3$ in equation (61) are functions of the metric of the coordinate transformation, and are defined as

$$h_i \equiv \begin{Bmatrix} f/(f_2 - f_1) \\ h_1 a_1 \\ h_1(a_2 - a_1)/f \end{Bmatrix} \tag{62}$$

Therefore, the 2DBL/2DPNS equation sets are recast onto the fixed $\{\theta', r'\}$ coordinate system. For example, all members of both sets possess common convection and diffusion operators. Equation (58) projected onto $\{\theta', r'\}$ serves the illustration as

$$\begin{aligned} L(\tilde{u}_\theta) = {} & \bar{\rho}\tilde{u}_\theta \frac{1}{r}\frac{\partial \tilde{u}_\theta}{\partial\theta'} - \bar{\rho}\tilde{u}_\theta\left[h_2 + r'h_3\right]\frac{\partial u_\theta}{\partial r'} + \bar{\rho}\tilde{u}_r h_1 \frac{\partial \tilde{u}\theta}{\partial r'} \\ & + \frac{1}{r}\bar{\rho}\tilde{u}_r\tilde{u}_\theta + \frac{1}{r}\frac{\partial p_c}{\partial\theta'} - \left[h_2 + r'h_3\right]\frac{\partial p_c}{\partial r'} \\ & - h_1\frac{\partial}{\partial r'}\left[\bar{\rho}\nu_{eff}\left(h_1\frac{\partial \tilde{u}_\theta}{\partial r} - \frac{\tilde{u}_\theta}{r}\right)\right] = 0 \end{aligned} \tag{63}$$

The transformation-induced radial pressure gradient on p_c vanishes identically for 2DBL, but only in 2DPNS for zero angle of attack. Note also that the influence of the x_1-(ie., θ) gradient of the inviscid pressure p_c is diminished as r^{-1} through the boundary layer. Therefore, even though p_c equals a constant in the 2DBL solution, its influence is distributed as

$$\frac{1}{r}\frac{\partial p_c}{\partial\theta'} = \frac{dp^I}{dx_1} \Big/ f_1\left[1 + r'/(h_1 f_1)\right] \tag{64}$$

where dp^I/dx_1 is the potential flow pressure gradient.

The upper and lower surface 2DBL solutions are computed independently up to the trailing edge. Thereat, the 2DPNS solution domain is defined as the interior of the region bounded by f_1^{ℓ} and f_1^{u}, see Figure 2. A return to rectangular Cartesian coordinates is permitted since the upper and lower surface boundary layers have acquired a common alignment. Alternatively, if the wake is curved, due to angle of attack for example, a single polar coordinate system would be useable. An alternative is to employ a grid-translation transformation that retains fine grid resolution in the region with extremal gradients. This transformation, which also permits grid stretching, is simply the Cartesian equivalent of equation (59), ie.

$$\begin{aligned} x_1' &= x_1 \\ x_2' &= \frac{x_2 - f_1(x_1)}{[f_2(x_1) - f_1(x_1)]f^{-1}} \end{aligned} \tag{65}$$

While the f_i could be general curves, piecewise linear segments of the form $ax_1 + b$ should be adequate. Then,

$$\begin{aligned} \frac{\partial}{\partial x_1} &= \frac{\partial}{\partial x_1'} - \left[h_2 + x_2' h_3\right]\frac{\partial}{\partial x_2'} \\ \frac{\partial}{\partial x_2} &= h_1 \frac{\partial}{\partial x_2'} \end{aligned} \tag{66}$$

Elliptic Solution Algorithm

Analysis of separated flows in the trailing edge vicinity usually require a complete two-dimensional Navier-Stokes (2DNS) solution to accurately resolve local velocity distributions. Analysis of the trailing edge region of a blunt-based airfoil at zero angle of attack is an example, and Figure 3 illustrates the geometry. The cylindrical coordinate system is the descriptor for the 2DBL/2DPNS solutions that provide initialization of the 2DNS solutions.

The switch-over from dual 2DBL solutions, to the single 2DPNS solution for the sharp trailing edge airfoil, occurs at $x_1/C = 1.0 - \eta$, where $\eta > 0$ provides the computational flexibility for the transition. For the blunt-based airfoil, an inviscid "extension" is extrapolated to a sharp intersection, defined to occur at $x_1/C = 1.0$ as shown in Figure 3. The 2DBL solution is pursued on the interval $x_1/C \leq 0.9$ up to the blunt base terminus. Each 2DPNS solution is initiated just prior to this location, and continued in the $\{\theta' \; r'\}$ coordinate system up to $x_1/C = 1.0$. The upper and lower 2DPNS solutions are then coupled

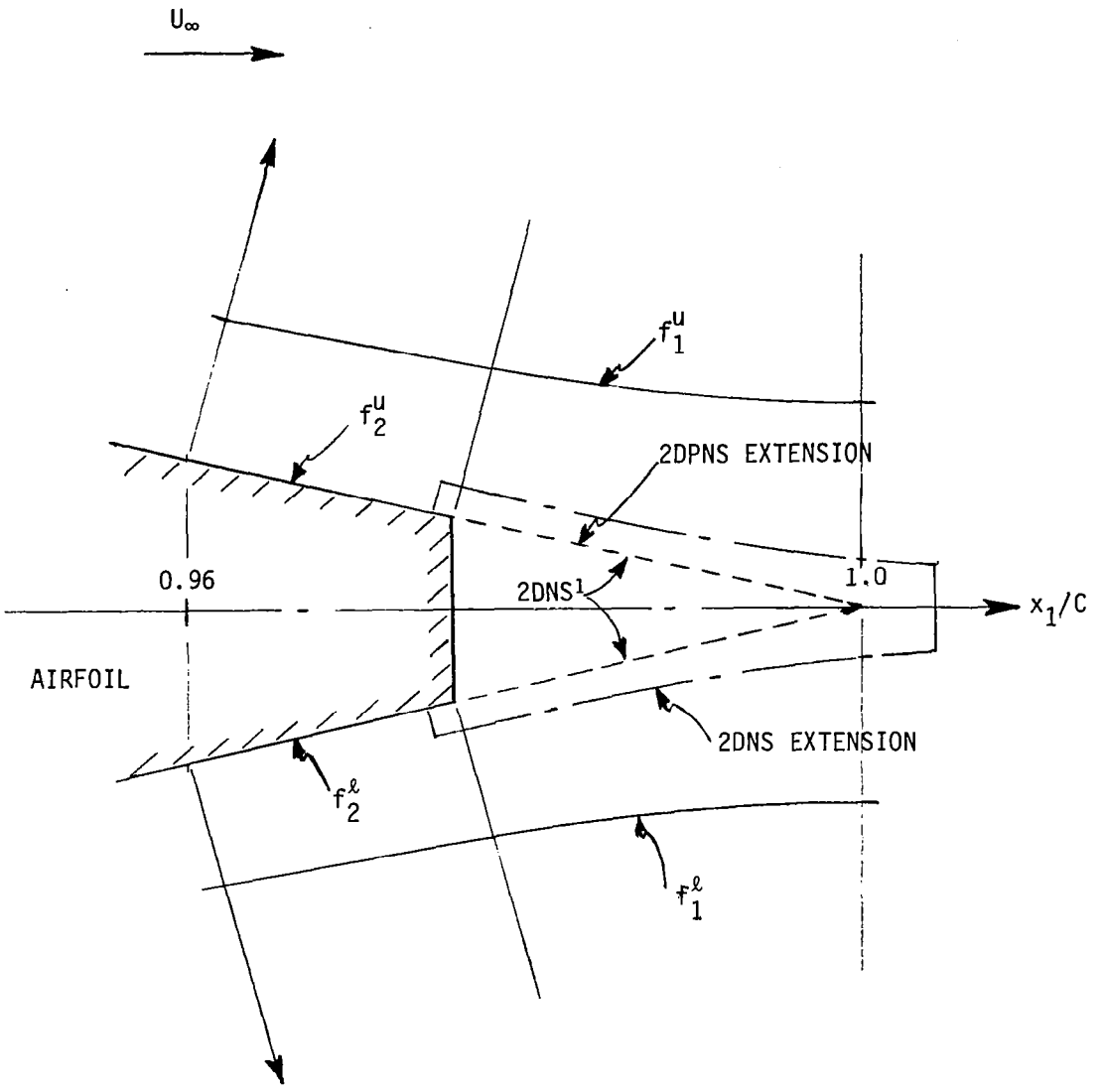

Figure 3. Blunt Base Airfoil 2DNS Solution Domains

in a rectangular coordinate description and marched into the wake. The 2DPNS upper and lower surface extension solutions are solved independently as is the case for the 2DBL solutions. The no-slip wall boundary condition on $\tilde{u}_1$ is removed on the extension, allowing the individual 2DPNS high shear regions to accelerate prior to actual merging.

The solution domain for a Phase D solution of the 2DNS equations lies in the immediate vicinity of the blunt-based trailing edge as illustrated in Figure 3. The two-dimensional Navier-Stokes equations for an isoenergetic flow are contained in equations (8)-(9) by the limited summation index convention $1 \leq i, j \leq 2$. The solution of the 2DNS equations for small Mach number and large Reynolds number is a difficult task. The 2DNS algorithm suggested is based upon the formulation developed for 2DPNS, extended to three-dimensional space, ie., 3DPNS. Specifically, equation (9) in expanded form is

$$L(\tilde{u}_i) = \bar{\rho} \frac{\partial \tilde{u}_i}{\partial t} + \bar{\rho} u_1 \frac{\partial \tilde{u}_i}{\partial x_1} + \bar{\rho} \tilde{u}_2 \frac{\partial \tilde{u}_i}{\partial x_2} + \frac{\partial \bar{p}}{\partial x_i}$$

$$- \frac{\partial}{\partial x_1} \left[\bar{\sigma}_{i1} - \overline{\rho u_i'' u_1''} \right] - \frac{\partial}{\partial x_2} \left[\bar{\sigma}_{i2} - \overline{\rho u_i'' u_2''} \right] = 0 \qquad (67)$$

The pressure field remains resolved according to equation (47). The solution for complementary pressure is given in equations (48)-(50) with $1 \leq \ell \leq 2$. The particular pressure is the solution to equations (51)-(52) with all subscripts allowed to range (1, 2). The x_1 derivatives contained within the j-summation in equation (52), for the 2DPNS formulation, are now the time derivatives from equation (67). The 2DNS velocity field $\tilde{u}_j$ is determined from application of the continuity equation as a differential continuity constraint.

Equation (67), and the corresponding 2DNS k and ε equations (30)-(31), restricted to two-dimensions, require Reynolds stress components for closure. The constitutive equation (25) is assumed a valid representation. In the blunt base region, all terms in equation (25) may be required retained, since the assumptions yielding the simplified forms in equation (28) are specifically parabolic.

The initial 2DNS solution domain is bounded by the inviscid extension employed for the 2DPNS solution and the base. Boundary conditions for $\{q\} = \{\tilde{u}_1, \tilde{u}_2, k, \varepsilon, p_c, p_p\}$ are provided thereupon by the 2DPNS solution. Upon a satisfactory 2DNS approach to steady-state, the 2DNS solution domain should be enlarged, as illustrated in Figure 3. The flow conditions on the new boundary are provided by the previous converged 2DPNS solution, and the 2DNS system is resolved on the interior of the expanded domain. The primary purpose in the final 2DNS solution is a more accurate prediction of the corner flow at the base. However, the discretization required to produce an adequate resolution is a significant limiting factor in terms of computer time and storage.

FINITE ELEMENT SOLUTION ALGORITHM

The several sets of partial differential equations that are required solved for the developed aerodynamic interaction algorithm, have been identified. For Phase B, equations (11)-(13) are appropriate. The 2DBL/2DPNS system for the parabolic Phase C operations are given by equations (32)-(37), (44), (48)-(52), and (54)-(55). The elliptic Phase D sequence requires solution of equations (67), (30) and (31) in addition to (48)-(52) and (54)-(55). Fortunately, in terms of developing a numerical solution procedure for the aerodynamic interaction algorithm, each member of the set belongs to the general class of second-order elliptic partial differential equations expressed

$$L(q) = \frac{\partial}{\partial x_\ell}\left[K(q)\,\frac{\partial q}{\partial x_\ell}\right] + f_1\left(q, \frac{\partial q}{\partial x_\ell}, p, x_i\right) + f_2(q,\chi) = 0 \tag{68}$$

In equation (68), q is any dependent variable, ie. $\{q\} \equiv \{\tilde{u}_i, k, \varepsilon, p_c, p_p, \phi\}$. K is the generalized diffusion coefficient, f_1 is a function of its argument that includes convection and any parameter p, and f_2 is an initial-value operator if present. For the 2DNS equations, χ is time t and $1 \leq \ell, i \leq 2$. For the 2DBL/2DPNS equation system, χ corresponds to the x_1 coordinate and $\ell = 2$, $1 \leq i \leq 2$. For the solution variables p_p, p_c, and ϕ, f_2 vanishes identically in all instances.

In all instances, the solution domain Ω, corresponds to the product of an n-dimensional Euclidean space R^n, spanned by the x_ℓ coordinate system $1 \leq \ell \leq n$, with a one-dimensional space spanned by the χ coordinate, ie.

$$\Omega \equiv R^n \times \chi \in x_\ell \times \left[\chi_o, \chi\right) \tag{69}$$

The boundary $\partial\Omega$ of the domain Ω is its intersection with another enveloping solution domain, or the infinite freestream, and

$$\partial\Omega \equiv \partial R \times \chi \in \bar{x}_\ell \times \left[\chi_o, \chi\right) \tag{70}$$

On $\partial\Omega$ the boundary conditions appropriate for solution of all variables are contained within the expression

$$\ell(q) = a_1 q + a_2\, k\, \frac{\partial q}{\partial x_\ell}\, \hat{n}_\ell + a_3 = 0 \tag{71}$$

Here, the $a_i(\bar{x}_\ell, \chi)$ are specified coefficients appropriate to each q. Except for p_c, p_p and ϕ, an initial condition is required specified for each q as

$$q(x_\ell, \chi_o) \equiv q_o(x_\ell) \tag{72}$$

The finite element numerical solution algorithm for equations (68)-(72) assumes all q and p interpolated on sub-domains Ω_e, which form the finite element discretization of Ω, as

$$q_e(x_\ell, \chi) = \{N_k(x_\ell)\}^T \{Q(\chi)\}_e \tag{73}$$

Determination of the sum of the expansion coefficients $\{Q\}_e$, which constitute the numerical solution, is accomplished using the Method of Weighted Residuals in the form,

$$S_e \left[\int_{R_e^2} \{N\} L(q_e) + \lambda \left[\int_{\partial R_e \cap \partial R} \{N\} \ell(q_e) + \varepsilon_q \frac{\partial}{\partial x_\ell} \int_{R_e^2} \{N\} L(\rho_e) \right] \right] \equiv \{0\} \tag{74}$$

where S_e is the assembly operator. The multiplier λ is evaluated to enforce cancellation of generated surface integrals with the prescribed boundary condition normal gradient. For $q_e = \tilde{u}_\ell$ only, $\varepsilon_q \neq 0$ and the last term expresses the explicit enforcement of the continuity equation (32), ie. equation (54) is a differential constraint on the transverse momentum equation solution. Inserting equation (68) into (74), and using the divergence theorem on the lead term, produces the equivalent matrix solution statement

$$S_e \left[-\int_{R_e^2} \frac{\partial}{\partial x_\ell} \{N\} K \frac{\partial q_e}{\partial x_\ell} d\tau + \int_{R_e^2} \{N\} \left[f_{1e} + f_{2e} \right] d\tau \right.$$

$$\left. - \int_{\partial R_e \cap \partial R} \{N\} [a_1 q_e + a_3] d\tau + \varepsilon_q \frac{\partial}{\partial x_\ell} \int_{R_e^2} \{N\} L(\rho_e) \right] \equiv \{0\} \tag{75}$$

The global rank of equation (75) is identical with the total number of node points on $R^n \cup \partial R$ at which the dependent variable requires solution. For f_2 non-vanishing, equation (75) is a system of first-order ordinary differential equations. For f_2 vanishing identically, it is large-order algebraic and the matrix structure is symmetric, sparse and banded. In this instance, standard matrix solution procedures are directly applicable.

An implicit numerical integration algorithm is suggested to solve equation (75) for the various initial-value problem descriptions. Completing the terms, the equivalent matrix statement for equation (75) is

$$S_e\left[[C]_e\{Q\}'_e + \left([U]_e + [K]_e\right)\{Q\}_e + \{f\}_e\right] \equiv \{0\} \tag{76}$$

where the square brackets denote square matrices of element rank, the curly brackets denote column matrices, and the superscript prime indicates the ordinary derivative with respect to χ. For the first three terms, which account for acceleration, convection and diffusion respectively, the explicit matrix forms are

$$[C]_e \equiv \begin{cases} \{\bar{\rho}\tilde{u}_1\}_e^T \displaystyle\int_{R_e^n} \{N\}\{N\}\{N\}^T d\tau & \chi \to x_1 \\ \displaystyle\int_{R_e^n} \{N\}\{N\}^T d\tau & \chi \to t \end{cases}$$

$$[U]_e \equiv \{\bar{\rho}\tilde{u}_\ell\}_e^T \int_{R_e^n} \{N\}\{N\}\frac{\partial\{N\}^T}{\partial x_\ell} d\tau$$

$$[K]_e \equiv \{\bar{\rho}\nu^{eff}\}_e^T \int_{R_e^n} \{N\}\frac{\partial\{N\}}{\partial x_\ell}\frac{\partial\{N\}^T}{\partial x_\ell} d\tau \tag{77}$$

All terms not explicitly involving the dependent variable $\{Q\}$ are contained in $\{f\}_e$.

An accurate single-step implicit integration algorithm is the trapezoidal rule

$$\{Q\}_{j+1} = \{Q\}_j + \frac{h}{2}\left[\{Q\}'_{j+1} + \{Q\}'_j\right] \tag{78}$$

In equation (78), j is the initial-value coordinate index, and h is integration step-size $\Delta\chi$. Following the usual matrix manipulations, insertion of equation (76) into (78) yields a large order, non-linear algebraic equation system. The Newton matrix iterative algorithm for solution of this system is

$$\left[J\left(\{Q\}^p_{j+1}\right)\right]\{\delta Q\}^{p+1}_{j+1} = -\left\{F\left(\{Q\}^p_{j+1}\right)\right\} \tag{79}$$

The dependent variable in equation (79) is the iteration vector, and

$$\{Q\}^{p+1}_{j+1} \equiv \{Q\}^p_{j+1} + \{\delta Q\}^{p+1}_{j+1} \tag{80}$$

where p is the iteration index. The right side of equation (79) is the homogeneous form of equation (78) evaluated with the $p^{\underline{th}}$ iterate, i.e.,

$$\{F\}^p_{j+1} = S_e\left[[C]_e\left(\{Q\}^p_{j+1} - \{Q\}_j\right) + \frac{h}{2}\left(\{g_e\}^p_{j+1} + \{g_e\}_j\right)\right] \tag{81}$$

where

$$\{g_e\}^p_\ell \equiv \left([U]_e + [K]_e\right)\{Q\}^p_\ell + \{f\}_e \tag{82}$$

In equations (81)-(82), the matrix operations constitute inner products on matrices of element rank, with the assembly operator yielding the equivalent global expression. The vanishing of {F}to within definition of a computed zero, yields equation (79) homogeneous, hence convergence of the iteration for any evaluation of the Jacobian. The initial estimate $\{Q\}^1_{j+1}$ for each iteration is typically $\{Q\}_j$.

By definition, the Jacobian is the derivative of equation (81) with respect to $\{Q\}^p$. It can be computationally evaluated as

$$[J] = S_e \left[[C]_e + \frac{h}{2} \left([K]_e + [U]_e \right) \right] \tag{83}$$

All operations again involve matrix inner products of an element rank. The rank of [J] equals the order of $\{\delta Q\}$; Dirichlet boundary constraints are applied within the evaluation of $\{F\}$.

NUMERICAL RESULTS

The developed numerical solution algorithm has been implemented into a computer program for the parabolic analysis for a sharp trailing edge airfoil. Phases A-C of the interaction algorithm, Table 1, have been assessed for accuracy and convergence for a NACA 63-012 airfoil with 0.61m chord for which experimental data are available for comparison (ref. 9).

Viscous-Corrected Potential Computation

The potential flow solution procedure is an extension of that reported in reference 10. The basic macro-element, and resultant finite element discretization of an appropriate region of R^2 is illustrated in Figure 4, as well as delineation of gradient boundary conditions. The solution of the integral boundary layer equation (13) yields the distribution of momentum thickness $\theta(x)$, hence displacement thickness $\delta^*(x)$, which in the subsequent potential flow solution augments the airfoil thickness distribution $t(x)/C$. The integral boundary layer solution is terminated at the trailing edge. The wake distribution of δ^* is a quadratic interpolation between the trailing edge value and zero thickness at 1.5C downstream.

Table 2 summarizes the results of the typical first three iterations of a Phase B analysis, for the NACA 63-012 for $\alpha = 0^o$ and C = 0.61m. The streamwise stations span $0.776 \leq x_1/C \leq 2.5$, where $x_1/C = 1.0$ is the trailing edge. The Phase B solutions for pressure coefficient converge to $\pm$ 0.0001 C_p after approximately seven iterations, and Table 3 summarizes typical results. At zero angle of attack, differences in C_p between natural laminar to turbulent transition, and tripping at 5% chord, are small for $\alpha = 0^o$. The δ^* augmentation procedure is equally applicable to non-zero angle of attack; results obtained for $\alpha = 6^o$ are illustrated, and convergence was achieved in seven iterations.

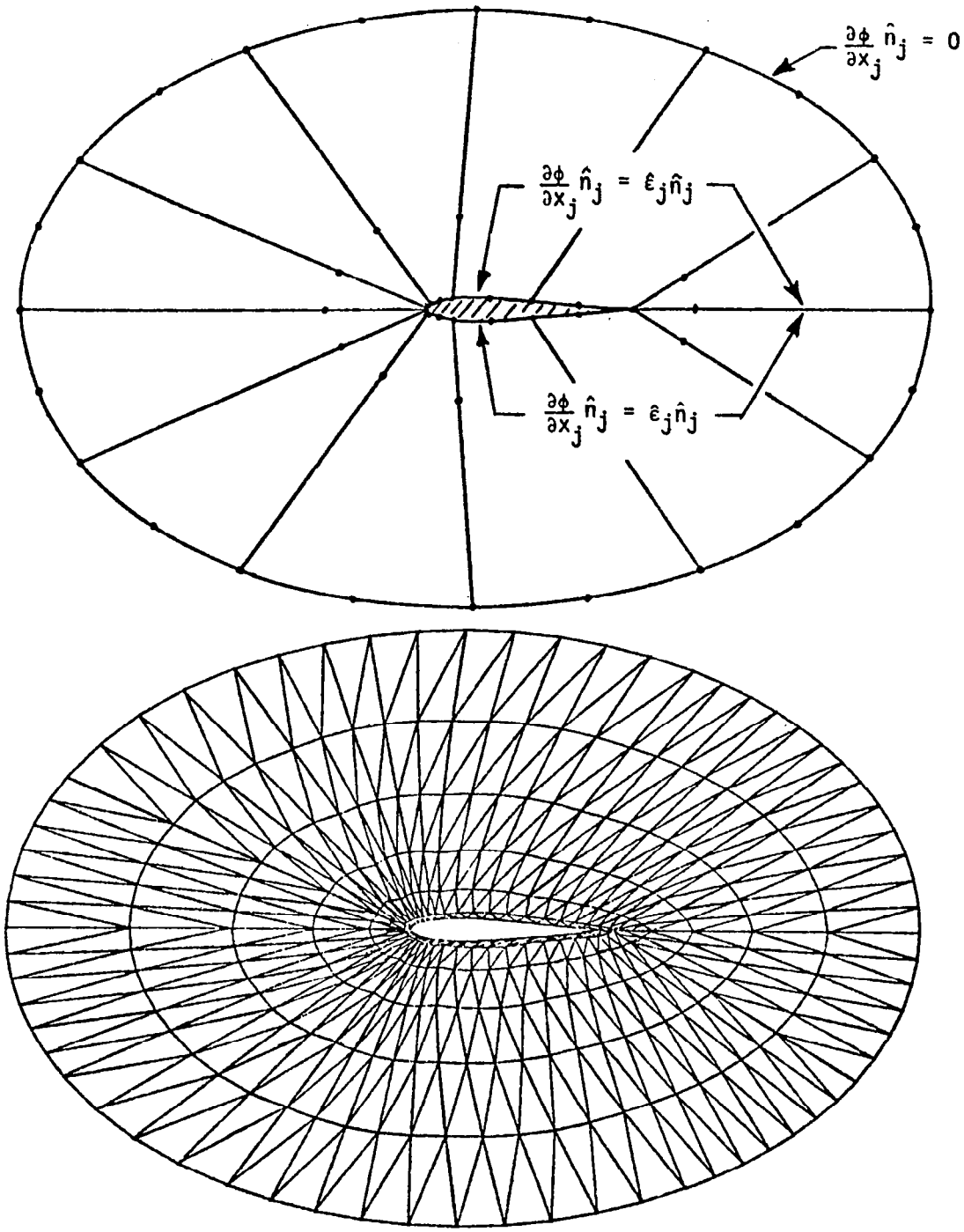

Fig. 4. Macro-Element and Finite Element Discretizations For Potential Flow Analysis of NACA 63-012 Airfoil.

Table 2

Viscous-Corrected Phase B Potential Flow
Pressure Distributions, Iterations 1-3
NACA 63-012 Airfoil, C = 0.61m, $\alpha = 0^{o}$

Station x_1/C	Pressure Coefficient $C_p(x_1)$ Iteration Number		
	1	2	3
0.776	-.0063	-.0231	-.0216
0.841	.0565	.0448	.0466
0.895	.1042	.0985	.1004
0.940	.1361	.1391	.1406
0.975	.1458	.1639	.1632
1.000	.1410	.1783	.1741
1.050	.0903	.0846	.0831
1.180	.0592	.0560	.0553
1.390	.0213	.0214	.0212
1.680	.0090	.0088	.0087
2.050	.0017	.0017	.0017
2.500	.0017	.0016	.0016

Table 3

Viscous-Corrected Phase B
Potential Flow Pressure Distributions
NACA 63-012 Airfoil, C = 0.61m

Station x_1/C	Pressure Coefficient Distribution, $C_p(x_1)$			
	Zero Degrees Angle of Attack		Six Degrees Angle of Attack	
	Natural Transition	Tripped at 5%C	Upper Surface	Lower Surface
0.776	-.0217	-.0210	-.1570	.1170
0.841	.0463	.0464	-.0596	.1518
0.895	.1001	.0992	.0158	.1764
0.940	.1402	.1386	.0738	.1880
0.975	.1632	.1608	.1124	.1789
1.000	.1746	.1715	.1367	.1575
1.050	.0833	.0817	.0797	.0868
1.180	.0557	.0546	.0683	.0434
1.390	.0212	.0209	.0453	-.0039
1.680	.0087	.0085	.0395	-.0278
2.050	.0017	.0017	.0270	-.0240
2.500	.0016	.0016	-.0049	.0084

Low Turbulence Reynolds Number Model

The primary requirement of the attached flow turbulent boundary layer analysis near the trailing edge is to establish initial conditions for the parabolic Navier-Stokes solutions in the wake. In turn, a suitable procedure is required to develop initial condition profiles for the boundary layer solution distributions. Cole's Law (ref. 3) is available to establish a $\tilde{u}_1$ mean velocity initial profile, and the continuity equation (32) yields the corresponding $\tilde{u}_2$ distribution. In certain instances, experimental data may be available to initialize the turbulence kinetic energy initial profiles. If corresponding Reynolds shear stress data are available then equation (29) could be employed to initialize isotropic dissipation function.

Several very practical problems emerge in establishing suitable initial-condition distributions for the 2DBL equations using the TKE closure procedure. Aerodynamic boundary layers are typically thin, hence experimental measurements of either mean or fluctuating velocity correlations are extremely difficult to obtain near the surface. For example, for the comparison data set summarized in the Appendix, hot wire probe dimensions limited the nearest approach to approximately 0.01m, at which location $\tilde{u}_1/u_e \approx 0.7$. Hence, most of the detail of the $\tilde{u}_1$ and k distributions eludes the experimentalist, and alternative methods are required developed. Furthermore, and of paramount impact for the current study, the numerical solution domain is required to reach to the wall, since flow evolution in the wake centerline region is specifically of primary interest.

A viable alternative approach involves use of mixing length theory to predict the near wall distributions of turbulent viscosity ν^t. As is well known, and recalling equation (39),

$$\nu^t = C_4 \frac{k^2}{\varepsilon} = (\omega \ell)^2 \left| \frac{\partial \tilde{u}_1}{\partial x_2} \right| \tag{84}$$

where $(\omega\ell)$ is the Van Driest-damped Prandtl mixing length ℓ, and ℓ is a piece-wise linear function of x_2. The functional form of ω, equation (84) is known and depends strictly on various specified parameters (ref. 3). Importantly, equation (84) depends solely on geometry and $\tilde{u}_1$, which is available from Cole's law in the absence of detailed data. For the current study, the TKE closure model was extended to the wall by assuming a low turbulence Reynold's number modification based upon Van Driest damping concepts. The ratio (k/ε) was assumed unaffected, and k and C_4 were modified in equation (84) as $k \Rightarrow \omega^{\alpha} k$ and $C_4 \Rightarrow \omega^{(2-\alpha)} C_4$, where $0 < \alpha \leq 2$ is a parameter to be optimized. Hence, the distribution of k in the near wall region, $0 < y+ < 80$ could be modified with the resultant distribution of C_4 affecting primarily the k and ε source terms, as dominated by $\overline{u_1' u_2'}$, see equations (36)-(37).

A sequence of numerical experiments is continuing on evaluation of the concept. One particularly demanding test case corresponds to the Bradshaw relaxing flow boundary layer, IDENT 2400 of reference 11. Figure 5 summarizes the accuracy of the basic MLT solution in terms of familiar boundary layer integral parameters. The standard value of the MLT parameter $\lambda = 0.09$ produced correct overall solution trends, but detailed discrepancies from data. Increasing to $\lambda = 0.11$ produced the quite acceptable agreement indicated. Using $\lambda = 0.11$ to compute the corresponding initial distribution of $\overline{u_1' u_2'}$, the flow was recomputed using the TKE closure model, see Figure 6.

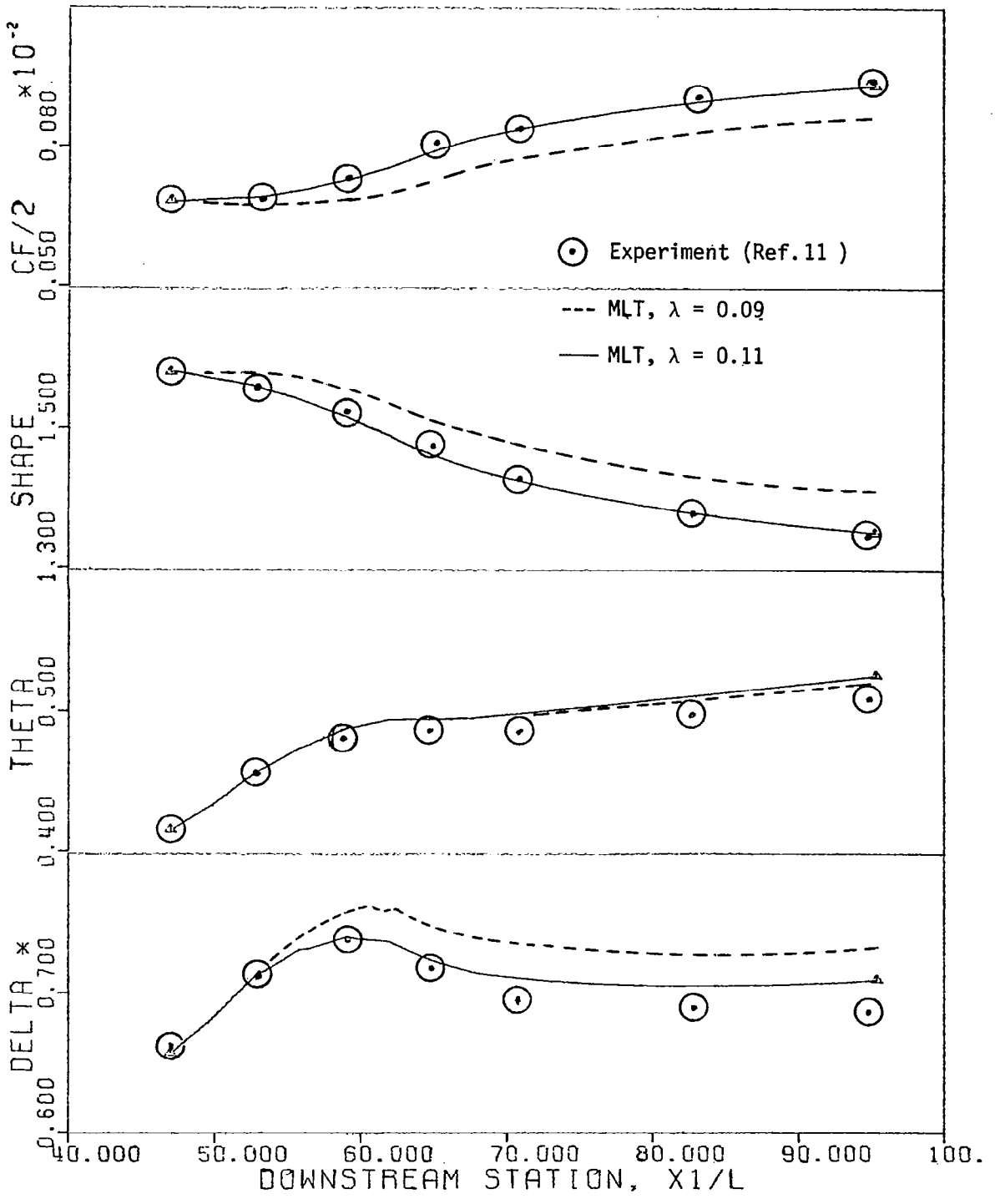

Fig. 5. Prediction of Bradshaw Turbulent Boundary Layer Test Case, Mixing Length Turbulence Closure Model.

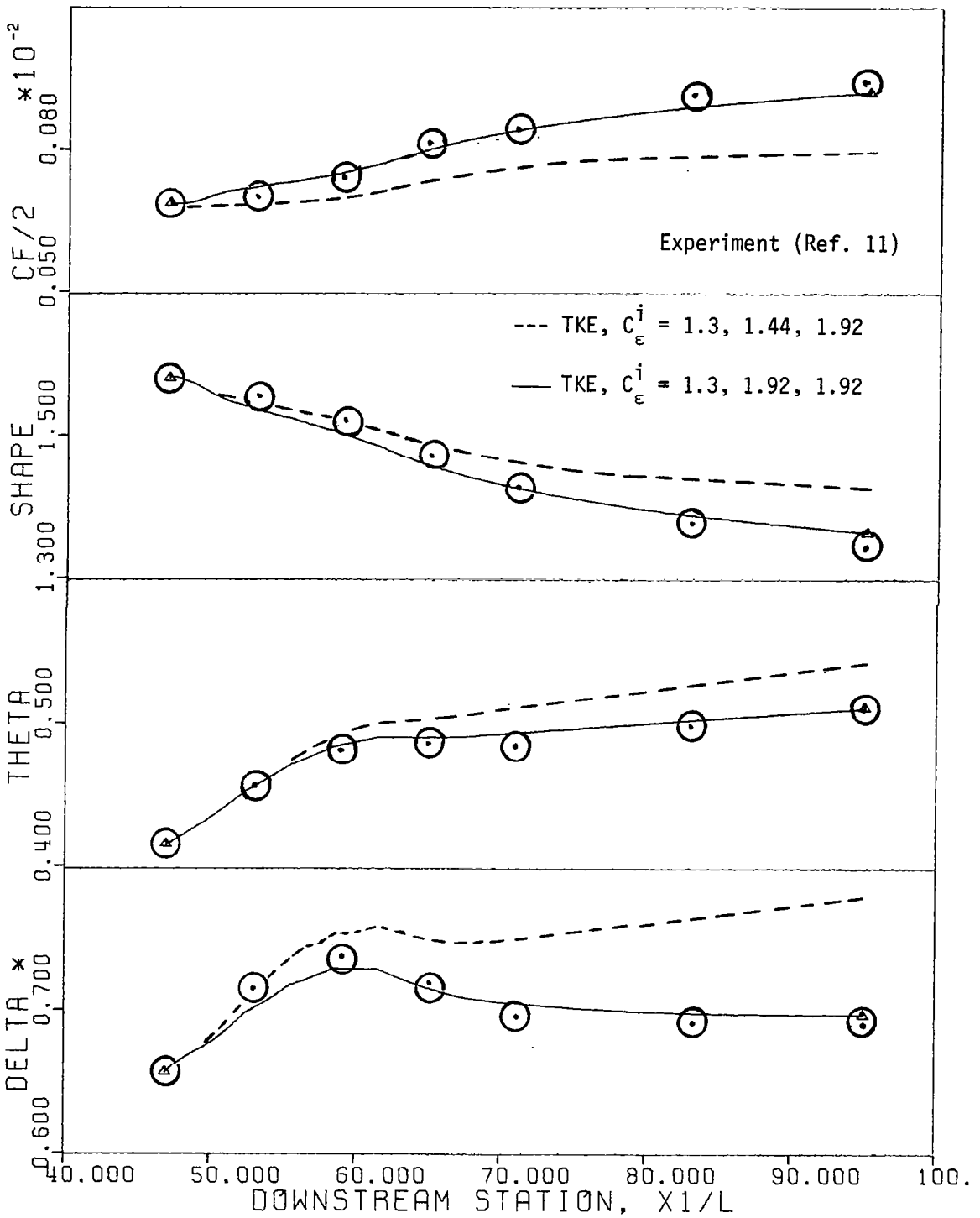

Fig. 6. Prediction of Bradshaw Turbulent Boundary Layer Test Case, Turbulence Kinetic Energy Closure Model.

As observed, for $\alpha = 1$, use of the "standard" TKE model constants $C_\varepsilon = 1.3$, $C_\varepsilon^1 = 1.44$, and $C_\varepsilon^2 = 1.92$ produce essentially correct trends but detailed inaccuracy. Setting $C_\varepsilon^2 = 1.92$ considerably improved the agreement as indicated. Figure 7 illustrates corresponding computed distributions of mean velocity and Reynolds shear stress at the initial and final stations, which are separated by a distance of 1.3m. Viewing the distribution of $\tilde{u}_1$, the near wall region undergoes significant acceleration and the final station solution is in excellent agreement with data. Over the same interval, the distribution of shear stress $\overline{u_1' u_2'}$ flattens considerably. These distributions are smooth as computed from the $\tilde{u}_1$, $\tilde{u}_2$, k and ε solutions, using the derived constitutive relation equation (28). The deviation of the sum $\overline{u_i' u_i'}/2$ about k was bounded by two percent throughout the solution field.

NACA 63-012 Interaction Analysis

The Phase A-C interaction analysis has been exercised for a NACA 63-012 airfoil for $M_\infty = 0.09$, $\alpha = 0^o$ and C = 0.61m. A thoroughly comprehensive data set has been obtained for this configuration on $0.90 \leq x_1/C \leq 1.10$, see reference 9. The Appendix lists these data at the first and last stations, and at two stations immediately bounding the trailing edge terminus. Figure 8a)-8d) are composite summaries of the measured mean and fluctuating velocities on the interval $0.9 \leq x_1/C \leq 0.9979$. All profiles are by and large parallel; the flattening of the $\overline{u_1' u_2'}$ distributions at the last two stations give indication of anticipation of the imminent trailing edge terminus.

The Phase C interaction analysis was initiated using the experimental data for $\tilde{u}_1$, $\overline{u_1'} \equiv (\overline{u_1' u_1'})^{\frac{1}{2}}$, and $\overline{u_1' u_2'}$ on the given interval at $x_1/C = 0.90$. Following considerable experimentation, Cole's law, MLT concepts, and the turbulence constitutive equation (28) were successfully employed to fill in the initial profiles between the wall and the first experimental data points. The 2DBL solution was then exercised on $0.9 \leq x_1/C \leq 1.000$, and the resultant free-stream distribution of $\tilde{u}_2$ inserted into the potential flow analysis, Phase B, to modify the inviscid flow C_p. Four sequences through this interaction, using 2DPNS to supplant 2DBL, were sufficient to render the freestream distribution of $\tilde{u}_2$ stationary to within $\pm$ 2%.

Figure 9 illustrates the evolution of the final 2DPNS solution on $0.9 \leq x/C \leq 1.0$, on a plot scale directly comparable to the experimental data distributions, Figure 8. In Figure 9, however, each curve is shifted to the left to retain definition of near wall gradients. Recall the data employed to initialize the solution were $\tilde{u}_1$, $\overline{u_1'}$, and $\overline{u_1' u_2'}$, with use of MLT concepts to complete the variable distributions. Figure 9a) illustrates the evolution of $\tilde{u}_1$, for the noted x_1/C stations. The experimental data at $x_1/C = 0.9$ and 0.9979 are plotted for comparison on the first and final computed solutions. Agreement at the first station is essentially by definition, and the final station comparison shows quite good agreement for the selection of $\alpha = 1$ in the low turbulence Reynolds model and the dissipation equation coefficients $C_\varepsilon^1 = 1.67$ and $C_\varepsilon^2 = 1.92$.

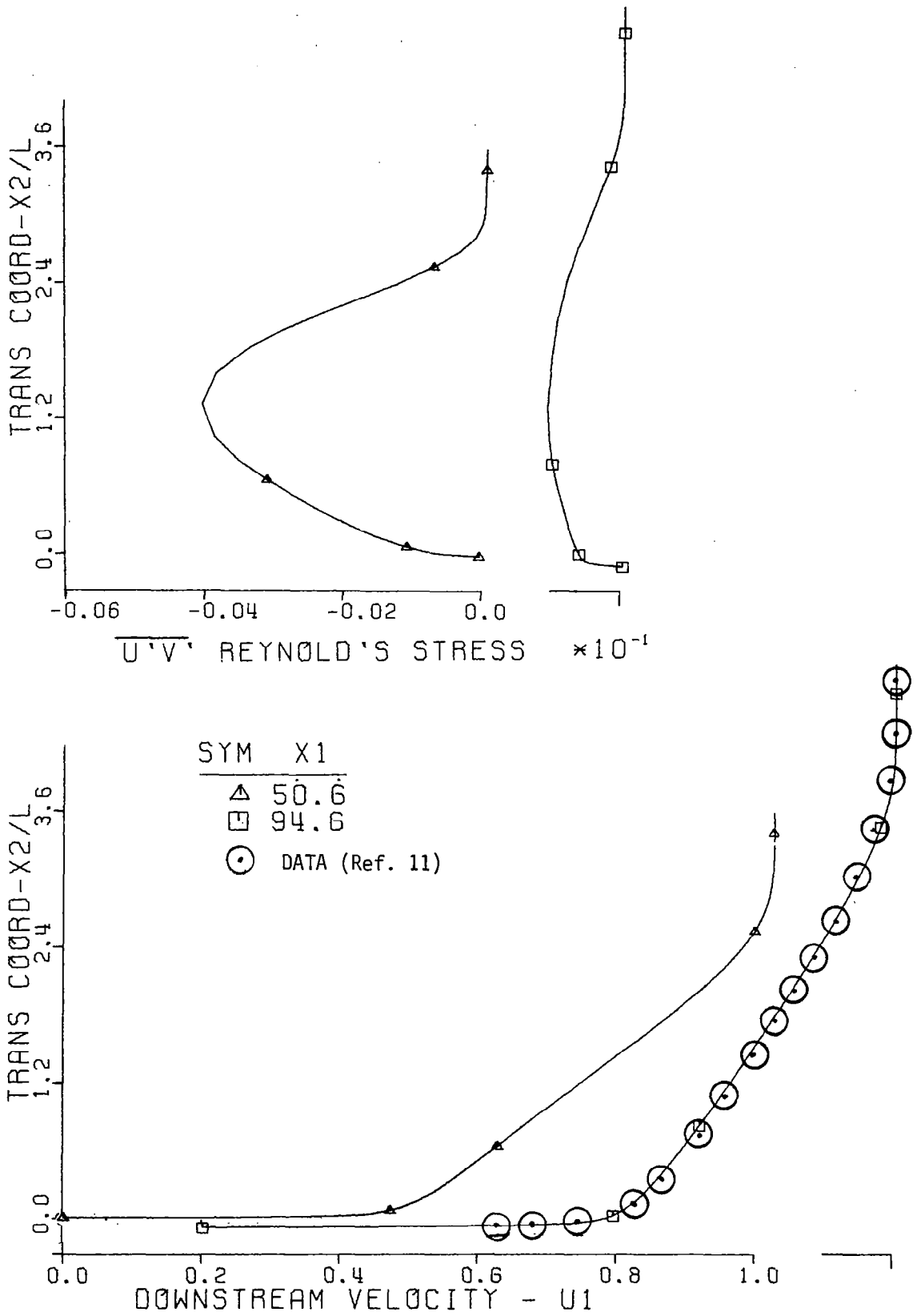

Fig. 7. Computed Mean and Fluctuating Velocity Profiles Bradshaw Turbulent Boundary Layer Test Case.

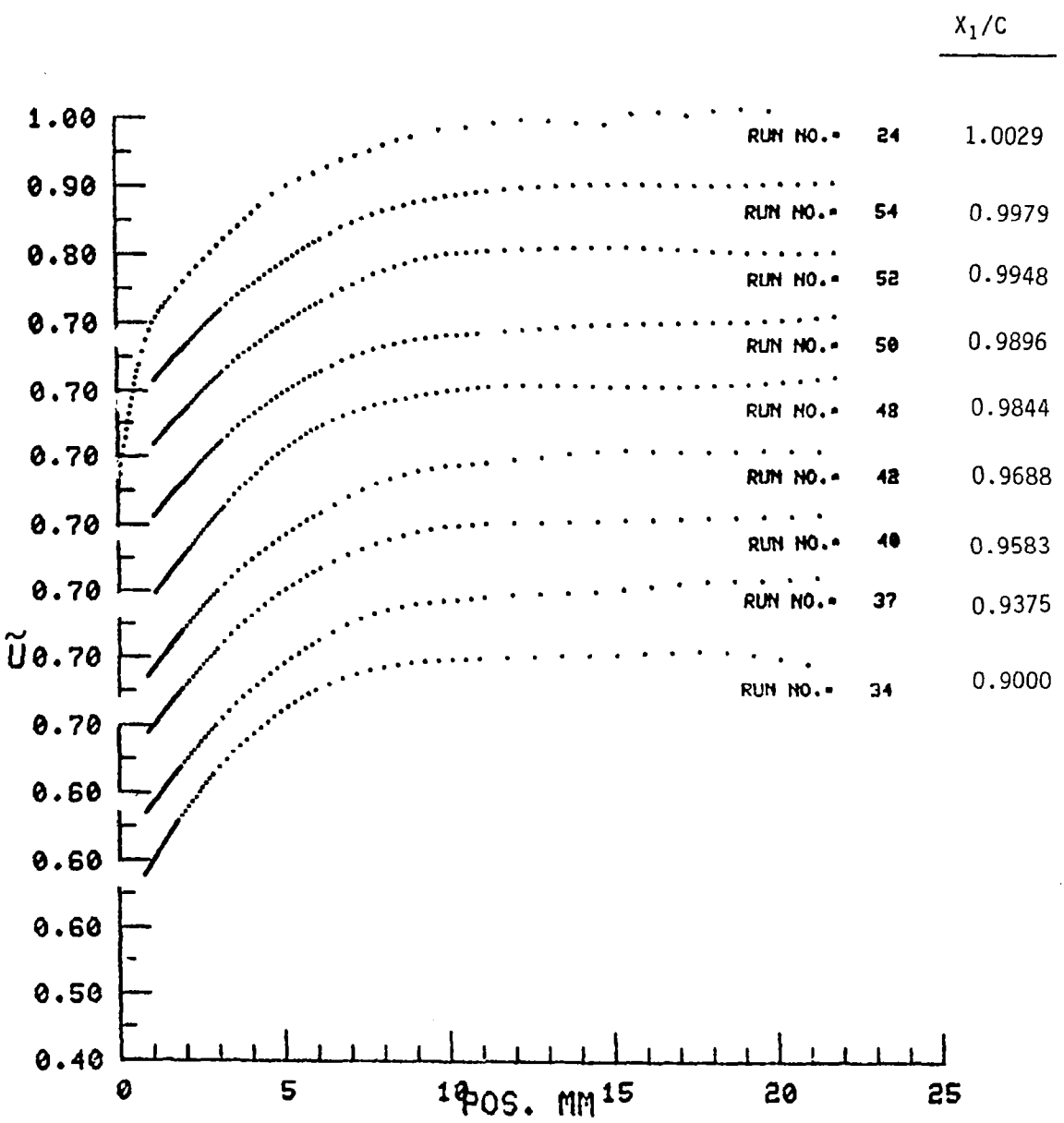

(a) Mean Velocity $\tilde{u}_1$

Fig. 8. Experimental Data for NACA 63-012, $\alpha = 0^o$, Ref. 9.

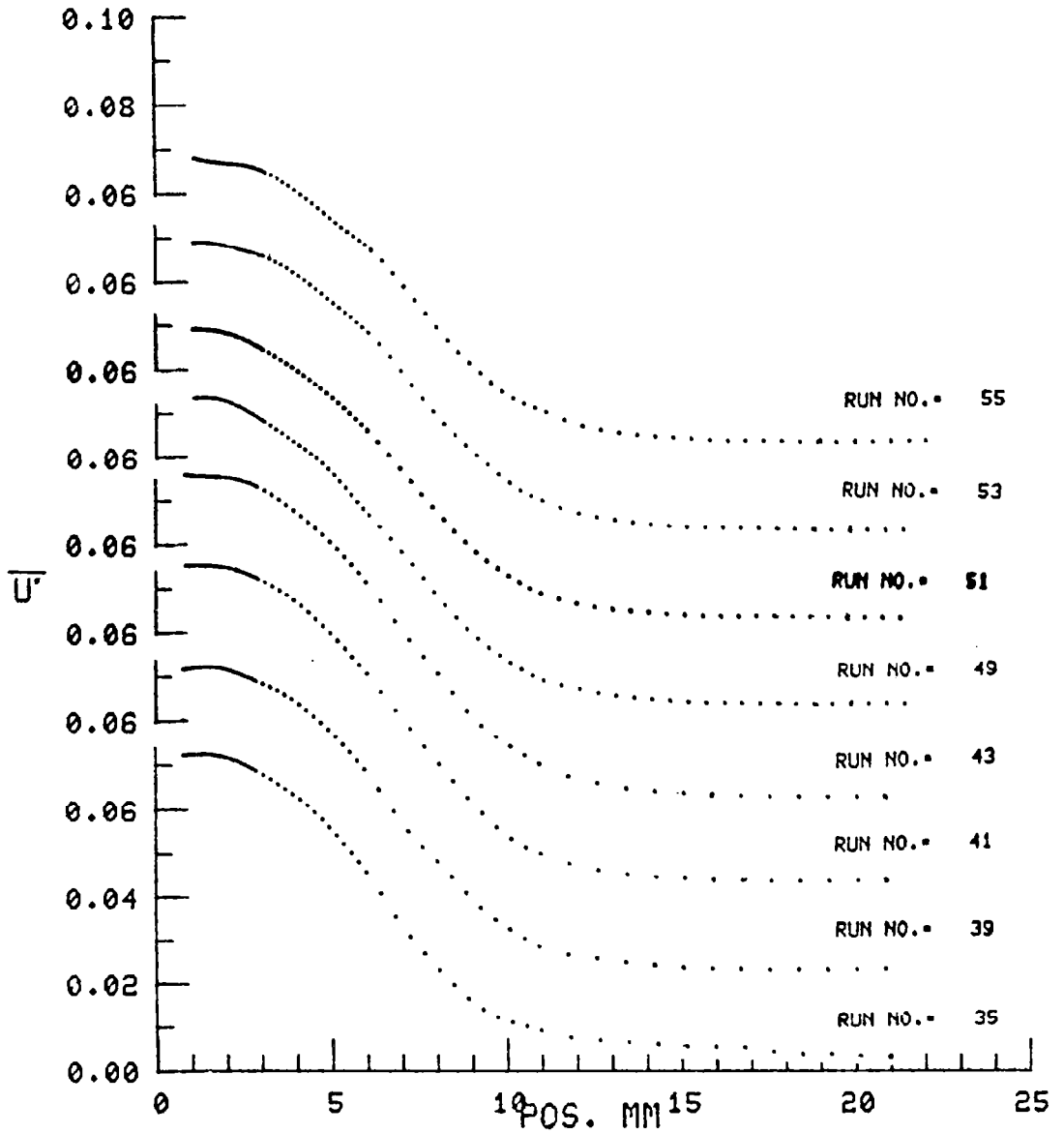

(b) Fluctuating Velocity $\overline{u_1'}$

Fig. 8. Continued.

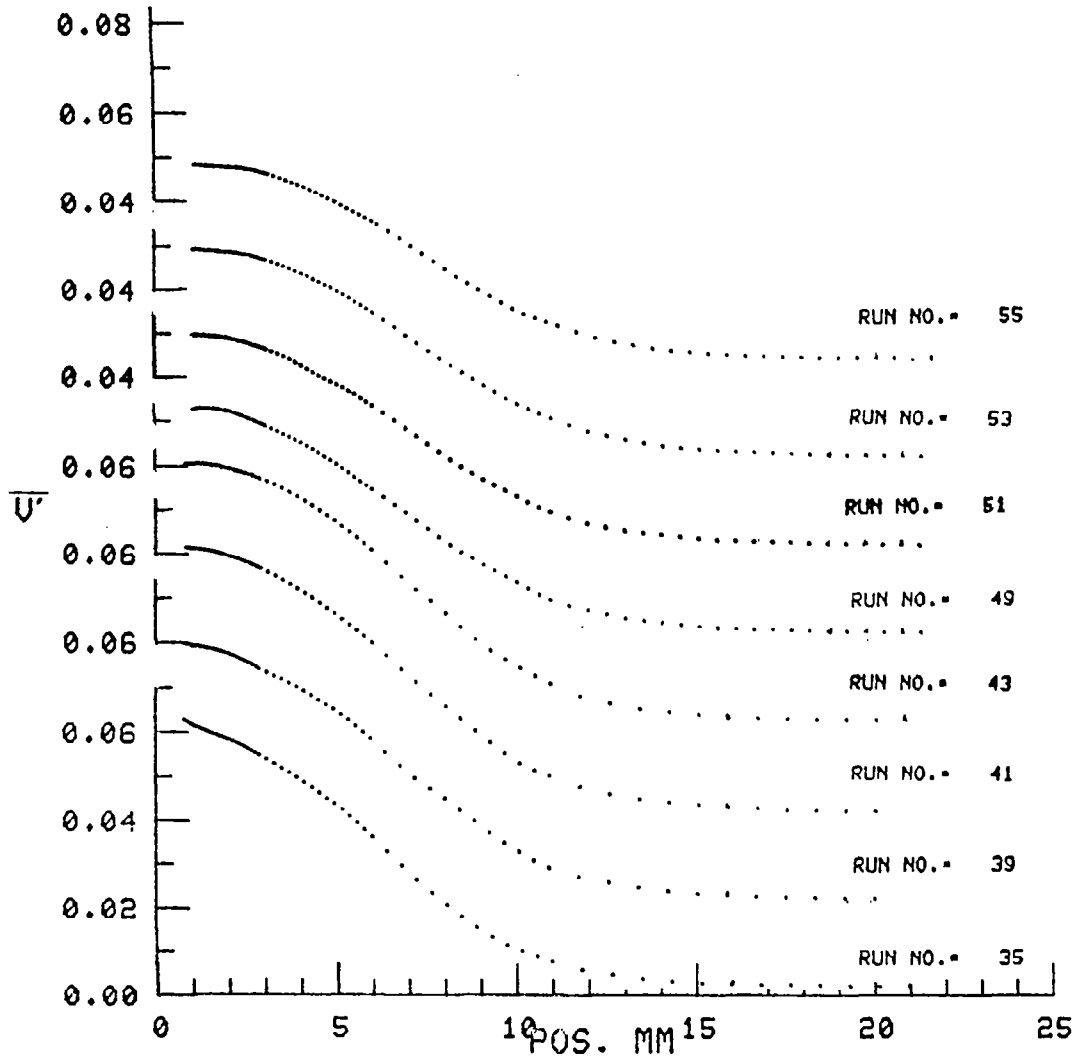

(c) Fluctuating Velocity $\overline{u_2'}$

Fig. 8. Continued.

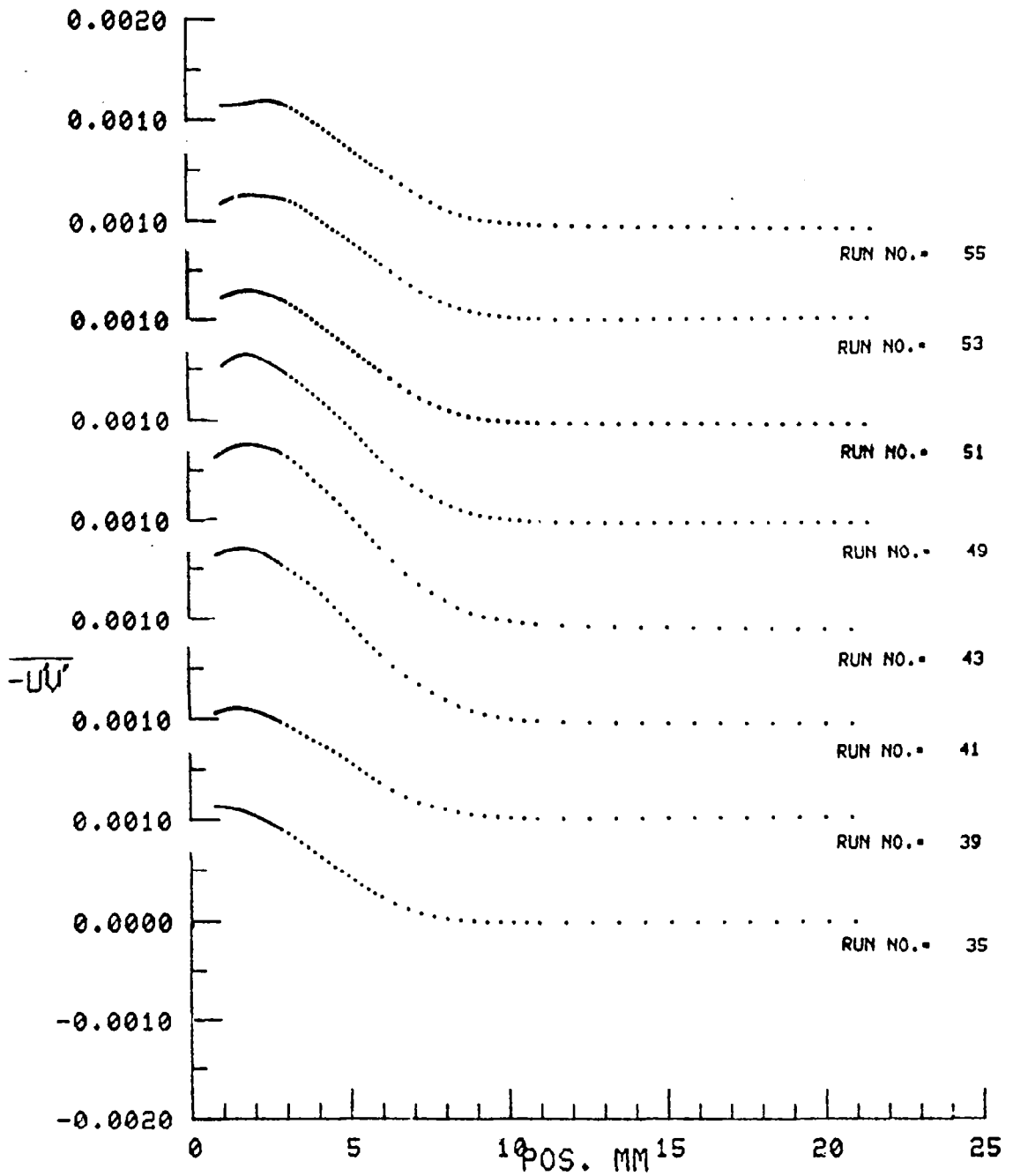

(d) Reynolds Stress - $\overline{u_1' u_2'}$

Fig. 8. Concluded.

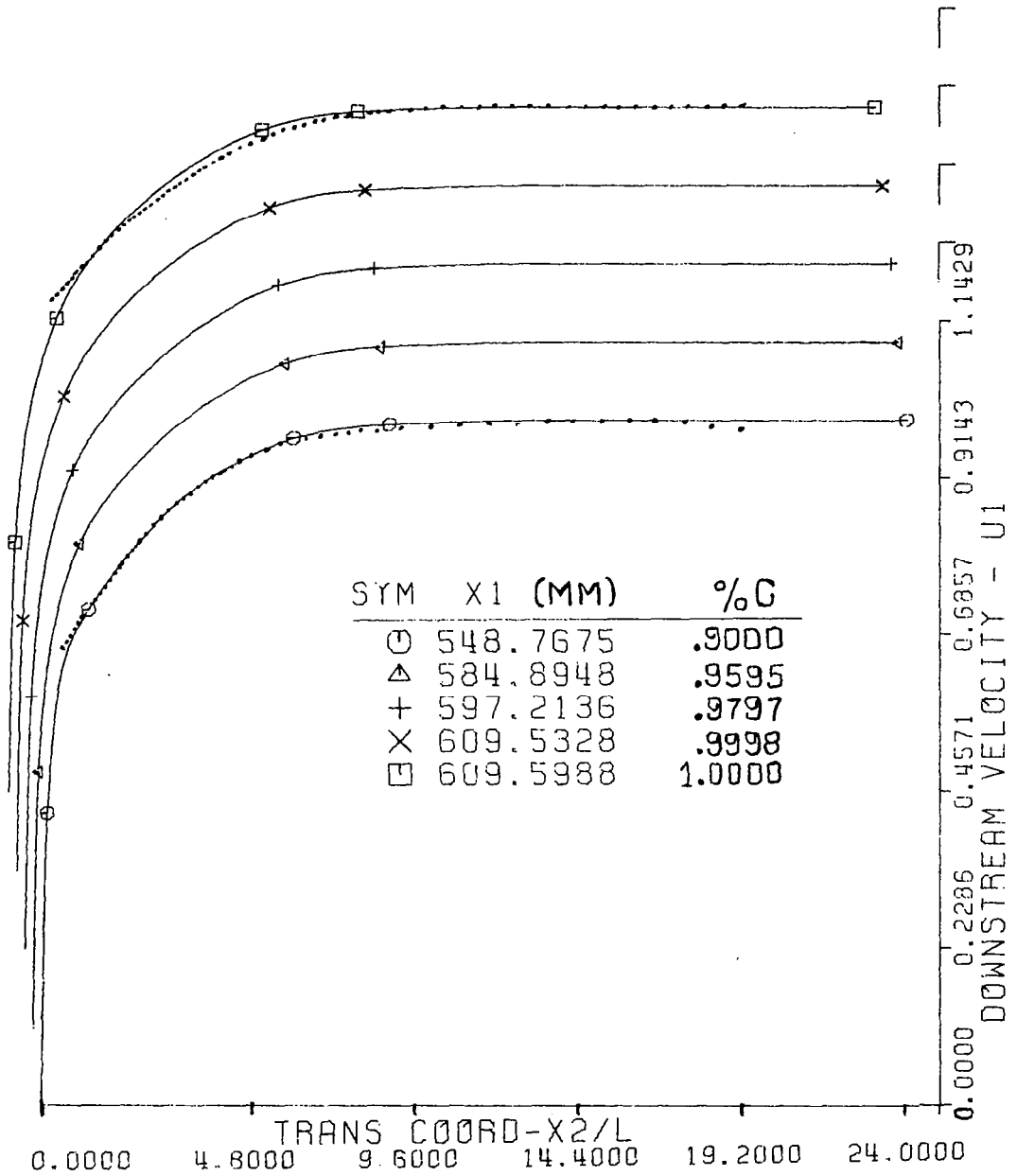

(a) Mean Velocity $\tilde{u}_1$

Fig. 9 Computed 2DBL/2DPNS Trailing Edge Solution.

In Figure 9b), the plot of $\overline{u_1'}$, the agreement with data at the first station is not exact. However, the 2DPNS solution has actually marched two percent chord. The computed solution recovers some of the initial disparity and the final station comparison is essential parallel curves with computation nominally 5% lower than data. The elevation in $\overline{u_1'}$ adjacent to the wall persists throughout the solution. Figure 9c) shows the comparison for $\overline{u_2'}$ at the selected stations. No agreement at the first station is required since the data for $\overline{u_2'}$ are not used for initialization. However, by the final station, the comparison between data and numerical prediction is acceptable. The near-wall peak in computed $\overline{u_2'}$ is somewhat subdued compared to that for $\overline{u_1'}$. A similar and modest near-wall peak is also computed in $\overline{u_1'u_2'}$, see Figure 9d. A modest disparity between data and prediction is illustrated at the initial profile and increases in magnitude and extent in proceeding to the final station where the maximum difference is about 20%. The magnitude of the near-wall peak remains nominally constant throughout the solution. Figure 9e is the plot of dissipation length scale ℓ_d.

$$\ell_d \equiv C_4 \frac{k^{3/2}}{\varepsilon} \tag{85}$$

where $\ell_d(x_2 \geq \delta)$ is defined equal to the value at $x_2 = \delta$.

In the overall view, the agreement between prediction and experiment is favorable and the final station solution fields for $\tilde{u}_1$, $\tilde{u}_2$, k and ε should be acceptable as initial data for the 2DPNS wake solution. The near wall model and the dissipation equation correlation constants can exert a profound influence on the numerical solutions. Figure 10 summarizes the impact of variation of model constants on the distributions of fluctuating parameters at $x_1/C = 1.0$. The dashed curves correspond to the results of Figure 9 for which $C_\varepsilon^2 - C_\varepsilon^1 = \Delta C_\varepsilon = 0.25$. The solid curve was obtained for $\Delta C_\varepsilon = 0.35$, while the dash-dot curve corresponds to $\Delta C_\varepsilon = 0.20$. The level of ΔC_ε reflects the difference between annihilation and production of dissipation, see equation (37). The larger levels tend to raise sharply all stress levels near the wall and to flatten the profiles away from the wall (near freestream).

Since the data case corresponds to $\alpha = 0^\circ$, these computed trailing edge lower boundary layer distributions can be reflected about the mean chord to initialize the 2DPNS wake solution on a discretization containing 80 elements. For solution comparison, Figures 11a)-11d) are composite plots of the experimental data distributions on the interval $1.0029 \leq x_1/C \leq 1.10$. The dominant action in the field near the trailing edge appears manifested primarily in $\overline{u_2'}$ which exhibits a noticeable peak which decays rapidly. The profiles of $\overline{u_1'}$ and $\overline{u_1'u_2'}$ also exhibit peaks with significantly smaller amplitudes.

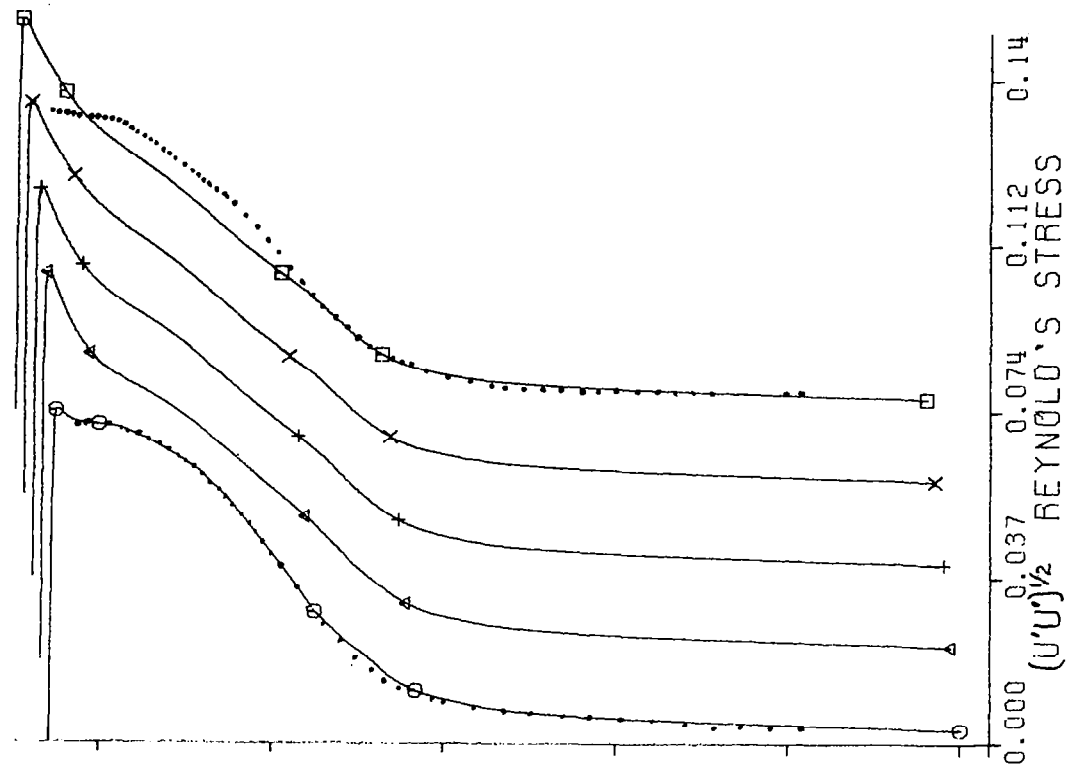

(b) Fluctuating Velocity $\overline{u_1'}$

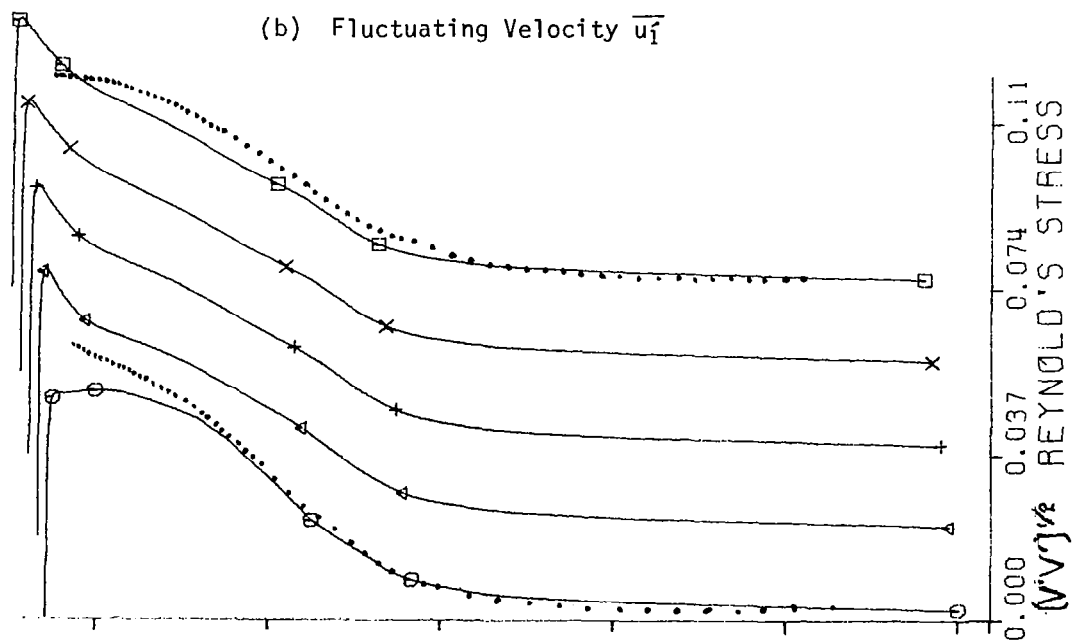

(c) Fluctuating Velocity $\overline{u_2'}$

Fig. 9. Continued.

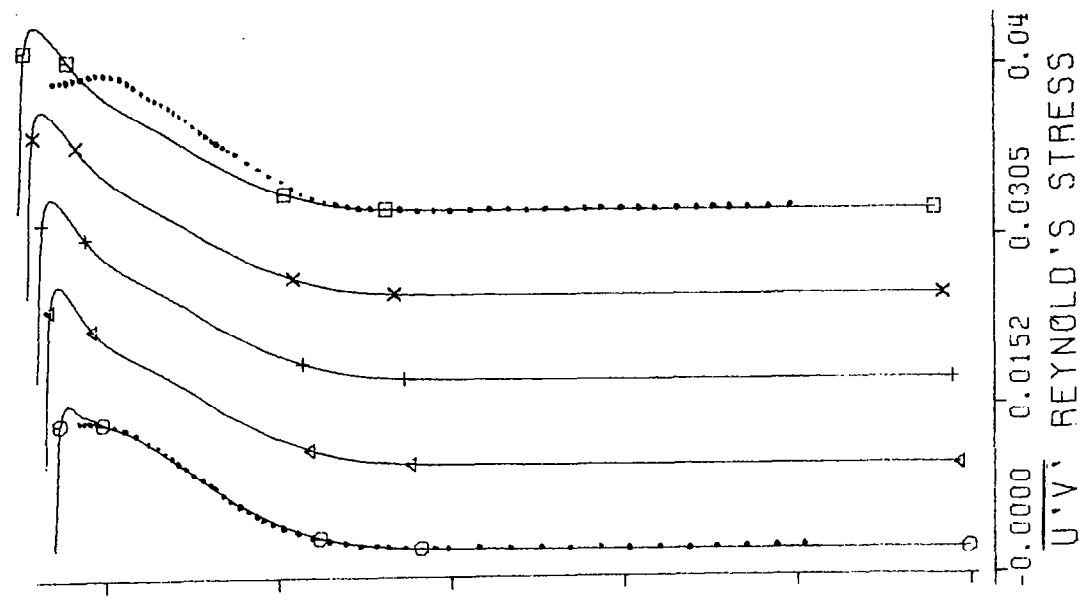

(d) Reynolds Stress $\overline{u_1' u_2'}$

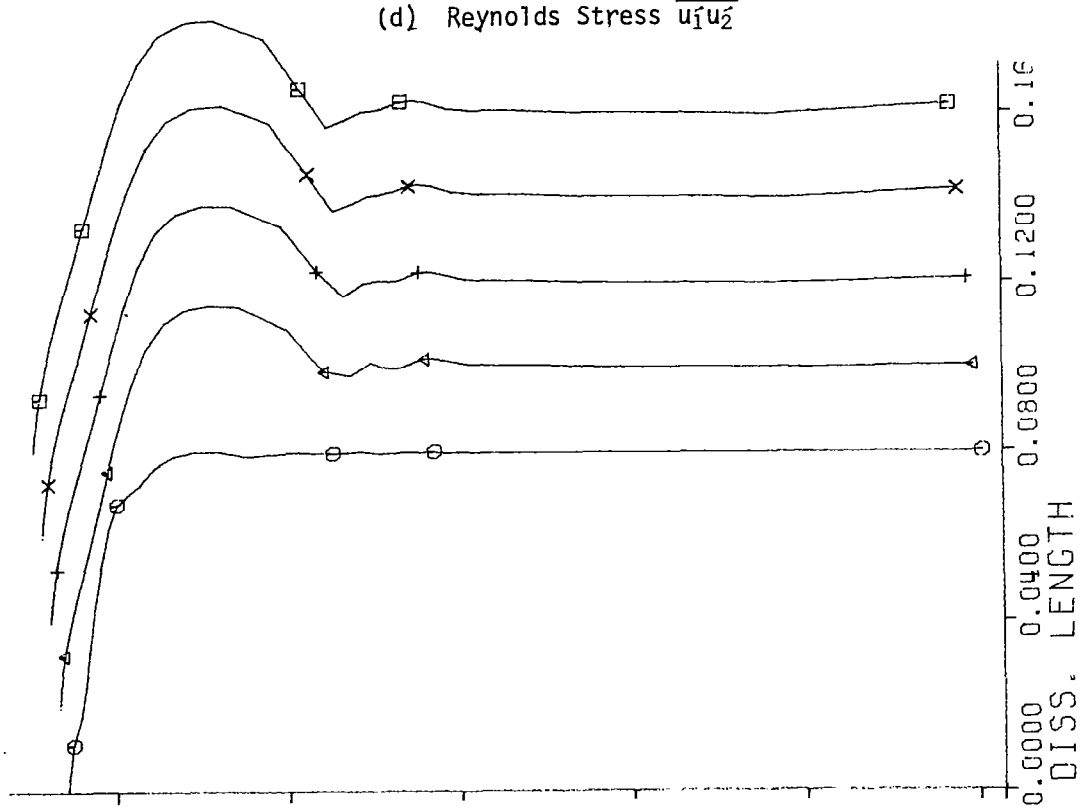

(e) Dissipation Length ℓ_d

Fig. 9. Concluded.

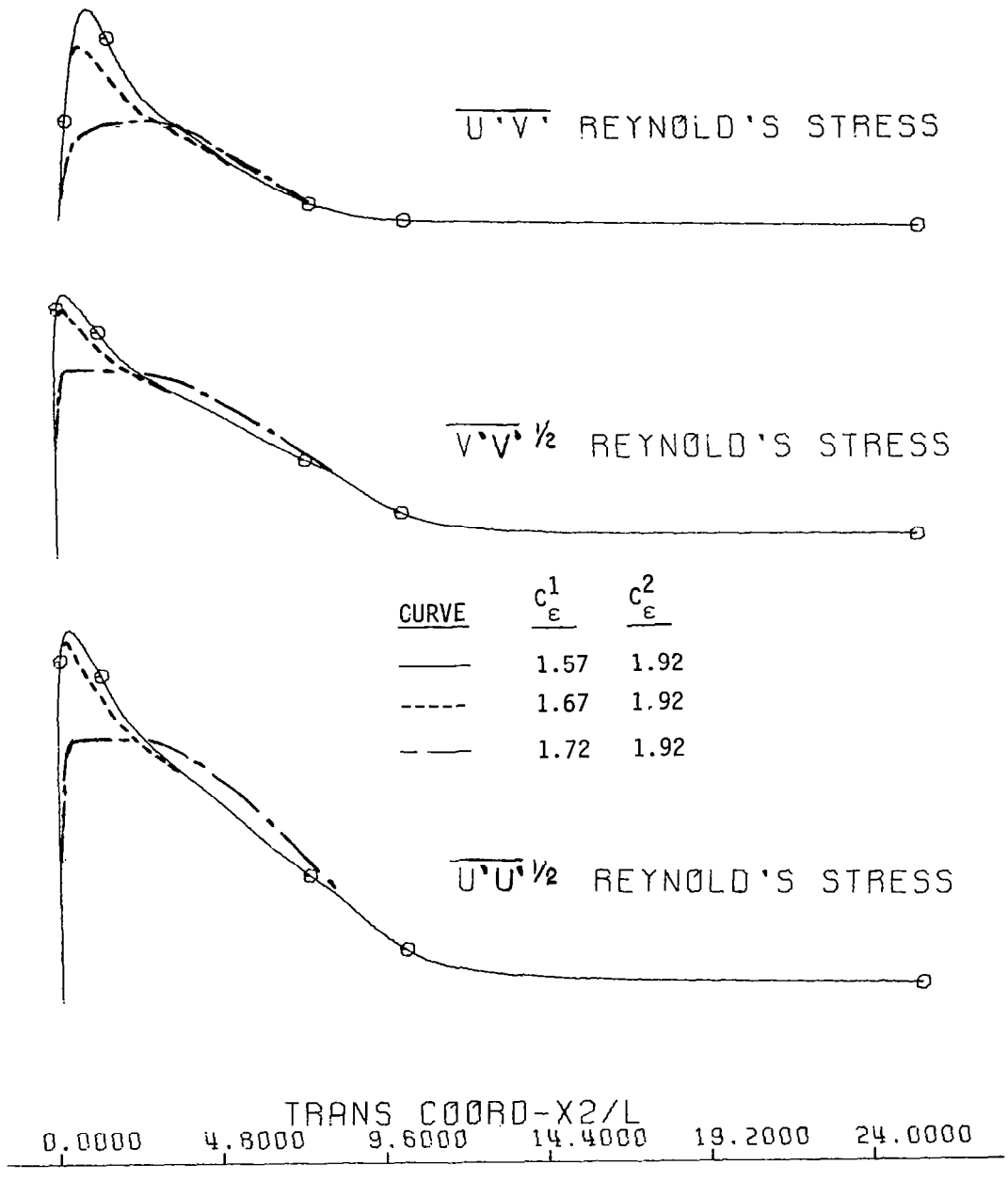

Fig. 10. Influence Of Dissipation Equation Constants On Computed Reynolds Stress Distributions, $x_1/C = 1.0$.

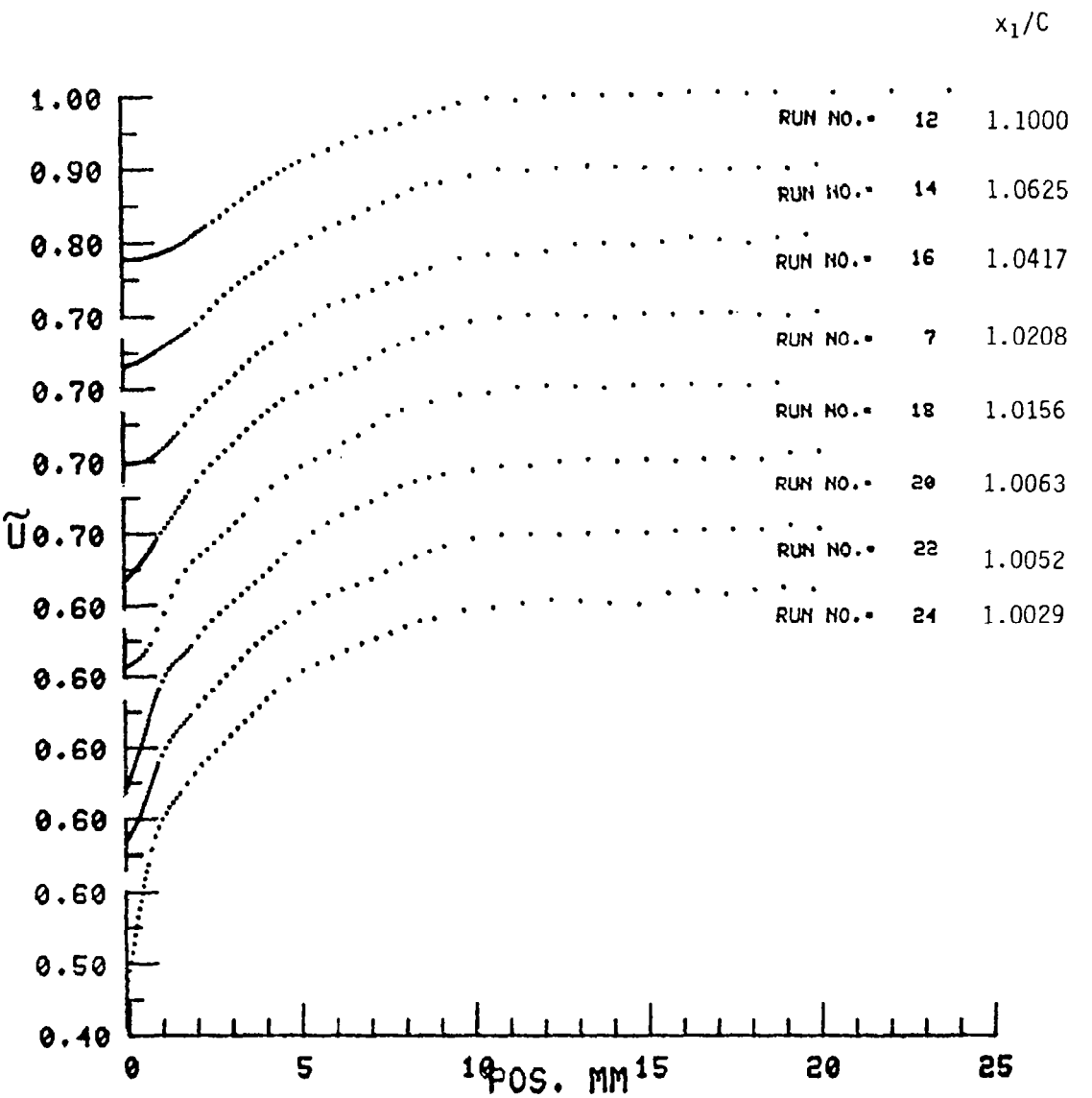

(a) Mean Velocity $\tilde{u}_1$

Fig. 11. Experimental Data for NACA 63-012, $\alpha = 0^{\circ}$, Ref. 9.

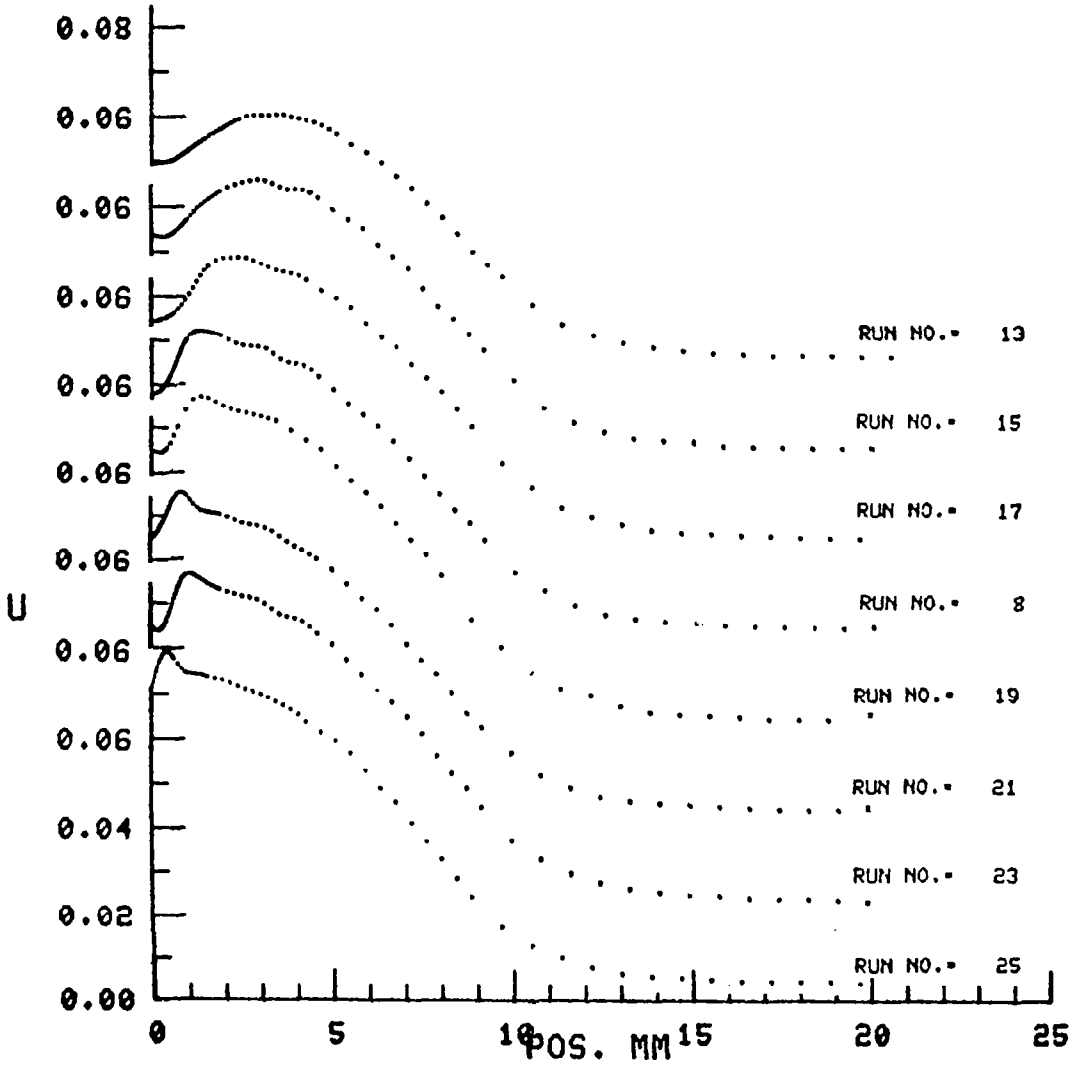

(b) Fluctuating Velocity $\overline{u_1'}$

Fig. 11. Continued.

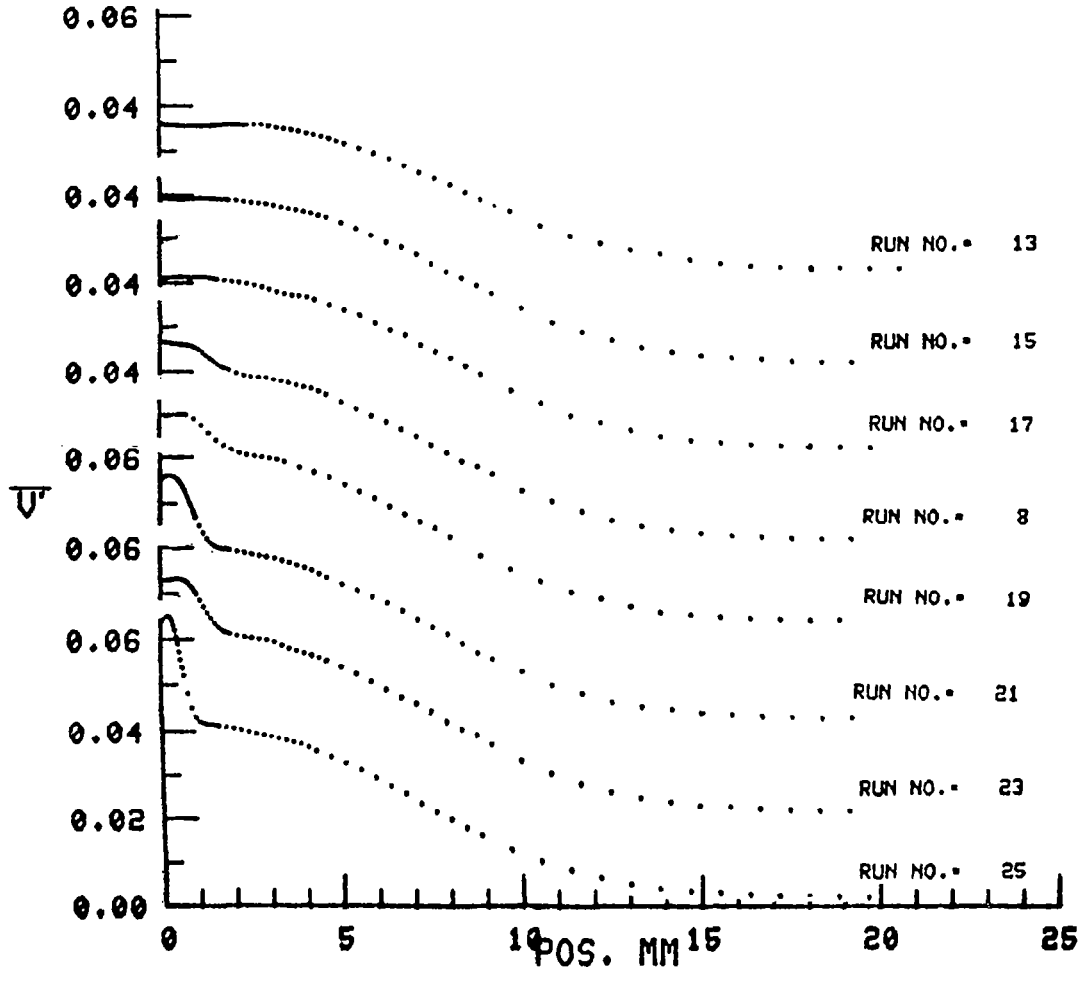

(c) Fluctuating Velocity $\overline{u_2'}$

Fig. 11. Continued.

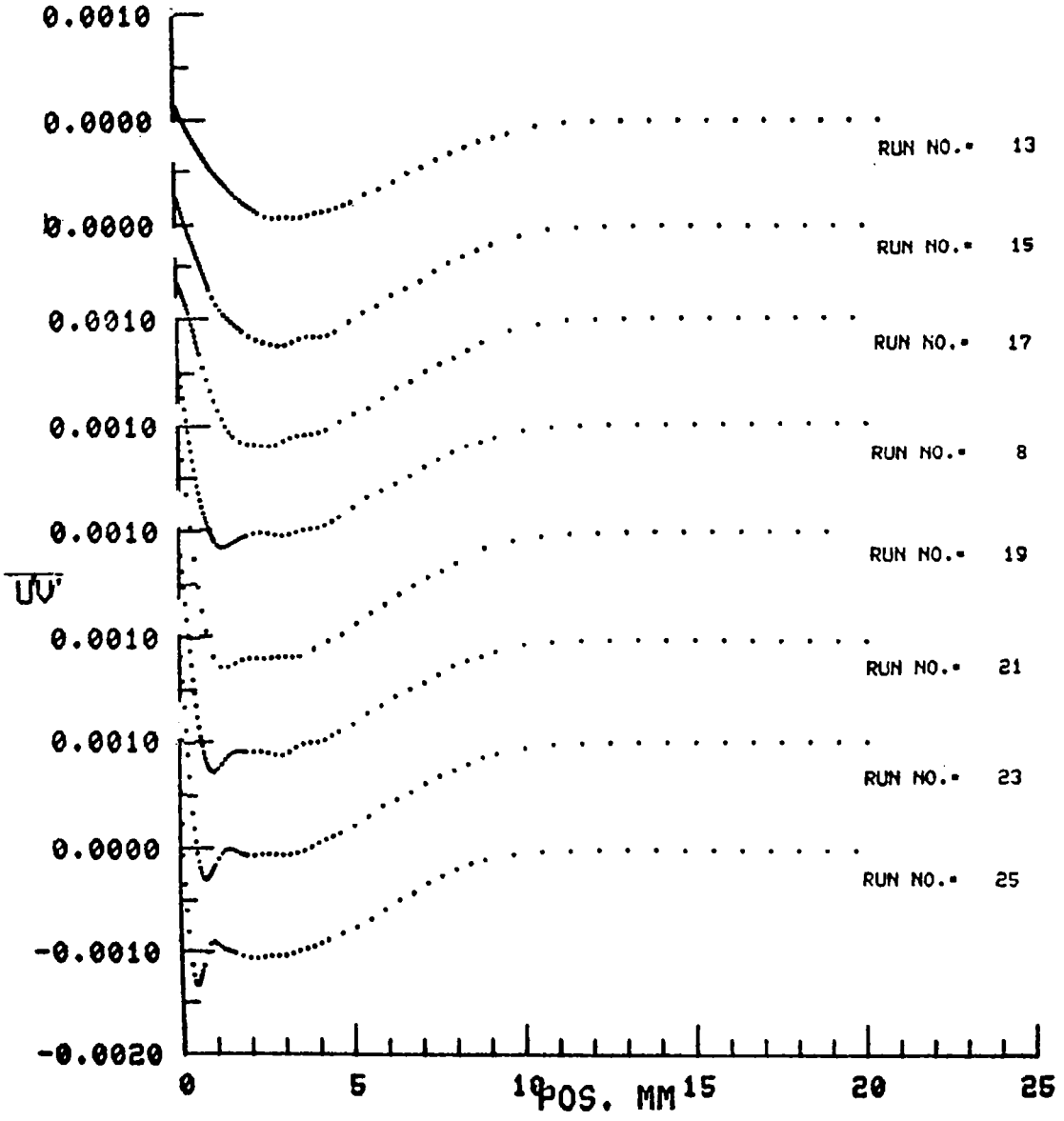

(d) Reynolds Stress $\overline{u_1' u_2'}$

Fig. 11. Concluded.

Using freestream pressure distribution of the final 2DBL/2DPNS iteration, 2DPNS wake solutions were generated on $1.0 < x_1/C < 1.10$. Figure 12 summarizes the computed solution which was obtained by eliminating the low turbulence Reynolds influence at the wall and setting the turbulence dissipation correlation coefficients to their standard values, $C_\varepsilon^\alpha = 1.3$, 1.44 and 1.92. In Figure 12, the experimental data profiles have been over-plotted at the nearest computational profile. Viewing the distributions of mean velocity $\tilde{u}_1$, good agreement occurs at $x_1/C = 1.0037$, but the 2DPNS solution progressively under predicts acceleration of the momentum deficit on the centerline. At $x_1/C = 1.10$, the maximum discrepancy is 8%. There also is evidence of modest under prediction of the lateral spread of the wake.

This is more graphic in the solutions for the fluctuating velocities $\overline{u_1'}$ and $\overline{u_2'}$, Figures 12b)-12c). For the former, recall that the trailing edge 2DPNS solution under-predicted data by about 5%, see Figure 9b). The experimental data indicates a nominal 10% increase in the level of $\overline{u_1'}$, uniformly over the profile, immediately downstream of the trailing edge (compare Run 55 curve in Figure 8b) to Run 25 curve on Figure 12b)). There is no mechanism in the numerical solution to elevate the initial data profile in this manner; hence, the nominal 20% difference persists throughout Figure 12b). Referring to the constitutive relation, equation (28), $\overline{u_1'u_1'}$ is dominately C_1 k, hence the levels of turbulence kinetic energy are correspondingly low. This is also evident in the freestream comparison of $\overline{u_2'}$, hence may account for the noted under-prediction of wake spreading.

The computed distributions of $\overline{u_1'}$ and $\overline{u_2'}$ about the wake centerline do exhibit a significant difference that is confirmed by the data. Both fluctuating velocities peak immediately downstream; thereafter, $\overline{u_1'}$ exhibits the characteristic double hump while $\overline{u_2'}$ achieves a nominally flat central plateau. For the computations, the sole difference between the two velocity distributions, see equation (28), is in the term $2C_4 \frac{k^2}{\varepsilon}$. For two-dimensional incompressible flows, the continuity equation (32) indicates that $\partial\tilde{u}_1/\partial x_1 = -\partial\tilde{u}_2/\partial x_2$. Hence, the second term in $\overline{u_1'u_1'}$ can be replaced by the negative of the second term in $\overline{u_2'u_2'}$. The resultant differences in $\overline{u_1'}$ and $\overline{u_2'}$ are in general agreement with the data which tends to confirm a viability for the Reynolds stress constitutive equation.

Figure 12d) compares the 2DPNS predictions for Reynolds shear stress $\overline{u_1'u_2'}$ to data. The low levels away from the center region can be attributed to overall under-prediction of the level of k. The development of the center region peak, and its decay and lateral spread, are in qualitative agreement with the data. Figure 12e) shows the computed distributions of turbulence kinetic energy, the profiles of which are essentially comparable to $\overline{u_1'}$.

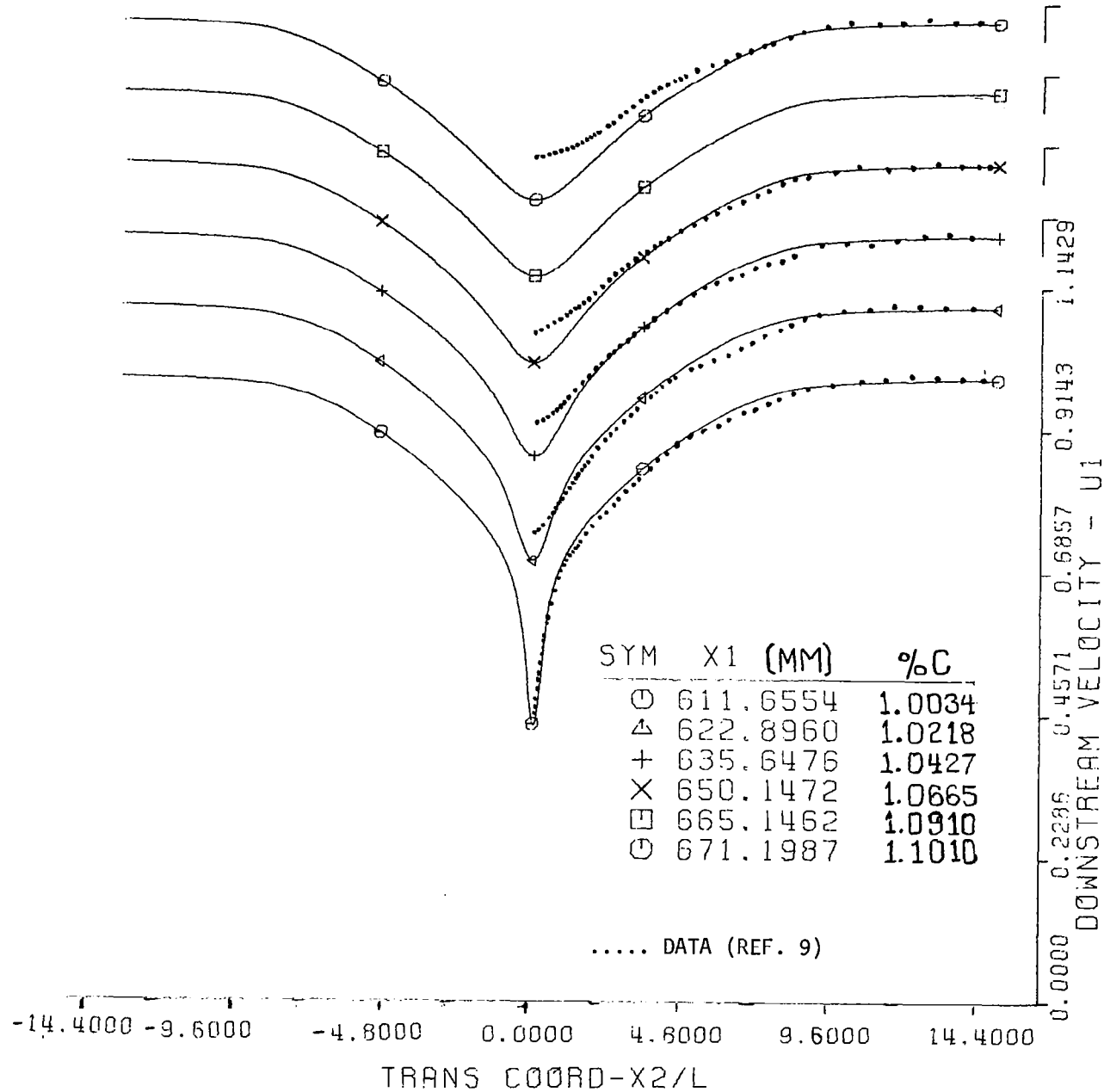

(a) Mean Velocity $\tilde{u}_1$

Fig. 12. Computed 2DPNS Wake Flow For NACA 63-012, $\alpha = 0^\circ$

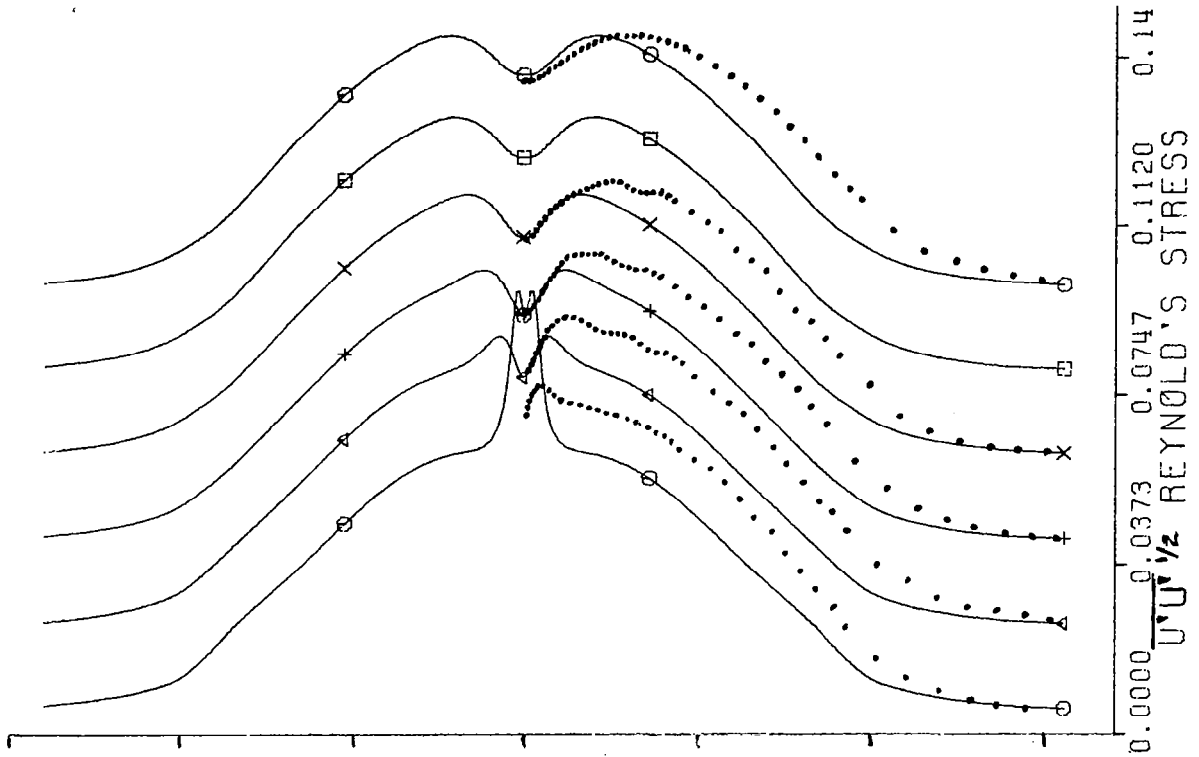

(b) Fluctuating Velocity $\overline{u_1'}$

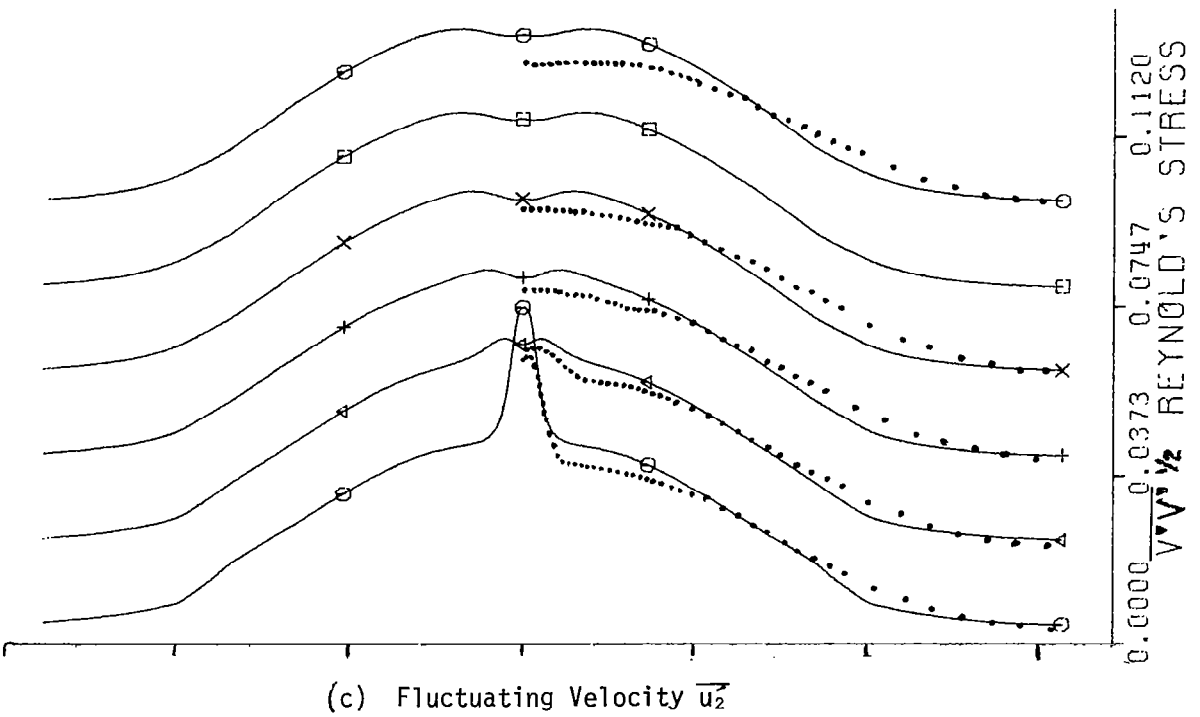

(c) Fluctuating Velocity $\overline{u_2'}$

Fig. 12 Continued.

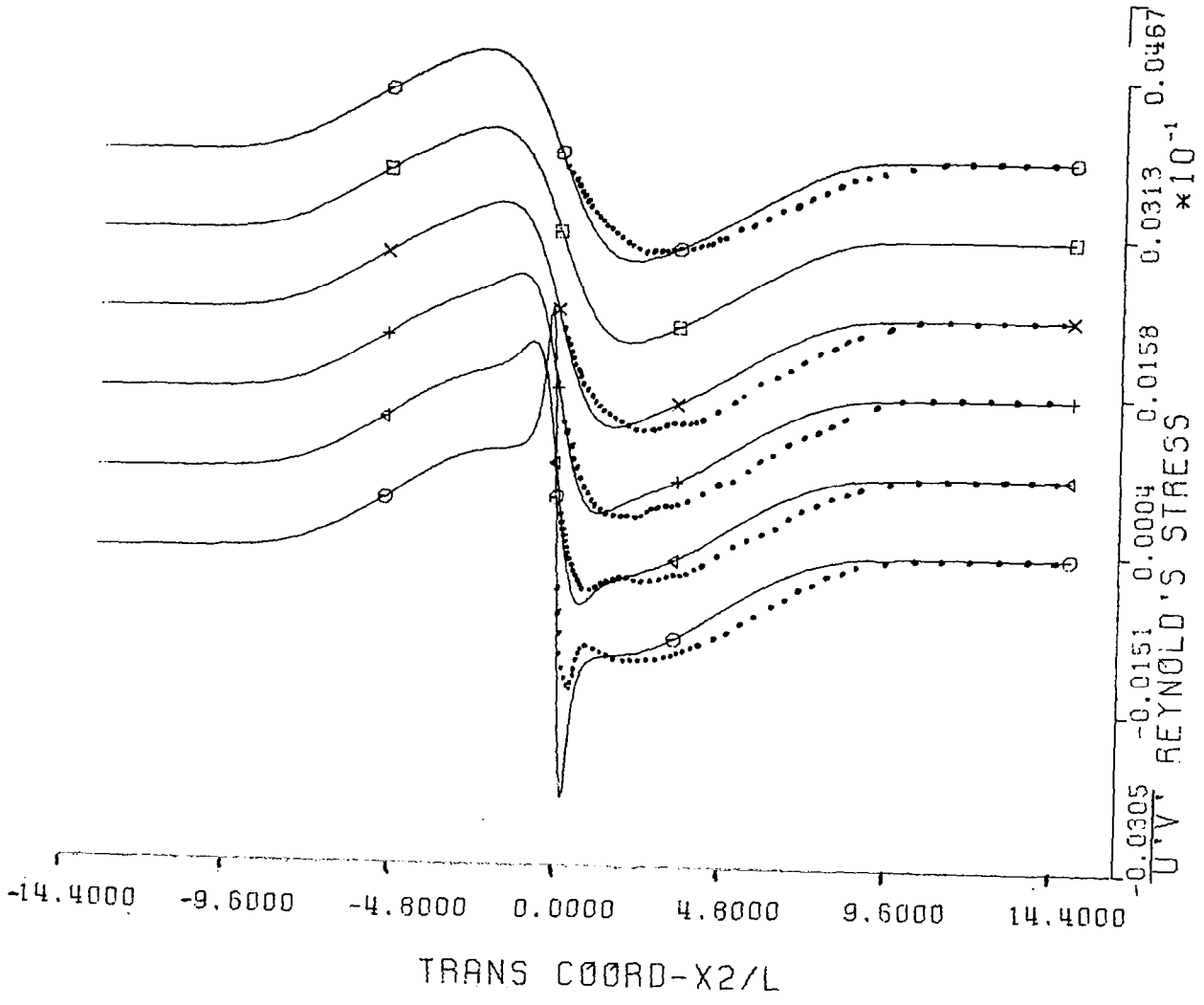

(d) Reynolds Stress $\overline{u_1 u_2}$

Fig. 12. Continued.

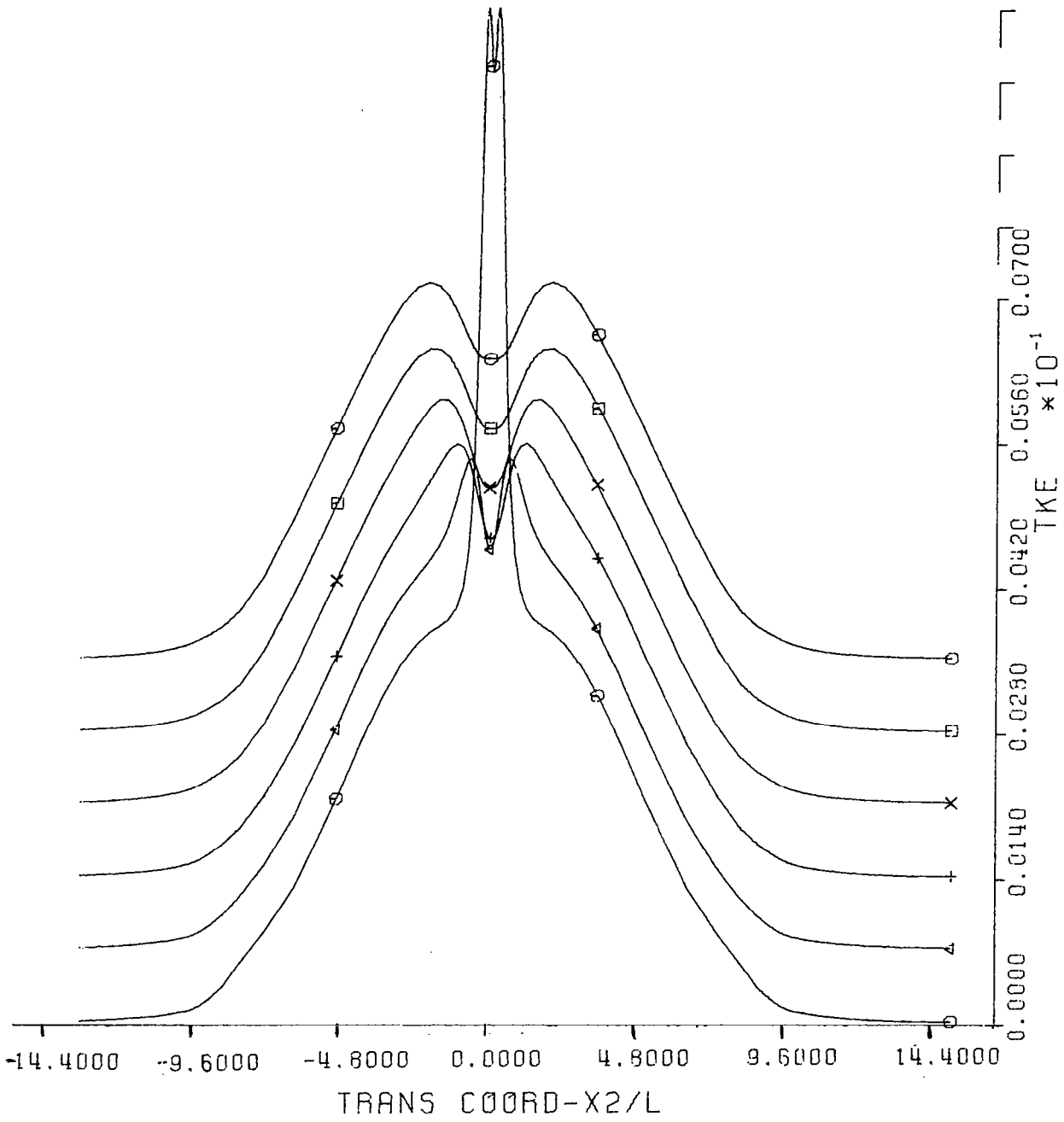

(e) Turbulence Kinetic Energy $\frac{1}{2}\overline{u_i'u_i'}$

Fig. 12. Concluded.

CONCLUSIONS

A theoretical analysis has yielded an interaction algorithm for prediction of mean and fluctuating velocity distributions in the vicinity of the sharp trailing edge of a subsonic airfoil. Governing systems of partial differential equations have been established and a numerical solution algorithm identified.

The results of numerical prediction for a NACA 63-012 airfoil have been compared with detailed experimental data. While some detailed quantitative differences exist, the results of the numerical solutions have exhibited quite notable qualitative agreement in delineation of differences in scalar components of the Reynolds stress tensor. Within the theoretical framework of the derived constitutive equation, exhibited differences in the wake fluctuating velocity distributions have been correlated directly with the action of the continuity equation. Interestingly, the parabolic order of magnitude analysis indicates this term is higher order, yet its impact on correlation with data is most important.

A considerable effort is required to generate initial data for the numerical predictions. The computational solutions are quite sensitive to boundary data, and in particular, a key required element was establishment of a low turbulence Reynolds number model, to account for the influence of the airfoil surface on the differential equation solutions for turbulence kinetic energy and isotropic dissipation function. The solution field of primary interest appears essentially dominated by the action of this model, minor modifications to which can cause truly significant solution differences. It is quite apparent that considerable theoretical attention should be applied to this specific topic, to render the developed procedure more widely applicable. Certainly there is little desirability in developing the Phase D analysis until this has been accomplished.

APPENDIX

Select Experimental Velocity Profiles For

NACA 63-012 Airfoil, $\alpha = 0^{o}$, $U_{\infty} = 30$ m/s, C = 0.61m

Untripped Boundary Layer

Run Numbers	Chord Station, x_1/c
34,35	0.9000
54,55	0.9979
24,25	1.0029
22,23	1.0052
12,13	1.1000

RUN NO.= 34 Y-STATION= 1 PROBE= 2 YMAX= 0.99312E+01 RUN NO.= 35

POSITION MM	U	UT	VT	U*V	TKE
0.77000E+00	0.67916E+00	0.72244E-01	0.62815E-01	0.11391E-02	0.91650E-02
0.81164E+00	0.68241E+00	0.72272E-01	0.62630E-01	0.11382E-02	0.91458E-02
0.85328E+00	0.68565E+00	0.72300E-01	0.62445E-01	0.11372E-02	0.91266E-02
0.89492E+00	0.68889E+00	0.72327E-01	0.62261E-01	0.11362E-02	0.91075E-02
0.93656E+00	0.69212E+00	0.72352E-01	0.62079E-01	0.11351E-02	0.90886E-02
0.97820E+00	0.69535E+00	0.72376E-01	0.61899E-01	0.11339E-02	0.90698E-02
0.10198E+01	0.69858E+00	0.72398E-01	0.61721E-01	0.11325E-02	0.90511E-02
0.10615E+01	0.70180E+00	0.72418E-01	0.61547E-01	0.11311E-02	0.90325E-02
0.11031E+01	0.70502E+00	0.72436E-01	0.61377E-01	0.11295E-02	0.90141E-02
0.11448E+01	0.70823E+00	0.72450E-01	0.61210E-01	0.11277E-02	0.89957E-02
0.11864E+01	0.71143E+00	0.72462E-01	0.61048E-01	0.11258E-02	0.89775E-02
0.12280E+01	0.71462E+00	0.72469E-01	0.60889E-01	0.11237E-02	0.89593E-02
0.12697E+01	0.71780E+00	0.72473E-01	0.60735E-01	0.11213E-02	0.89411E-02
0.13113E+01	0.72097E+00	0.72473E-01	0.60585E-01	0.11187E-02	0.89229E-02
0.13530E+01	0.72413E+00	0.72469E-01	0.60439E-01	0.11159E-02	0.89046E-02
0.13946E+01	0.72728E+00	0.72460E-01	0.60298E-01	0.11129E-02	0.88862E-02
0.14362E+01	0.73041E+00	0.72446E-01	0.60160E-01	0.11096E-02	0.88676E-02
0.14779E+01	0.73353E+00	0.72427E-01	0.60026E-01	0.11081E-02	0.88488E-02
0.15195E+01	0.73664E+00	0.72404E-01	0.59894E-01	0.11024E-02	0.88296E-02
0.15612E+01	0.73973E+00	0.72375E-01	0.59766E-01	0.10984E-02	0.88101E-02
0.16028E+01	0.74281E+00	0.72340E-01	0.59640E-01	0.10942E-02	0.87901E-02
0.16444E+01	0.74586E+00	0.72301E-01	0.59516E-01	0.10898E-02	0.87695E-02
0.16861E+01	0.74890E+00	0.72256E-01	0.59393E-01	0.10851E-02	0.87484E-02
0.17277E+01	0.75193E+00	0.72205E-01	0.59270E-01	0.10803E-02	0.87265E-02
0.17694E+01	0.75493E+00	0.72148E-01	0.59148E-01	0.10752E-02	0.87039E-02
0.18110E+01	0.75791E+00	0.72086E-01	0.59026E-01	0.10700E-02	0.86805E-02
0.19151E+01	0.76529E+00	0.71907E-01	0.58715E-01	0.10562E-02	0.86181E-02
0.20192E+01	0.77253E+00	0.71692E-01	0.58392E-01	0.10416E-02	0.85493E-02
0.21233E+01	0.77963E+00	0.71443E-01	0.58050E-01	0.10263E-02	0.84739E-02
0.22274E+01	0.78659E+00	0.71160E-01	0.57686E-01	0.10105E-02	0.83915E-02
0.23315E+01	0.79340E+00	0.70846E-01	0.57298E-01	0.99434E-03	0.83022E-02
0.24356E+01	0.80006E+00	0.70501E-01	0.56887E-01	0.97785E-03	0.82066E-02
0.25397E+01	0.80656E+00	0.70128E-01	0.56456E-01	0.96105E-03	0.81052E-02
0.26438E+01	0.81291E+00	0.69729E-01	0.56007E-01	0.94388E-03	0.79989E-02
0.27479E+01	0.81909E+00	0.69306E-01	0.55545E-01	0.92625E-03	0.78886E-02
0.28520E+01	0.82512E+00	0.68861E-01	0.55075E-01	0.90803E-03	0.77751E-02
0.30602E+01	0.83671E+00	0.67920E-01	0.54118E-01	0.86937E-03	0.75418E-02
0.32684E+01	0.84770E+00	0.66925E-01	0.53149E-01	0.82719E-03	0.73037E-02
0.34766E+01	0.85809E+00	0.65890E-01	0.52158E-01	0.78159E-03	0.70620E-02
0.36848E+01	0.86794E+00	0.64815E-01	0.51126E-01	0.73346E-03	0.68148E-02
0.38930E+01	0.87726E+00	0.63679E-01	0.50034E-01	0.68416E-03	0.65585E-02
0.41012E+01	0.88611E+00	0.62448E-01	0.48879E-01	0.63494E-03	0.62889E-02
0.43094E+01	0.89450E+00	0.61087E-01	0.47668E-01	0.58651E-03	0.60039E-02
0.45176E+01	0.90248E+00	0.59576E-01	0.46421E-01	0.53898E-03	0.57041E-02
0.47258E+01	0.91005E+00	0.57920E-01	0.45150E-01	0.49209E-03	0.53932E-02
0.49340E+01	0.91725E+00	0.56147E-01	0.43856E-01	0.44567E-03	0.50759E-02
0.51422E+01	0.92408E+00	0.54291E-01	0.42527E-01	0.39992E-03	0.47561E-02
0.53504E+01	0.93054E+00	0.52368E-01	0.41137E-01	0.35546E-03	0.44347E-02
0.55586E+01	0.93665E+00	0.50366E-01	0.39664E-01	0.31307E-03	0.41099E-02
0.57668E+01	0.94240E+00	0.48246E-01	0.38096E-01	0.27343E-03	0.37789E-02
0.59750E+01	0.94780E+00	0.45970E-01	0.36441E-01	0.23690E-03	0.34412E-02
0.63914E+01	0.95750E+00	0.40951E-01	0.32988E-01	0.17327E-03	0.27652E-02
0.68078E+01	0.96576E+00	0.35726E-01	0.29592E-01	0.12152E-03	0.21520E-02
0.72242E+01	0.97263E+00	0.30961E-01	0.26450E-01	0.51478E-04	0.16582E-02
0.76406E+01	0.97822E+00	0.26858E-01	0.23554E-01	0.52674E-04	0.12762E-02
0.80570E+01	0.98266E+00	0.23179E-01	0.20798E-01	0.32958E-04	0.96983E-03
0.84734E+01	0.98613E+00	0.19757E-01	0.18116E-01	0.19023E-04	0.71854E-03
0.88898E+01	0.98879E+00	0.16671E-01	0.15552E-01	0.81631E-05	0.51979E-03
0.93062E+01	0.99080E+00	0.14120E-01	0.13259E-01	-0.31663E-06	0.37518E-03
0.97226E+01	0.99232E+00	0.12092E-01	0.11406E-01	-0.58276E-05	0.28118E-03
0.10139E+02	0.99348E+00	0.11116E-01	0.10015E-01	-0.83922E-05	0.22386E-03
0.10555E+02	0.99440E+00	0.10188E-01	0.88957E-02	-0.89117E-05	0.18293E-03
0.10972E+02	0.99518E+00	0.92051E-02	0.78172E-02	-0.83367E-05	0.14584E-03
0.11805E+02	0.99662E+00	0.77190E-02	0.58556E-02	-0.69271E-05	0.93871E-04
0.12637E+02	0.99798E+00	0.70776E-02	0.46772E-02	-0.61147E-05	0.71968E-04
0.13470E+02	0.99908E+00	0.65381E-02	0.37925E-02	-0.57560E-05	0.57130E-04
0.14303E+02	0.99982E+00	0.61044E-02	0.32250E-02	-0.53343E-05	0.47664E-04
0.15136E+02	0.10007E+01	0.56407E-02	0.28794E-02	-0.50991E-05	0.40109E-04
0.15969E+02	0.10022E+01				

RUN NO.= 54 Y-STATION= 11 PROBE= 2 YMAX= 0.92511E+01 RUN NO.= 55

POSITION MM	U	UT	VT	U*V	TKE
0.10910E+01	0.71605E+00	0.68240E-01	0.48389E-01	0.11488E-02	0.69982E-02
0.11326E+01	0.71835E+00	0.68171E-01	0.48356E-01	0.11490E-02	0.69855E-02
0.11743E+01	0.72064E+00	0.68102E-01	0.48322E-01	0.11493E-02	0.69729E-02
0.12159E+01	0.72294E+00	0.68034E-01	0.48288E-01	0.11495E-02	0.69603E-02
0.12576E+01	0.72523E+00	0.67966E-01	0.48255E-01	0.11499E-02	0.69479E-02
0.12992E+01	0.72752E+00	0.67899E-01	0.48223E-01	0.11504E-02	0.69358E-02
0.13408E+01	0.72981E+00	0.67834E-01	0.48191E-01	0.11510E-02	0.69238E-02
0.13825E+01	0.73210E+00	0.67770E-01	0.48160E-01	0.11517E-02	0.69121E-02
0.14241E+01	0.73438E+00	0.67708E-01	0.48129E-01	0.11527E-02	0.69008E-02
0.14658E+01	0.73665E+00	0.67648E-01	0.48100E-01	0.11538E-02	0.68898E-02
0.15074E+01	0.73893E+00	0.67590E-01	0.48071E-01	0.11551E-02	0.68792E-02
0.15490E+01	0.74119E+00	0.67534E-01	0.48043E-01	0.11565E-02	0.68690E-02
0.15907E+01	0.74345E+00	0.67480E-01	0.48016E-01	0.11582E-02	0.68592E-02
0.16323E+01	0.74570E+00	0.67429E-01	0.47990E-01	0.11601E-02	0.68498E-02
0.16740E+01	0.74795E+00	0.67381E-01	0.47965E-01	0.11622E-02	0.68408E-02
0.17156E+01	0.75018E+00	0.67334E-01	0.47941E-01	0.11645E-02	0.68322E-02
0.17572E+01	0.75241E+00	0.67291E-01	0.47917E-01	0.11669E-02	0.68241E-02
0.17989E+01	0.75463E+00	0.67249E-01	0.47894E-01	0.11695E-02	0.68163E-02
0.18405E+01	0.75684E+00	0.67210E-01	0.47871E-01	0.11722E-02	0.68088E-02
0.18822E+01	0.75904E+00	0.67173E-01	0.47848E-01	0.11750E-02	0.68017E-02
0.19238E+01	0.76124E+00	0.67138E-01	0.47826E-01	0.11779E-02	0.67948E-02
0.19654E+01	0.76342E+00	0.67105E-01	0.47803E-01	0.11808E-02	0.67881E-02
0.20071E+01	0.76559E+00	0.67073E-01	0.47779E-01	0.11837E-02	0.67816E-02
0.20487E+01	0.76774E+00	0.67042E-01	0.47755E-01	0.11866E-02	0.67752E-02
0.20904E+01	0.76989E+00	0.67011E-01	0.47730E-01	0.11894E-02	0.67687E-02
0.21320E+01	0.77203E+00	0.66981E-01	0.47704E-01	0.11922E-02	0.67621E-02
0.22153E+01	0.77626E+00	0.66920E-01	0.47645E-01	0.11972E-02	0.67483E-02
0.22986E+01	0.78044E+00	0.66854E-01	0.47578E-01	0.12013E-02	0.67330E-02
0.23818E+01	0.78457E+00	0.66778E-01	0.47498E-01	0.12042E-02	0.67154E-02
0.24651E+01	0.78864E+00	0.66689E-01	0.47405E-01	0.12058E-02	0.66946E-02
0.25484E+01	0.79265E+00	0.66581E-01	0.47296E-01	0.12056E-02	0.66699E-02
0.26317E+01	0.79661E+00	0.66451E-01	0.47169E-01	0.12037E-02	0.66407E-02
0.27150E+01	0.80051E+00	0.66295E-01	0.47025E-01	0.12000E-02	0.66064E-02
0.27982E+01	0.80435E+00	0.66111E-01	0.46862E-01	0.11943E-02	0.65666E-02
0.28815E+01	0.80813E+00	0.65895E-01	0.46681E-01	0.11868E-02	0.65213E-02
0.29648E+01	0.81185E+00	0.65648E-01	0.46483E-01	0.11775E-02	0.64704E-02
0.30481E+01	0.81551E+00	0.65370E-01	0.46271E-01	0.11666E-02	0.64143E-02
0.31314E+01	0.81912E+00	0.65062E-01	0.46046E-01	0.11543E-02	0.63533E-02
0.32979E+01	0.82616E+00	0.64364E-01	0.45567E-01	0.11264E-02	0.62191E-02
0.34645E+01	0.83298E+00	0.63579E-01	0.45067E-01	0.10954E-02	0.60733E-02
0.36310E+01	0.83959E+00	0.62731E-01	0.44560E-01	0.10629E-02	0.59208E-02
0.37976E+01	0.84601E+00	0.61843E-01	0.44049E-01	0.10298E-02	0.57649E-02
0.39642E+01	0.85225E+00	0.60923E-01	0.43527E-01	0.99617E-03	0.56063E-02
0.41307E+01	0.85832E+00	0.59971E-01	0.42977E-01	0.95183E-03	0.54436E-02
0.42973E+01	0.86426E+00	0.58980E-01	0.42380E-01	0.92618E-03	0.52747E-02
0.44638E+01	0.87005E+00	0.57942E-01	0.41722E-01	0.88876E-03	0.50980E-02
0.46304E+01	0.87573E+00	0.56860E-01	0.41002E-01	0.84949E-03	0.49143E-02
0.47970E+01	0.88129E+00	0.55751E-01	0.40232E-01	0.80879E-03	0.47268E-02
0.49635E+01	0.88674E+00	0.54638E-01	0.39436E-01	0.76752E-03	0.45405E-02
0.51301E+01	0.89209E+00	0.53549E-01	0.38640E-01	0.72672E-03	0.43605E-02
0.52966E+01	0.89734E+00	0.52501E-01	0.37867E-01	0.68729E-03	0.41902E-02
0.54632E+01	0.90249E+00	0.51494E-01	0.37126E-01	0.64976E-03	0.40300E-02
0.56298E+01	0.90752E+00	0.50506E-01	0.36413E-01	0.61411E-03	0.38767E-02
0.57963E+01	0.91245E+00	0.49498E-01	0.35707E-01	0.57985E-03	0.37251E-02
0.59629E+01	0.91724E+00	0.48426E-01	0.34986E-01	0.54623E-03	0.35691E-02
0.61294E+01	0.92191E+00	0.47250E-01	0.34229E-01	0.51253E-03	0.34042E-02
0.64417E+01	0.93027E+00	0.44720E-01	0.32682E-01	0.44783E-03	0.30680E-02
0.67540E+01	0.93805E+00	0.41853E-01	0.31009E-01	0.38229E-03	0.27133E-02
0.70663E+01	0.94522E+00	0.38838E-01	0.29288E-01	0.31958E-03	0.23662E-02
0.73786E+01	0.95173E+00	0.35761E-01	0.27533E-01	0.26226E-03	0.20369E-02
0.76909E+01	0.95758E+00	0.32588E-01	0.25709E-01	0.21031E-03	0.17229E-02
0.80032E+01	0.96278E+00	0.29361E-01	0.23850E-01	0.16335E-03	0.14309E-02
0.83155E+01	0.96739E+00	0.26285E-01	0.22087E-01	0.12269E-03	0.11788E-02
0.86278E+01	0.97147E+00	0.23564E-01	0.20514E-01	0.90301E-04	0.97610E-03
0.89401E+01	0.97508E+00	0.21178E-01	0.19069E-01	0.66282E-04	0.81214E-03
0.92524E+01	0.97829E+00	0.18926E-01	0.17597E-01	0.48339E-04	0.66786E-03
0.95647E+01	0.98117E+00	0.16694E-01	0.16054E-01	0.33933E-04	0.53643E-03
0.98770E+01	0.98377E+00	0.14626E-01	0.14581E-01	0.22253E-04	0.42654E-03

RUN NO.= 24 Y-STATION= 12 PROBE= 2 YMAX= 0.96688E+01 RUN NO.= 25

POSITION MM	U	UT	VT	U*V	TKE
0.10228E-03	0.46376E+00	0.71479E-01	0.63700E-01	0.53782E-03	0.91669E-02
0.41742E-01	0.47674E+00	0.72655E-01	0.64144E-01	0.24029E-03	0.93933E-02
0.83382E-01	0.48969E+00	0.73801E-01	0.64527E-01	-0.48063E-04	0.96102E-02
0.12502E+00	0.50256E+00	0.74886E-01	0.64789E-01	-0.31860E-03	0.98055E-02
0.16666E+00	0.51533E+00	0.75884E-01	0.64879E-01	-0.56376E-03	0.99676E-02
0.20830E+00	0.52796E+00	0.76771E-01	0.64757E-01	-0.77747E-03	0.10087E-01
0.24994E+00	0.54040E+00	0.77526E-01	0.64394E-01	-0.95547E-03	0.10157E-01
0.29158E+00	0.55262E+00	0.78136E-01	0.63778E-01	-0.10955E-02	0.10173E-01
0.33322E+00	0.56458E+00	0.78591E-01	0.62907E-01	-0.11973E-02	0.10134E-01
0.37486E+00	0.57623E+00	0.78887E-01	0.61796E-01	-0.12625E-02	0.10042E-01
0.41650E+00	0.58755E+00	0.79028E-01	0.60473E-01	-0.12944E-02	0.99024E-02
0.45814E+00	0.59848E+00	0.79022E-01	0.58975E-01	-0.12977E-02	0.97285E-02
0.49978E+00	0.60899E+00	0.78884E-01	0.57347E-01	-0.12779E-02	0.95114E-02
0.54142E+00	0.61905E+00	0.78632E-01	0.55640E-01	-0.12410E-02	0.92788E-02
0.58306E+00	0.62863E+00	0.78290E-01	0.53904E-01	-0.11932E-02	0.90350E-02
0.62470E+00	0.63769E+00	0.77882E-01	0.52190E-01	-0.11401E-02	0.87893E-02
0.72880E+00	0.65800E+00	0.76741E-01	0.48280E-01	-0.10146E-02	0.82201E-02
0.83290E+00	0.67487E+00	0.75709E-01	0.45270E-01	-0.93506E-03	0.77812E-02
0.93700E+00	0.68847E+00	0.75008E-01	0.43317E-01	-0.91146E-03	0.75025E-02
0.10411E+01	0.69924E+00	0.74669E-01	0.42275E-01	-0.92614E-03	0.73627E-02
0.11452E+01	0.70783E+00	0.74572E-01	0.41836E-01	-0.95368E-03	0.73112E-02
0.12493E+01	0.71498E+00	0.74536E-01	0.41685E-01	-0.97674E-03	0.72932E-02
0.13534E+01	0.72141E+00	0.74430E-01	0.41602E-01	-0.99103E-03	0.72705E-02
0.14575E+01	0.72765E+00	0.74221E-01	0.41489E-01	-0.10010E-02	0.72302E-02
0.15616E+01	0.73403E+00	0.73964E-01	0.41334E-01	-0.10124E-02	0.71793E-02
0.17698E+01	0.74730E+00	0.73570E-01	0.40993E-01	-0.10423E-02	0.70930E-02
0.19780E+01	0.76018E+00	0.73299E-01	0.40680E-01	-0.10616E-02	0.70276E-02
0.21862E+01	0.77149E+00	0.72758E-01	0.40363E-01	-0.10598E-02	0.69230E-02
0.23944E+01	0.78163E+00	0.71994E-01	0.40010E-01	-0.10480E-02	0.67839E-02
0.26026E+01	0.79178E+00	0.71324E-01	0.39624E-01	-0.10389E-02	0.66572E-02
0.28108E+01	0.80238E+00	0.70782E-01	0.39254E-01	-0.10384E-02	0.65511E-02
0.30190E+01	0.81272E+00	0.70195E-01	0.38908E-01	-0.10355E-02	0.64411E-02
0.32272E+01	0.82208E+00	0.69437E-01	0.38496E-01	-0.10158E-02	0.63034E-02
0.34354E+01	0.83082E+00	0.68561E-01	0.38034E-01	-0.98764E-03	0.61471E-02
0.36436E+01	0.84002E+00	0.67715E-01	0.37634E-01	-0.96618E-03	0.60016E-02
0.38518E+01	0.85025E+00	0.66798E-01	0.37206E-01	-0.94665E-03	0.58462E-02
0.40600E+01	0.86092E+00	0.65521E-01	0.36532E-01	-0.91759E-03	0.56276E-02
0.42682E+01	0.87094E+00	0.63992E-01	0.35671E-01	-0.88163E-03	0.53674E-02
0.46846E+01	0.88727E+00	0.61744E-01	0.34283E-01	-0.81823E-03	0.49876E-02
0.51010E+01	0.89982E+00	0.59844E-01	0.32975E-01	-0.74770E-03	0.46686E-02
0.55174E+01	0.90861E+00	0.57138E-01	0.31292E-01	-0.67226E-03	0.42439E-02
0.59338E+01	0.91697E+00	0.53288E-01	0.29495E-01	-0.57848E-03	0.37096E-02
0.63502E+01	0.92720E+00	0.49238E-01	0.27615E-01	-0.48639E-03	0.31870E-02
0.67666E+01	0.93582E+00	0.46212E-01	0.25941E-01	-0.41767E-03	0.28086E-02
0.71830E+01	0.94291E+00	0.41491E-01	0.23737E-01	-0.32649E-03	0.22850E-02
0.75994E+01	0.95035E+00	0.37117E-01	0.21808E-01	-0.25379E-03	0.18532E-02
0.80158E+01	0.95872E+00	0.33102E-01	0.20002E-01	-0.19597E-03	0.14958E-02
0.84322E+01	0.96654E+00	0.28678E-01	0.18018E-01	-0.14001E-03	0.11471E-02
0.88486E+01	0.97069E+00	0.24506E-01	0.16199E-01	-0.10013E-03	0.86296E-03
0.96814E+01	0.98146E+00	0.17489E-01	0.13049E-01	-0.45223E-04	0.47615E-03
0.10514E+02	0.98509E+00	0.13052E-01	0.10446E-01	-0.19192E-04	0.27947E-03
0.11347E+02	0.99059E+00	0.10225E-01	0.85708E-02	-0.70776E-05	0.17801E-03
0.12180E+02	0.99459E+00	0.80144E-02	0.66179E-02	-0.67578E-06	0.10803E-03
0.13013E+02	0.99335E+00	0.64932E-02	0.50898E-02	0.21451E-05	0.68068E-04
0.13845E+02	0.99031E+00	0.58891E-02	0.41133E-02	0.21738E-05	0.51600E-04
0.14678E+02	0.98835E+00	0.54490E-02	0.35733E-02	0.23232E-05	0.42460E-04
0.15511E+02	0.10035E+01	0.50132E-02	0.31564E-02	0.18381E-05	0.35096E-04
0.16344E+02	0.10055E+01	0.46971E-02	0.27429E-02	0.18178E-05	0.29586E-04
0.17177E+02	0.10013E+01	0.46658E-02	0.24711E-02	0.17335E-05	0.27876E-04
0.18009E+02	0.10067E+01	0.45649E-02	0.23485E-02	0.18892E-05	0.26354E-04
0.18842E+02	0.10097E+01	0.45572E-02	0.21867E-02	0.18805E-05	0.25549E-04
0.19675E+02	0.10066E+01	0.41435E-02	0.20592E-02	0.15094E-05	0.21409E-04

RUN NO.= 22 Y-STATION= 13 PROBE= 2 YMAX= 0.95869E+01 RUN NO.= 23

POSITION MM	U	UT	VT	U*V	TKE
0.33622E-01	0.57268E+00	0.64440E-01	0.52896E-01	0.77967E-03	0.69506E-02
0.75262E-01	0.57593E+00	0.64215E-01	0.52927E-01	0.62551E-03	0.69248E-02
0.11690E+00	0.57923E+00	0.64029E-01	0.52961E-01	0.47186E-03	0.69046E-02
0.15854E+00	0.58262E+00	0.63920E-01	0.53000E-01	0.31929E-03	0.68949E-02
0.20018E+00	0.58614E+00	0.63920E-01	0.53047E-01	0.16845E-03	0.68997E-02
0.24182E+00	0.58981E+00	0.64053E-01	0.53099E-01	0.20087E-04	0.69223E-02
0.28346E+00	0.59368E+00	0.64337E-01	0.53155E-01	-0.12492E-03	0.69647E-02
0.32510E+00	0.59776E+00	0.64777E-01	0.53211E-01	-0.26558E-03	0.70275E-02
0.36674E+00	0.60207E+00	0.65372E-01	0.53260E-01	-0.40079E-03	0.71101E-02
0.40838E+00	0.60661E+00	0.66109E-01	0.53296E-01	-0.52940E-03	0.72108E-02
0.45002E+00	0.61139E+00	0.66968E-01	0.53309E-01	-0.65023E-03	0.73266E-02
0.49166E+00	0.61638E+00	0.67923E-01	0.53292E-01	-0.76217E-03	0.74536E-02
0.53330E+00	0.62157E+00	0.68942E-01	0.53236E-01	-0.86421E-03	0.75871E-02
0.57494E+00	0.62694E+00	0.69991E-01	0.53134E-01	-0.95550E-03	0.77220E-02
0.61658E+00	0.63245E+00	0.71037E-01	0.52981E-01	-0.10354E-02	0.78532E-02
0.65822E+00	0.63807E+00	0.72047E-01	0.52772E-01	-0.11036E-02	0.79757E-02
0.69986E+00	0.64375E+00	0.72993E-01	0.52507E-01	-0.11599E-02	0.80851E-02
0.74150E+00	0.64946E+00	0.73852E-01	0.52186E-01	-0.12047E-02	0.81775E-02
0.78314E+00	0.65514E+00	0.74605E-01	0.51812E-01	-0.12384E-02	0.82504E-02
0.82478E+00	0.66075E+00	0.75242E-01	0.51389E-01	-0.12617E-02	0.83022E-02
0.86642E+00	0.66627E+00	0.75757E-01	0.50924E-01	-0.12756E-02	0.83324E-02
0.90806E+00	0.67163E+00	0.76152E-01	0.50423E-01	-0.12814E-02	0.83416E-02
0.94970E+00	0.67682E+00	0.76431E-01	0.49894E-01	-0.12801E-02	0.83311E-02
0.10538E+01	0.68885E+00	0.76694E-01	0.48499E-01	-0.12548E-02	0.82341E-02
0.11579E+01	0.69934E+00	0.76502E-01	0.47087E-01	-0.12130E-02	0.80697E-02
0.12620E+01	0.70827E+00	0.76060E-01	0.45743E-01	-0.11694E-02	0.78775E-02
0.13661E+01	0.71581E+00	0.75521E-01	0.44527E-01	-0.11334E-02	0.76861E-02
0.14702E+01	0.72230E+00	0.74978E-01	0.43482E-01	-0.11087E-02	0.75123E-02
0.15743E+01	0.72812E+00	0.74481E-01	0.42633E-01	-0.10954E-02	0.73649E-02
0.16784E+01	0.73362E+00	0.74055E-01	0.41987E-01	-0.10908E-02	0.72471E-02
0.17825E+01	0.73908E+00	0.73707E-01	0.41525E-01	-0.10915E-02	0.71571E-02
0.18866E+01	0.74464E+00	0.73421E-01	0.41208E-01	-0.10937E-02	0.70888E-02
0.19948E+01	0.75621E+00	0.72907E-01	0.40810E-01	-0.10941E-02	0.69808E-02
0.23030E+01	0.76797E+00	0.72370E-01	0.40514E-01	-0.10925E-02	0.68788E-02
0.25112E+01	0.77939E+00	0.71961E-01	0.40287E-01	-0.11031E-02	0.68014E-02
0.27194E+01	0.79031E+00	0.71707E-01	0.40137E-01	-0.11207E-02	0.67529E-02
0.29276E+01	0.80086E+00	0.71280E-01	0.39926E-01	-0.11203E-02	0.66749E-02
0.31358E+01	0.81127E+00	0.70402E-01	0.39462E-01	-0.10906E-02	0.65137E-02
0.33440E+01	0.82169E+00	0.69182E-01	0.38753E-01	-0.10470E-02	0.62880E-02
0.35522E+01	0.83208E+00	0.68086E-01	0.38050E-01	-0.10145E-02	0.60835E-02
0.37604E+01	0.84208E+00	0.67515E-01	0.37532E-01	-0.10033E-02	0.59670E-02
0.39686E+01	0.85115E+00	0.67195E-01	0.37181E-01	-0.99824E-03	0.58931E-02
0.41768E+01	0.85899E+00	0.66425E-01	0.36658E-01	-0.97707E-03	0.57561E-02
0.43850E+01	0.86591E+00	0.65101E-01	0.36064E-01	-0.93808E-03	0.55388E-02
0.45932E+01	0.87269E+00	0.63776E-01	0.35361E-01	-0.89759E-03	0.53178E-02
0.50096E+01	0.88744E+00	0.61503E-01	0.33917E-01	-0.82378E-03	0.49330E-02
0.54260E+01	0.90049E+00	0.58015E-01	0.32284E-01	-0.71338E-03	0.44080E-02
0.58424E+01	0.90958E+00	0.54974E-01	0.30559E-01	-0.63499E-03	0.39560E-02
0.62588E+01	0.91790E+00	0.51366E-01	0.28741E-01	-0.54870E-03	0.34645E-02
0.66752E+01	0.92492E+00	0.48901E-01	0.27056E-01	-0.47859E-03	0.31234E-02
0.70916E+01	0.93184E+00	0.45590E-01	0.25786E-01	-0.41662E-03	0.27402E-02
0.75080E+01	0.94286E+00	0.41798E-01	0.24072E-01	-0.33758E-03	0.23265E-02
0.79244E+01	0.95321E+00	0.36977E-01	0.21746E-01	-0.25616E-03	0.18402E-02
0.83408E+01	0.96226E+00	0.32865E-01	0.20133E-01	-0.20567E-03	0.14855E-02
0.87572E+01	0.97094E+00	0.29336E-01	0.18770E-01	-0.16952E-03	0.12129E-02
0.91736E+01	0.97806E+00	0.25074E-01	0.16630E-01	-0.11040E-03	0.90526E-03
0.10006E+02	0.98885E+00	0.17342E-01	0.13099E-01	-0.45149E-04	0.47234E-03
0.10839E+02	0.99442E+00	0.13034E-01	0.10385E-01	-0.17792E-04	0.27774E-03
0.11672E+02	0.99540E+00	0.99688E-02	0.81609E-02	-0.45191E-05	0.16598E-03
0.12505E+02	0.99358E+00	0.78692E-02	0.63752E-02	-0.28847E-06	0.10257E-03
0.13338E+02	0.99640E+00	0.66145E-02	0.51095E-02	0.20071E-05	0.69858E-04
0.14170E+02	0.99878E+00	0.58911E-02	0.42095E-02	0.20563E-05	0.52425E-04
0.15003E+02	0.99671E+00	0.54115E-02	0.35690E-02	0.18750E-05	0.42022E-04
0.15836E+02	0.99992E+00	0.51149E-02	0.30707E-02	0.18760E-05	0.35592E-04
0.16669E+02	0.10014E+01	0.48058E-02	0.27473E-02	0.18074E-05	0.30644E-04
0.17502E+02	0.10015E+01	0.46263E-02	0.26165E-02	0.15171E-05	0.28248E-04
0.18334E+02	0.10019E+01	0.46385E-02	0.24179E-02	0.19172E-05	0.27362E-04
0.19167E+02	0.10073E+01	0.45090E-02	0.22401E-02	0.18845E-05	0.25350E-04
0.20000E+02	0.10026E+01	0.43464E-02	0.21752E-02	0.14818E-05	0.23622E-04

RUN NO.= 12 Y-STATION= 22 PROBE= 2 YMAX= 0.92040E+01 RUN NO.= 13

POSITION MM	U	UT	VT	U*V	TKE
0.40343E-01	0.77914E+00	0.49674E-01	0.36093E-01	0.12123E-03	0.37702E-02
0.81983E-01	0.77909E+00	0.49670E-01	0.36041E-01	0.92523E-04	0.37661E-02
0.12362E+00	0.77905E+00	0.49669E-01	0.35991E-01	0.63987E-04	0.37623E-02
0.16526E+00	0.77901E+00	0.49671E-01	0.35944E-01	0.35782E-04	0.37591E-02
0.20690E+00	0.77899E+00	0.49679E-01	0.35900E-01	0.80415E-05	0.37568E-02
0.24854E+00	0.77899E+00	0.49695E-01	0.35861E-01	-0.19130E-04	0.37556E-02
0.29018E+00	0.77901E+00	0.49721E-01	0.35827E-01	-0.45667E-04	0.37557E-02
0.33182E+00	0.77906E+00	0.49759E-01	0.35799E-01	-0.71545E-04	0.37575E-02
0.37346E+00	0.77914E+00	0.49810E-01	0.35776E-01	-0.96774E-04	0.37610E-02
0.41510E+00	0.77926E+00	0.49877E-01	0.35759E-01	-0.12140E-03	0.37664E-02
0.45674E+00	0.77941E+00	0.49961E-01	0.35746E-01	-0.14550E-03	0.37739E-02
0.49838E+00	0.77959E+00	0.50062E-01	0.35738E-01	-0.16916E-03	0.37834E-02
0.54002E+00	0.77982E+00	0.50182E-01	0.35734E-01	-0.19246E-03	0.37951E-02
0.58166E+00	0.78009E+00	0.50321E-01	0.35732E-01	-0.21549E-03	0.38089E-02
0.62330E+00	0.78039E+00	0.50478E-01	0.35731E-01	-0.23832E-03	0.38248E-02
0.66494E+00	0.78074E+00	0.50653E-01	0.35732E-01	-0.26100E-03	0.38425E-02
0.70658E+00	0.78113E+00	0.50845E-01	0.35733E-01	-0.28353E-03	0.38621E-02
0.74822E+00	0.78155E+00	0.51052E-01	0.35734E-01	-0.30592E-03	0.38833E-02
0.78986E+00	0.78201E+00	0.51273E-01	0.35735E-01	-0.32811E-03	0.39059E-02
0.83150E+00	0.78251E+00	0.51505E-01	0.35734E-01	-0.35006E-03	0.39297E-02
0.87314E+00	0.78304E+00	0.51745E-01	0.35733E-01	-0.37169E-03	0.39544E-02
0.91478E+00	0.78361E+00	0.51992E-01	0.35730E-01	-0.39291E-03	0.39798E-02
0.95642E+00	0.78421E+00	0.52243E-01	0.35727E-01	-0.41366E-03	0.40057E-02
0.99806E+00	0.78485E+00	0.52496E-01	0.35723E-01	-0.43386E-03	0.40320E-02
0.10397E+01	0.78551E+00	0.52750E-01	0.35719E-01	-0.45347E-03	0.40584E-02
0.10813E+01	0.78621E+00	0.53002E-01	0.35715E-01	-0.47247E-03	0.40847E-02
0.11230E+01	0.78693E+00	0.53252E-01	0.35711E-01	-0.49086E-03	0.41110E-02
0.11646E+01	0.78769E+00	0.53498E-01	0.35709E-01	-0.50868E-03	0.41372E-02
0.12063E+01	0.78848E+00	0.53741E-01	0.35707E-01	-0.52597E-03	0.41631E-02
0.12479E+01	0.78929E+00	0.53981E-01	0.35708E-01	-0.54279E-03	0.41889E-02
0.12895E+01	0.79014E+00	0.54216E-01	0.35710E-01	-0.55923E-03	0.42146E-02
0.13312E+01	0.79102E+00	0.54449E-01	0.35715E-01	-0.57535E-03	0.42402E-02
0.13728E+01	0.79192E+00	0.54678E-01	0.35723E-01	-0.59123E-03	0.42658E-02
0.14145E+01	0.79286E+00	0.54905E-01	0.35733E-01	-0.60690E-03	0.42914E-02
0.14561E+01	0.79383E+00	0.55130E-01	0.35746E-01	-0.62240E-03	0.43171E-02
0.15602E+01	0.79641E+00	0.55681E-01	0.35789E-01	-0.66040E-03	0.43812E-02
0.16643E+01	0.79918E+00	0.56217E-01	0.35839E-01	-0.69681E-03	0.44448E-02
0.17684E+01	0.80215E+00	0.56735E-01	0.35882E-01	-0.73067E-03	0.45063E-02
0.18725E+01	0.80530E+00	0.57235E-01	0.35903E-01	-0.76117E-03	0.45648E-02
0.19766E+01	0.80859E+00	0.57722E-01	0.35894E-01	-0.78827E-03	0.46202E-02
0.20807E+01	0.81197E+00	0.58207E-01	0.35860E-01	-0.81279E-03	0.46740E-02
0.21848E+01	0.81542E+00	0.58694E-01	0.35820E-01	-0.83592E-03	0.47281E-02
0.22889E+01	0.81890E+00	0.59178E-01	0.35797E-01	-0.85849E-03	0.47835E-02
0.23930E+01	0.82237E+00	0.59635E-01	0.35809E-01	-0.88032E-03	0.48386E-02
0.26012E+01	0.82930E+00	0.60320E-01	0.35901E-01	-0.91599E-03	0.49274E-02
0.28094E+01	0.83630E+00	0.60540E-01	0.35883E-01	-0.93058E-03	0.49527E-02
0.30176E+01	0.84357E+00	0.60456E-01	0.35600E-01	-0.92680E-03	0.49223E-02
0.32258E+01	0.85124E+00	0.60459E-01	0.35227E-01	-0.92238E-03	0.48962E-02
0.34340E+01	0.85917E+00	0.60632E-01	0.34972E-01	-0.92440E-03	0.48993E-02
0.36422E+01	0.86705E+00	0.60637E-01	0.34748E-01	-0.92084E-03	0.48842E-02
0.38504E+01	0.87451E+00	0.60247E-01	0.34387E-01	-0.90409E-03	0.48122E-02
0.40586E+01	0.88138E+00	0.59701E-01	0.33951E-01	-0.88429E-03	0.47169E-02
0.42668E+01	0.88771E+00	0.59282E-01	0.33578E-01	-0.86976E-03	0.46418E-02
0.44750E+01	0.89368E+00	0.58870E-01	0.33217E-01	-0.85388E-03	0.45691E-02
0.46832E+01	0.89943E+00	0.58209E-01	0.32741E-01	-0.83112E-03	0.44603E-02
0.48914E+01	0.90492E+00	0.57313E-01	0.32145E-01	-0.80615E-03	0.43181E-02
0.50996E+01	0.90998E+00	0.56309E-01	0.31504E-01	-0.77907E-03	0.41632E-02
0.55160E+01	0.91831E+00	0.53977E-01	0.30277E-01	-0.70304E-03	0.38302E-02
0.59324E+01	0.92548E+00	0.52120E-01	0.29200E-01	-0.65093E-03	0.35691E-02
0.63488E+01	0.93403E+00	0.49923E-01	0.27993E-01	-0.58367E-03	0.32759E-02
0.67652E+01	0.94311E+00	0.46900E-01	0.26387E-01	-0.49852E-03	0.28959E-02
0.71816E+01	0.94931E+00	0.44086E-01	0.24747E-01	-0.43608E-03	0.25560E-02
0.75980E+01	0.95367E+00	0.40716E-01	0.23361E-01	-0.36537E-03	0.22036E-02
0.80144E+01	0.96080E+00	0.37510E-01	0.21923E-01	-0.30618E-03	0.18870E-02
0.84308E+01	0.97023E+00	0.33702E-01	0.20201E-01	-0.24700E-03	0.15439E-02
0.88472E+01	0.97725E+00	0.29645E-01	0.18466E-01	-0.19556E-03	0.12198E-02
0.92636E+01	0.98218E+00	0.26732E-01	0.17146E-01	-0.15895E-03	0.10086E-02
0.96800E+01	0.98857E+00	0.24057E-01	0.15837E-01	-0.12320E-03	0.82957E-03

REFERENCES

1. Baker, A. J. and Manhardt, P.D., "Numerical Prediction of Mean and Fluctuating Velocities for Jet-Flap Flows," AIAA J., Vol. 16, No. 8, p. 807-814, 1978.

2. Ferzinger, J.H., "Large Eddy Numerical Simulations of Turbulent Flows," AIAA Paper No. 78-347, 1978.

3. Cebeci, T. and Smith, A.M.O., Analysis of Turbulent Boundary Layers, Academic Press, New York, 1974.

4. Tennekes, H. and Lumley, J.L., A First Course in Turbulence, MIT Press, U.S.A., 1972.

5. Launder, B.E., Reece, G.J. and Rodi, W., "Progress in the Development of A Reynolds-Stress Turbulence Closure," J. Flu. Mech., V. 68, Pt. 3 pp. 537-566, 1975.

6. Hanjalic, K. and Launder, B.E., "A Reynolds Stress Model of Turbulence and its Application to Thin Shear Flows," J. Flu. Mech., V. 52, Pt. 4, pp. 609-638, 1972.

7. Gessner, F. B., and Emery, A. F., "A Reynolds Stress Model for Turbulent Corner Flows - Pt. 1: Development of the Model," J. Flu. Engr. Trans. ASME, pp. 261-268, 1976.

8. Lumley, J.L., "Toward A Turbulent Constitutive Relation," J. Flu. Mech., Vol. 41, Pt. 2, p. 413-434, 1970.

9. Yu, J.C., "Mean Flow and Reynolds Stress Measurements in the Vicinity of the Trailing Edge of a NACA 63-012 Airfoil," NASA TM-80224, 1980.

10. Baker, A.J. and Manhardt, P.D., "Finite Element Analysis of Low Speed Viscous and Inviscid Aerodynamic Flows," NASA CR-2908, 1977.

11. Proceedings, AFOSR-IFP-Stanford Conference on Computation of Turbulent Boundary Layers - 1968, Vol. I., Eds. S.J. Kline, G. Sovran, M.V Morkovan, D.J. Cockrell, Vol. II, Eds, D.A., Coles, E.A., Hirst, Stanford University, 1969.

1. Report No.	2. Government Accession No.	3. Recipient's Catalog No.
NASA CR-3301		

4. Title and Subtitle	5. Report Date
An Interaction Algorithm for Prediction of Mean and Fluctuating Velocities in Two-Dimensional Aerodynamic Wake Flows	July 1980
	6. Performing Organization Code

7. Author(s)	8. Performing Organization Report No.
A. J. Baker and J. A. Orzechowski	CoMCo 80 TR-1.0

9. Performing Organization Name and Address	10. Work Unit No.
Computational Mechanics Consultants, Inc. 3601-A Chapman Highway Knoxville, TN 37920	11. Contract or Grant No. NAS1-14855/Mod. 1

12. Sponsoring Agency Name and Address	13. Type of Report and Period Covered
National Aeronautics & Space Administration Washington, DC 20546	Contractor Report
	14. Sponsoring Agency Code

15. Supplementary Notes

Langley Technical Monitor: Thomas B. Gatski
Final Report

16. Abstract

A theoretical analysis is presented yielding sets of partial differential equations for determination of turbulent aerodynamic flowfields in the vicinity of an airfoil trailing edge. A four-phase interaction algorithm is derived to complete the analysis. Following input, the first computational phase is an elementary viscous-corrected two-dimensional potential flow solution yielding an estimate of the inviscid-flow induced pressure distribution. Phase C involves solution of the turbulent two-dimensional boundary layer equations over the trailing edge, with transition to a two-dimensional parabolic Navier-Stokes equation system describing the near-wake merging of the upper and lower surface boundary layers. An iteration provides refinement of the potential flow induced pressure coupling to the viscous flow solutions. The final phase is a complete two-dimensional Navier-Stokes analysis of the wake flow in the vicinity of a blunt-bases airfoil. A finite element numerical algorithm is presented which is applicable to solution of all partial differential equation sets of inviscid-viscous aerodynamic interaction algorithm. Numerical results are discussed.

17. Key Words (Selected by Author(s))	18. Distribution Statement
Numerical Solution Aerodynamics Turbulent Wake Navier-Stokes	Unclassified - Unlimited Subject Category 02

19. Security Classif. (of this report)	20. Security Classif. (of this page)	21. No. of Pages	22. Price
Unclassified	Unclassified	68	A04

For sale by the National Technical Information Service, Springfield, Virginia 22161

NASA-Langley, 1980